Universidad del País Vasco Euskal Herriko Unibertsitatea
FACULTY OF ENGINEERING BILBAO
UNIVERSITY OF THE BASQUE COUNTRY

MASTER'S DEGREE IN

TELECOMMUNICATION ENGINEERING

MASTER'S THESIS

AppQP: NEW MEASUREMENT METHOD FOR NON-INTENTIONAL EMISSIONS IN LOW VOLTAGE GRID FROM 2 kHz TO 150 kHz

Student *Gallarreta, Canteli, Alexander*
Director *de la Vega, Moreno, David*
Co-director *Fernández, Pérez, Igor*
Department *Communications Engineering*
Academic course *2020/2021*

Bilbao, 11 Jun 2021

ACKNOWLEDGEMENTS

I would like to dedicate this Master's Thesis to:

- My parents, for giving me the wings to fly.
- The members of TSR, because with you going to work is even fun.
- My colleagues and teachers of the Smart Grids research line ("los chispas"), for putting up with me every day and giving me this incredible opportunity.
- My tutor, David de la Vega, for treating me like a colleague and passing on his passion for research to me.

Master Amaierako Lan hau honako pertsona hauei eskaini nahiko nieke:

- Nire gurasoei, hegan egiteko hegoak emateagatik.
- TRSko kideei, zuekin lanera joatera dibertigarria ere badelako.
- Smart Grids ikerketa lerroko nire lankide eta irakasleei ("los chispas"), egunero jasateagatik eta aukera zoragarri hau emateagatik.
- Master Amaierako Lan honen zuzendariari, David de la Vegari, lankide bat bezala tratatzeagatik eta ikerketarako berak duen grina transmititzeagatik.

Este Trabajo Fin de Máster se lo quería dedicar a:

- Mi madre y mi padre, por darme las alas para volar.
- Los y las integrantes de TSR, porque con vosotros ir a trabajar es hasta divertido.
- Mis compañerxs y profesorxs de la línea de investigación de Smart Grids ("los chispas"), por aguantarme a diario y por darme esta increíble oportunidad.
- El director de este Trabajo Fin de Máster, David de la Vega, por tratarme como a un compañero más y por transmitirme su pasión por la investigación.

ABSTRACT

This Master's Thesis is focused on the methods to measure the Non-Intentional Emissions (NIE) in the Low Voltage (LV) grid. These measurement methods have commonly been related to Electromagnetic Interference (EMI) of Electromagnetic Compatibility (EMC) tests. Nevertheless, these procedures are intended to be performed in controlled test environments, i.e. laboratories. Additionally, in the LV grid, Compatibility Levels (CL) for emissions in this medium must be complied with. The waveforms which exceed the CL in the LV grid can affect the correct operation of the rest of the equipment connected to the grid and the communications propagated through this.

Furthermore, this medium is a very hostile environment for communications, as it has very changeable properties that are dependent on the consumption, type, number, et cetera of the connected devices. For these reasons, it is essential to correctly characterise the electromagnetic emissions that exist in the LV network. For this purpose, measurement methods that provide the amplitude of the emissions in the spectrum must be used, which have to be designed for the low-voltage network.

This Master's Thesis addresses these issues with two main works. First, a comparison has been made with the existing NIE measurement methods, both in the literature and in the EMC and Power Quality (PQ) standards. The second contribution of this work is the proposed three EMI measurement methods for the characterisation of the network waveforms. A digital implementation of CISPR 16-1-1 has been defined, a procedure with which the CL of the grid must be verified. Secondly, a new measurement method, the RMS-A method, has been developed in this work, which allows to calculate the RMS values of the spectrum in the CISPR Band A. Additionally, other new EMI method has been designed, the Approximated Quasi-Peak (AppQP), which provides values similar to CISPR 16-1-1; however, it has lower computational complexity and needs fewer memory requirements.

Keywords: AppQP, EMC, EMI, Non-Intentional Emissions, CISPR 16-1-1, Quasi-Peak, IEC 61000-4-7

LABURPENA

Master Amaierako Lan honek Behe Tentsioko (BT) sareko emisio ez-intentzionalak neurtzeko metodoak ditu ardatz. Neurketa-metodo hauek Bateragarritasun Elektromagnetikoko (EMC) proben Interferentzia Elektromagnetikoko (EMI) prozedurekin lotu ohi dira. Hala ere, proba horiek kontrolatutako inguruneetan egiteko diseinatuta daude, hau da, laborategietan burutzeko sortu ziren. Gainera, BT sareetan existitzen diren emisioetarako Bateragarritasun Mailak (CL, *Compatibility Levels* ingelesez) definitu dira, zeinak gainditu ezin izango diren, sarera konektaturiko gainontzeko ekipoen funtzionamendu egokian edota ingurune horren bidez hedatzen diren komunikazioetan (PLC, *Power Line Communications* ingelesez) eragin baitezakete.

Bestalde, BT sarea oso ingurune desegokia da komunikazioetarako, oso propietate aldakorrak baititu, konektatutako gailuen kontsumoaren, motaren, kopuruaren eta abarren araberakoa baita. Horregatik, garrantzitsua da BT sarean dauden emisio elektromagnetikoak behar bezala ezaugarritzea. Horretarako, espektroko emisioen anplitudea neurtzen duten neurketa-metodoak erabili behar dira, eta behe-tentsioko sarerako diseinatuta egon behar dute.

Master Amaierako Lan honek bi ekarpen nagusirekin heltzen die gai horiei. Lehenengoan, gaur egun existitzen diren EMI metodoen konparazioa egin da; bai literaturan, bai EMC (*Electromagnetic Compatibility*) eta energiaren kalitatearen estandarretan definitutako metodoak erabiliz. Lan honen bigarren ekarpenean, sareko emisioak ezaugarritzeko hiru EMI neurketa metodo proposatzen dira. CISPR 16-1-1 estandarraren inplementazio digitala definitu da, parametro finkoak dituena. Izan ere, metodo horrekin sareko emisioen maila neurtu behar da CL-ak betetzen direla egiaztatzeko. Bigarrenik, lan honetan neurketa-metodo berri bat garatu da, RMS-A metodoa, espektroaren RMS balioak CISPRren A bandan kalkulatzeko aukera ematen duena. Beste alde betetik, beste EMI metodo berri bat diseinatu da, Approximated Quasi-Peak (AppQP) deitua, CISPR 16-1-1 metodoaren antzeko balioak ematen dituena, baina kostu konputazional txikiagoa duena eta memoria-baliabide gutxiago behar dituena.

Gako-hitzak: AppQP, EMC, EMI, emisio ez-intentsionalak, CISPR 16-1-1, Quasi-Peak, IEC 61000-4-7

RESUMEN

Este Trabajo Fin de Máster se centra en los métodos de medida de las Emisiones No Intencionales (NIE) en la red de Baja Tensión (BT). Este tipo de métodos de medida han sido comúnmente relacionados con los ensayos de Interferencia Electromagnética (EMI) de las pruebas de Compatibilidad Electromagnética (EMC). Sin embargo, estos procedimientos están pensados para ser realizados en entornos de prueba controlados, es decir, en laboratorios. Además, se han definido Niveles de Compatibilidad (CL) para las emisiones existentes en la red de BT, los cuales no deben de superarse, pues podrían afectar al correcto funcionamiento del resto de equipos conectados a la red y a las comunicaciones que se propagan a través de este medio (PLC).

Por otro lado, este medio es un entorno muy hostil para las comunicaciones, ya que tiene propiedades muy cambiantes que dependen del modo de funcionamiento, tipo, número, etc. de los dispositivos conectados. Por estas razones, es importante caracterizar correctamente las emisiones electromagnéticas que existen en la red de BT. Para ello, es necesario utilizar métodos de medida que proporcionen, de forma precisa, valores relacionados con la amplitud de las emisiones en el espectro, los cuales deben estar diseñados para las características concretas de la red de baja tensión y para la naturaleza de las emisiones.

Este Trabajo Fin de Master aborda estas cuestiones con dos aportaciones principales. En la primera, se ha realizado una comparativa de los métodos de medida de NIE existentes, tanto en la literatura como en los estándares de EMC y de Calidad de la Energía (PQ). La segunda aportación de este trabajo son los tres métodos de medida de EMI propuestos para la caracterización de las emisiones en la red eléctrica. Se ha definido una implementación digital del estándar del CISPR 16-1-1 con parámetros fijos, procedimiento con el que se deben verificar los CL de las emisiones de la red. En segundo lugar, en este trabajo se ha desarrollado un nuevo método de medición, el método RMS-A, que permite calcular los valores RMS del espectro en la banda A del CISPR. En segundo lugar, en este trabajo se ha desarrollado un nuevo método de medida, el método RMS-A, que permite calcular los valores RMS del espectro en la banda A de CISPR. Además, se ha diseñado otro nuevo método para la medida de NIE, el Approximated Quasi-Peak (AppQP), que proporciona valores similares a los de la norma CISPR 16-1-1, pero con un coste computacional menor y menos recursos de memoria.

Palabras clave: AppQP, EMC, EMI, Emisiones No Intencionales (NIE), CISPR 16-1-1, Quasi-Peak, IEC 61000-4-7

INDEX

INDEX OF FIGURES

INDEX OF TABLES

LIST OF ACRONYMS

ADC	Analog-to-Digital Converter
AppQP	Approximated Quasi-Peak
AWGN	Additive White Gaussian Noise
B_6	Resolution bandwidth at – 6 dB (as defined in CISPR 16-1-1)
CENELEC	*Comité Européen de Normalisation Electrotechnique*
CISPR	*Comité International Spécial des Perturbations Radioélectriques*
CL	Compatibility Levels
DFT	Discrete Fourier Transform
EMC	Electromagnetic Compatibility
EMI	Electromagnetic Interference
EMPIR	European Metrology Programme for Innovation and Research
EURAMET	The European Association of National Metrology Institutes
EV	Electric Vehicle
FFT	Fourier Fast Transform
FSS	Frequency Step Size
IEC	International Electrotechnical Commission
IEEE TIM	IEEE Transactions on Instrumentation and Measurement
IIR	Infinite Impulse Response
LNE	*Laboratoire national de métrologie et d'essais*
LV	Low Voltage
METAS	Federal Institute of Metrology
NIE	Non-Intentional Emissions
NPL	National Physics Laboratory
OFDM	Orthogonal Frequency Division Multiplexing
PLC	Power Line Communications
POC	Point Of Connection
PQ	Power Quality

PRIME	PoweRline Intelligent Metering Evolution
PSD	Power Spectral Density
PV	Photovoltaic
QP	Quasi-Peak
RBW	Resolution Bandwidth
RC	Resistor-Capacitor
REE	*Red Eléctrica de España*
RMS	Root Mean Square
RMS-A	IEC 61000-4-7 method adapted to CISPR Band A
RMSE	Root Mean Square Error
RSS	Root Sum Square
SG	Smart Grid
STFT	Short-Time Fourier Transform
SupraEMI	Supra Electromagnetic Interference (project accepted in EMPIR-18 call)
TC	Transformation Centre
TR	Technical Report
TSR	*Tratamiento de la Señal y Radiocomunicaciones*
TUD	*Technische Universität Dresden*
UNICAMPANIA	*Università degli Studi della Campania 'Luigi Vanvitelli'*
UPV/EHU	*Universidad del País Vasco/Euskal Herriko Unibertsitatea*
VSL	Dutch national metrology institute
WP	Work Package

1. Introduction

In recent decades, the way how electricity is generated and consumed has changed radically. This circumstance has changed the classical model of energy production and distribution. In the past, there was hierarchical production-distribution-consumption scheme, in which the roles of electricity producers, electricity companies and consumers were very well defined. In the current model, which is much more decentralised, consumers can also be electricity producers due to the popularisation of photovoltaic panels in private homes. This change in the electricity market model caused electricity companies, which must ensure the quality of electricity supply, to computerise their electricity distribution networks. In this wave of grid modernisation, telemetry arrived to stay.

Currently, the information collected by the telemetry equipment of the low voltage network is sent through the network itself. The grid is a rather hostile environment for communications due to the changing properties of the grid, and there are telemetry devices in the network that cannot communicate with each other. This issue has led to numerous research studies in the last decade, in which the propagation properties (impedance, attenuation, emissions, etcetera) of the network have been characterised. The latter, the emissions, are still under study, as there is no straightforward regulatory procedure for calculating the spectrum of the waveforms existing in this medium above 9 kHz. Since the mechanisms used to assess these PQ characteristics above 9 kHz are mostly inherited from EMC compatibility testing, so they are adapted to measurements in laboratory conditions but not to field trials on the LV grid. Therefore, a window of opportunity opens for investigating procedures to achieve emission spectrum in the distribution network of electric utilities.

This Master's Thesis is framed within the characterisation of the waveforms of the low voltage GRID, more precisely in the development of the measurement methods necessary to obtain a more detailed characterization of the amplitude of these emissions for the frequency range used by PLC in Europe (CENELEC Band A, up to 90 kHz). The work starts with a comparison of the most relevant published NIE measurement methods, both in the literature and in EMC and PQ standards. Once the strengths and weaknesses of the existing methods are known, the acquired knowledge has been used to design and implement two EMI measurement methods for the characterisation of LV network waveforms. Specifically, a digital implementation of the CISPR 16-1-1 standard has been defined, since it is the normative procedure to verify the CL of the grid. Moreover, a new measurement method, the RMS-A method, has been developed in this work, which allows to calculate the RMS values of the spectrum in the CISPR Band A. In addition, a new EMI method, the Approximate Quasi-Peak (AppQP), has been designed, which provides values similar to those of the digital implementation of CISPR 16-1-1 method, but with less computational complexity and less memory requirements.

2. Context

In the last years, utilities have revamped the control and management of their Low Voltage (LV) distribution networks by incorporating automation functionalities. This evolution has resulted in a modern electricity grid known as Smart Grid (SG), due to the automation of new equipment incorporated or renewed in the grid. According to *Red Eléctrica de España*, the operator of electricity transmission grids in Spain, 'a smart grid concerns an electricity network that can intelligently integrate the behaviour and actions of all users connected to it - generators, consumers and those that do both - in order to ensure a sustainable and economically efficient energy system, with low losses and high levels of quality and security of supply [1].

The development and implementation of SG and associated technologies in Spain has been significant as the IET/290/2012 law, published on 16 February 2012, obliged utilities to replace the electricity meters by smart electricity metering devices (or SM, Smart Meters) compatible with the SG in their LV distribution grids, with a deadline of 31 December 2018 [2].

The smart meters carry out various actions, such as electricity consumption measurements, remote power quality metering and, in some cases, remote management. These data flows are sent via the electricity cable to concentrators located in the electricity transformers of the neighbourhoods, from which the data are transmitted to the control centres of the utilities.

These communications occur on a transmission channel that was not developed for data transmission, a highly changeable and unstable electrical network, whose propagation properties depend on the number and working conditions of the connected equipment. In addition, the cables used in these networks are not always properly shielded, so that electromagnetic effects may generate interference in these communications. For this reason, it is crucial to know how to characterise the changes in the propagation properties that this network may undergo, as well as to measure the electromagnetic emissions produced by the devices connected to it, which are known as EMI (Electromagnetic Interference).

Currently, Non-Intentional Emissions (NIE) generated by the devices connected to the LV grid must not exceed certain threshold levels. These amplitude levels, known as Compatibility Levels (CL), are not constant across the spectrum and decrease as the frequency increases, as regulated in IEC 61000-2-2 [3]–[5]. In addition, the amplitude levels of the CLs above 9 kHz are defined for a specific detector of an EMI measurement method: Quasi-Peak (QP) detector CISPR 16-1-1 standard's method [6].

The Quasi-Peak detector, as defined in CISPR 16-1-1, is based on a heterodyne EMI receiver, whose behaviour to give the values of the corresponding spectra is determined by its electronic components. In addition, the standard governing this detector has quite considerable tolerances in the detector's configuration parameters and, therefore, many different implementations of this measurement method are accepted. Furthermore, ±2 dB of uncertainties (which corresponds to -20% to +26%) in measurements are allowed in the standard. Thus, spectrum measurements made with different meters may not be comparable even if both are meters complying with the standard [6].

Most modern EMI methods are based on digitising the measured signals and applying DFTs (Discrete Fourier Transform) to obtain the signal spectra. These standard-compliant digital implementations have a very high computational cost and require significant memory resources for their execution. Moreover, due to the wide implementation tolerances and the allowed uncertainties in the standard, results from different implementations are not always

comparable. Consequently, a reference digital implementation that demands low computational cost and memory resources is required.

In the last decades, different EMI measurement methods were proposed for laboratory EMC tests, where the reproducibility conditions are ensured as the measurement environment is controlled. Nevertheless, most of these alternative EMI measurement methods are not optimized for LV grid measurements, for the following reasons.

- It is impossible to preserve the reproducibility conditions in a changing medium as it is the LV distribution grid[7].
- The results provided by different EMI methods have a considerable deviation, due to the different configurations allowed by the standard that can be used to compute the spectrum (window overlap in Discrete Fourier Transforms, window shape, measurement length, detectors, etcetera) [7].
- Alternative EMI methods provide results with RMS (Root Mean Square) detectors, which is the most common detector for the rest of EMI methods, therefore, the obtained spectra could not be used to evaluate the emissions levels with respect to CL, as these are in form of QP values.
- There is no link between RMS detector's results and CISPR 16-1-1 QP results; thus, there is no alternative EMI method whit which EMC test could be performed. This fact has been pointed out in different researches and it is an issue that is under discussion in different standardisation working groups (as IEC77A WG9).

For all mentioned reasons, it is important to develop a novel EMI measurement method for the low voltage grid, with a fixed configuration that ensures reproducibility, with low computational cost and few memory resources required and based on a detector that provides results comparable to the Quasi-Peak values of CISPR 16-1-1.

The development of a new normative EMI measurement method is one of the objectives of the European *SupraEMI* consortium. This project, which is funded by the European Union and EURAMET (The European Association of National Metrology Institutes) through EMPIR (European Metrology Programme for Innovation and Research) and Horizon 2020 programmes, is integrated by different European research institutions, metrology organizations and universities, such as the National Physics Laboratory (NPL, UK), *Laboratoire national de métrologie et d'essais* (LNE, France), *Technische Universität Dresden* (TUD, Germany), Federal Institute of Metrology (METAS, Switzerland), *Università degli Studi della Campania 'Luigi Vanvitelli'* (UNICAMPANIA, Italy), University of the Basque Country (UPV/EHU, Spain) and Dutch national metrology institute (VSL, Dutchland). The *Tratamiento de la Señal y Radiocomunicaciones* (TSR) research group, located at Faculty of Engineering in Bilbao, is the member responsible for representing the UPV/EHU in SupraEMI project. As mentioned before, this project aims to create a new normative EMI method, being the working group IEC77A WG9 (Task Force for the redefinition of Annex C of IEC 61000-4-30 (Power Quality Measurements)) of IEC (International Electrotechnical Commission) the principal stakeholder organization [8].

This Master's Thesis is part of the aforementioned European project; therefore, the work presented here is directly linked to the development of a new normative EMI measurement method, which was presented to a IEC Working Group that was formed with this purpose.

3. Aim and scope of the project

In this section of the document, the aim and the scope of the project are explained.

3.1. Aim of the project

As explained in the previous section, the CL of NIE in the LV grid are defined for a specific detector and for an EMI method: the Quasi-Peak detector, implemented as it is described in the CISPR 16-1-1 measurement method. Since this method is defined only for laboratory conditions, with wide tolerances that hinder reproducibility and it requires high computational cost and significant memory resources, new technical solutions are demanded to overcome these limitations. Thus, the aim of this project is the **definition, development and validation of a new measurement method of NIE in the LV grid for the CISPR Band A (2 kHz – 150 kHz)**.

This objective is addressed in two ways: firstly, with the definition of a reference digital implementation of the CISPR 16-1-1 method with fixed parameters; secondly, with the proposal of a new EMI measurement methods.

For the achievement of this objective, the following partial objectives are defined:

- As a first step, and before defining a new measurement method to characterise NIEs, a **comparison of the existing research and normative measurement methods** is made. This will allow the evaluation of the most relevant approaches to characterize the level of different types of NIE in the entire frequency range, for signals with different variation over time. As these methods rely on different requirements (memory and processing resources, initial requirements), this comparison will allow the evaluation of the accuracy vs requirements of its technique.

- For this comparison, test signals with known values are needed as a reference. These test signals must be similar to the signals present in the LV grid, at least in the amplitude values, the spectral shape and the variation over time. As the values of any recording from the grid depend on the data processing algorithms and the calculation procedures applied within each method, the test signals must be based on mathematical models. As the CISPR-16-1-1 is focused on laboratory measurements, these test signals are not defined in the standard. In the literature, there is no technique to develop these test signals, either. Therefore, **a novel method to develop test signals with similar characteristics to the signals present in the LV grid is developed** in this this Master's Thesis. They will contain known voltage levels, spectral shape and variation over time, for the whole frequency range. They will allow a detailed assessment of the accuracy of the measurement methods evaluated in the comparison.

- The CISPR 16-1-1 only defines the characteristics that must fulfil an analogue QP receiver, based on a super-heterodyne architecture. The CISPR TR 16-3 [9] outlines some characteristics that a digital implementation of the CISPR 16-1-1 QP receiver, based on Fourier analysis, should address, but without defining such implementation. In this Master's Thesis, **a reference digital implementation of the CISPR 16-1-1 QP method is defined**, in order to provide a deterministic method, with no configuration tolerances and without reproducibility issues. This way, it allows the deployment of the CISPR 16-1-1 method by third party manufacturers or researchers in a unique unambiguous way.

- Currently there is no measurement method for spectrum calculation that provides RMS results in the CISPR Band A. Therefore, this project **defines and implements an EMI method**

that computes RMS spectra for the 2 to 150 kHz band. This new method is aligned with the standard method for the 2 to 9 kHz band, the IEC 61000-4-7 normative method, since this new method could be considered as an extension of the standard for higher frequencies.

- Last, **a new EMI measurement method which provide QP values is defined, developed and tested**. This method meets specific requirements to be technically innovative with respect to CISPR 16-1-1. The EMI method is based on digitized signals, assessment of the frequency values by means of DFTs and it requires 75 % less computational cost and memory resources than the digital implementation of CISPR 16-1-1. Additionally, the results in the frequency domain must be similar to the QP values of the CISPR 16-1-1. To evaluate the accuracy of the proposed method, results must have a difference lower than 10% compared with the Quasi-Peak results provided by the digital implementation of CISPR 16-1-1 defined in this TFM.

3.2. Scope of the project

As explained above, the new EMI measurement methods described in this Master's Thesis, which have been developed thanks to the participation of the TSR research group (UPV/EHU) in the European research project, are some of the new EMI measurement methods presented in the SupraEMI consortium. The partners of the European project selected these methods as 'preferred option' to be proposed as normative EMI measurement methods to IEC77A WG9, the working group of IEC which is in charge of the redefinition of Annex C of IEC 61000-4-30 standard.

Since the new EMI methods that are developed in this project has a normative nature, and they will be discussed in the SupraEMI consortium and in standardisation bodies, the obtained results will be evaluated by international external experts with an accredited professional experience in this subject.

As all the mentioned working groups are specialised in PQ (Power Quality) metrology, the accuracy of the results is a key aspect in the contributions submitted for discussion. For this reason, an important statistical analysis to evaluate the precision of the results provided by the proposed solution has to be developed in this project.

4. Benefits of the project

In this section the technical and economic benefits of the project are going to be described.

4.1. Technical benefits

In this Master's Thesis, a reference digital implementation of CISPR 16-1-1 and new EMI measurement methods are proposed. These two contributions are going to provide a solution to three issues that nowadays are being discussed in the Power Quality engineering area. The first one is the reproducibility problems of CISPR 16-1-1 methods, due to the large tolerances that are allowed in the standard. This issue will be solved by defining a reference digital implementation of CISPR 16-1-1 with fixed parameters. The other two issues that are going to be resolved with this work are, firstly, the lack of link between QP results of CISPR 16-1-1 and the RMS detectors' spectrum results of the rest of EMI measurement method; and secondly, the possibility of computing Quasi-Peak results with, at least, a 75% less computational cost and memory resources. These last benefits are going to be achieve by the new EMI methods.

4.2. Economic benefits

Having new EMI methods for measuring NIE requiring less computational cost and memory resources than the corresponding normative measurement method (CISPR 16-1-1) could be an opportunity for manufacturers. Since the digital CISPR 16-1-1 has a quite significant computational complexity, implementing this meter on cheap devices is not possible. Therefore, the new method could be used by EMC manufacturers to create inexpensive EMI methods, which could be massively deployed in the LV electricity grid. These devices might attract the interest of electricity distribution operators, which have to ensure the quality of power supply in their respective networks. Moreover, electricity companies could use these methods to perform continuous NIE measurements and to detect emissions above the compatibility level defined by different standardization bodies.

5. Structure of the work

This section summarizes the organisation of the work performed in this Master's Thesis and describes how all the scientific content has been distributed throughout this document. The following diagram contains the main tasks and how they are linked. The shadowed boxes indicate the methods developed in this work.

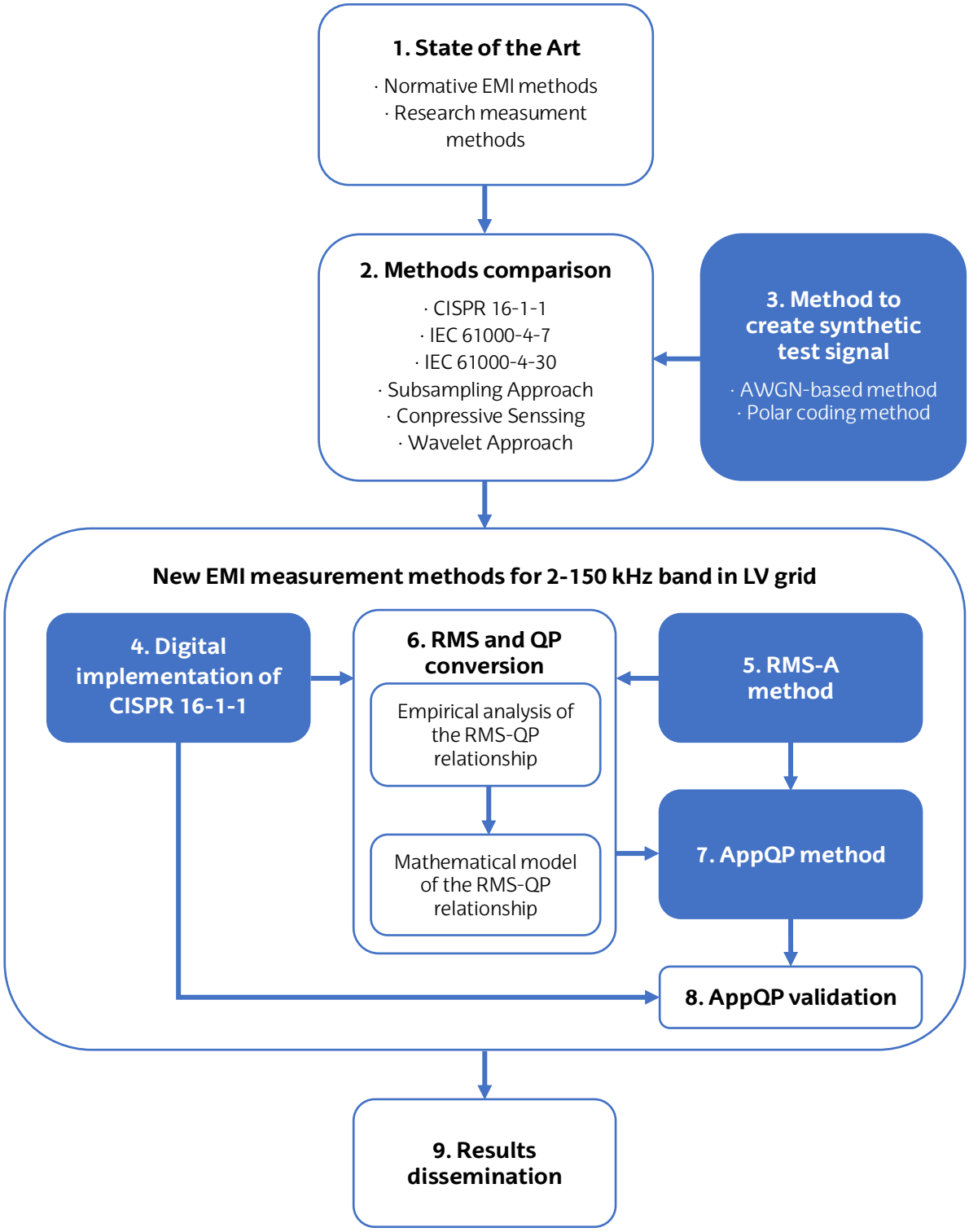

Figure 1: Overview of work's structure

The first task in this Master's thesis, as indicated in **box 1** of *Figure 1*, is the bibliographic compilation of the normative and the published EMI measurement methods, for the subsequent analysis and comparison. The methods are described in *Section 6,* 'State of the art'. The aim of this section is to select and analyze the main EMI measurement methods for their application in the LV grid, both normative and experimental.

Then, the selected methods are compared, as shown in **box 2**. The results of the comparison are described in *Chapter 9*, with particular focus on the accuracy in frequency, amplitude over the spectrum and on the integral values (energy in the spectrum for a given frequency range). The objective of this section is to learn about existing methods in order to be able to create a new one, from the strengths and weaknesses of each method.

The comparison of the methods requires the development of ad-hoc test signals, similar to the complex signals that can be found in the LV distribution grid, which contain different types of conducted noise and emissions and known PSD values. The **box 3** in the figure outlines the methods developed in this Master's Thesis to create synthetic test signals that fulfill the previous conditions. These methods are described in *Section 8.1*. They are based on the AWGN and the polar coding principles to generate synthetic test signals of configurable amplitude, spectral shape and time patterns, as they are calculated theoretically.

The core of this work is the design and development of new measurement methods should adapted to the characteristics of the network emissions. The first method is the CISPR 16-1-1, which is indicated in **box 4** and specified in *Chapter 11*, based on a QP detector and selected by the IEC to assess the Compatibility Levels of LV grid emissions,. A digital implementation of this method, which solves the weakness of the wide tolerances and the reproducibility issues of this method, has been created in this Master's thesis. This method, as it is defined in the standard, requires a high computational burden and controlled laboratory conditions.

Nonetheless, a new measurement method is needed since CISPR 16-1-1 method is not applicable for LV grid conditions and it requires high computational complexity. One of the new measurement methods developed in this project, the RMS-A method, is is described in *Chapter 12* of this work (**box 5** of the figure). This method is based on the IEC 61000-4-7 method, with some modifictions to measure and characterise LV grid NIE. In addition, it needs less computational requirements to compute the spectrum of the waveforms. This method provides RMS spectra.

Once the digital CISPR 16-1-1 and the method for LV grid measurements (RMS-A method) are described, the relation between the QP spectra (CISPR 16-1-1) and the RMS spectra (RMS-A) is analysed, based on empirical tests. This study is performed with 30 LV grid signals in which the behaviour of the method with different input waveforms is analysed. The relationship is used to create a mathematical model, in order to design a conversion procedure from RMS spectra to QP spectra. This relationship is pointed out in **box 6**, and described in detail in *Section 10*.

The relationship between RMS and QP spectra can be used to design a novel method to compute the QP spectra from the RMS spectra (**box 7**). The AppQP method is another new EMI measurement method created in this project, based on applying the mathematical relation between RMS and QP spectra (box 6) to the RMS values obtained with RMS-A (box 5) to obtain QP values with low computational and memory resources. The QP results of this method can be used to evaluate the CL of the emissions present in the LV grid. This EMI method is explained in detail in *Chapter 13.1*.

The AppQP method is evaluated to assess its accuracy, as shown in box 8 and explained in sections *13.2* and *13.3*. For this purpose, 29 LV grid recordings, not included in the definition of the conversion procedure between RMS and QP spectra, are used. Additionally, the computational burden of the AppQP method and the source of the differences between CISPR 16-1-1 and AppQP spectra are studied.

Finally, all the innovative results obtained in this Master's Thesis have been or will be be published and scientific journals and conferences, and presented to standardization bodies, as indicated in box 9. Although this information is described in the *Section 15.2*, a brief summary is given here.

Working groups of the standardisation organisations:

- IEC (International Electrotechnical Commission), working group S77A/WG9: the research described in boxes 2, 4, 5, 6, 7 and 8 have already been presented.
- CENELEC (*Comité Européen de Normalisation Electrotechnique*), WG11: the research in boxes 4 - 8 will be presented in the next meetings.

Papers in reseach journals

- Comparison of the measurement methods (boxes 2 and 3): published in *IEEE Trasactions on Instruments and Measurements* (IEEE TIM) [7].
- Reproducibility issues of CISPR 16-1-1 (boxes 1, 2 and 4): paper in preparation to be subimitted to IEEE TIM.
- Digital implementation of CISPR 16-1-1, AppQP method and the relation between QP and RMS spectra (boxes 4 to 8): paper in preparation to be submitted to IEEE TIM.

Workshops:

- SupraEMI Webinar-Workshop: results obtained in boxes 2 and 3 [10].

6. State of the art

This section provides an overview of the state of the art of the different types of EMI measurement methods that are regulated and/or part of a standard. Additionally, relevant experimental methods proposed in the literature are included.

6.1. CISPR 16-1-1

The CISPR 16-1-1 is a normative EMC (Electromagnetic Compatibility) measurement method that was standardized by the *Comité International Spécial des Perturbations Radioélectriques* (CISPR) [6].

This method is based on a heterodyne EMI method, defined as a black-box approach, whose behaviour is determined by the tolerances of its electronic components. Despite this fact, digital implementations, which are based on DFTs, are allowed to measure emissions as long as the signals are sampled continuously in the analysed measurement interval.

The standard defines five bands to analyse spectra of the emissions: A (9 kHz to 150 kHz), B (0.15 MHz to 30 MHz), C (30 MHz to 300 MHz), D (300 MHz to 1000 MHz) and E (1 GHz to 18 GHz). Nevertheless, the description below is for the band A, since the Approximated Quasi-Peak (the new EMI measuring method proposed in this work) is only applicable from 2 kHz to 150 kHz.

A digital implementation for the band A could be the following:

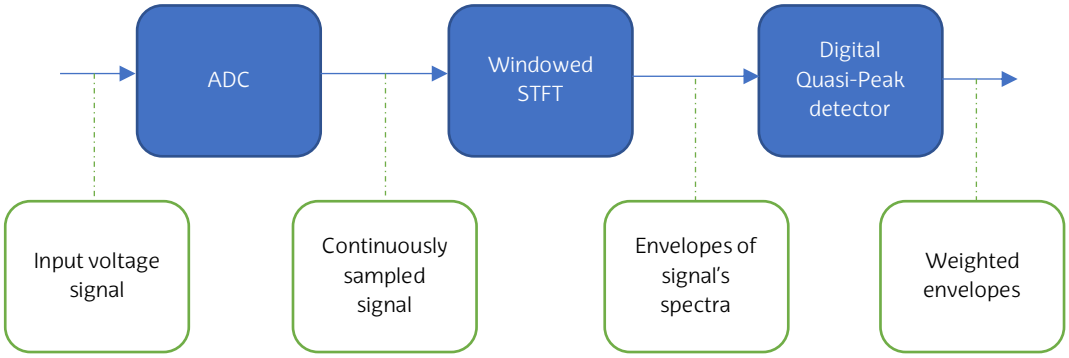

Figure 2: Schematic of a digital implementation of CISPR 16-1-1

First of all, the input voltage signal must be sampled continuously, since the method is gapless. This could be done using an Analog-to-Digital Converter (ADC). Before sampling the analogue signal, a low-pass filter must be applied to remove the frequency components above 150 kHz. This analogue signal processing intends to avoid the aliasing that waveforms above 150 kHz could cause. Following the Nyquist-Shannon theorem, signals should be sampled at a frequency equal to or higher than 300 kHz, which corresponds to twice the maximum frequency to be analysed in the band A of CISPR 16-1-1.

Once the signal has been sampled, a windowed STFT (Short-Time Fourier Transform) is applied to compute the spectra of the signal. For the band A of CISPR 16-1-1, the windows must have a resolution bandwidth (B_6) of 200 Hz at –6 dB, as it is shown in *Figure 3*. In general, the windows used in CISPR 16-1-1 digital implementations are not rectangular. They have variable shape in the time domain, since a rectangular window of 20 ms does not reach the resolution bandwidth required by the standard. Due to the shape of the windows and in order to measure all the energy of the analysed signal, the STFT must have a temporal overlap. However, the standard does not

provide a fixed value for the temporal overlap of windows in DFTs calculations. In contrast, in CISPR 16-1-1, other requirements for the windowing are defined, as the standard provides a mask for the spectral shape of windows. Nevertheless, these limits in the spectral selectivity of EMI methods allows quite considerable tolerances, which is one of the most important deviations between different CISPR 16-1-1 implementations and an important source reproducibility issue.

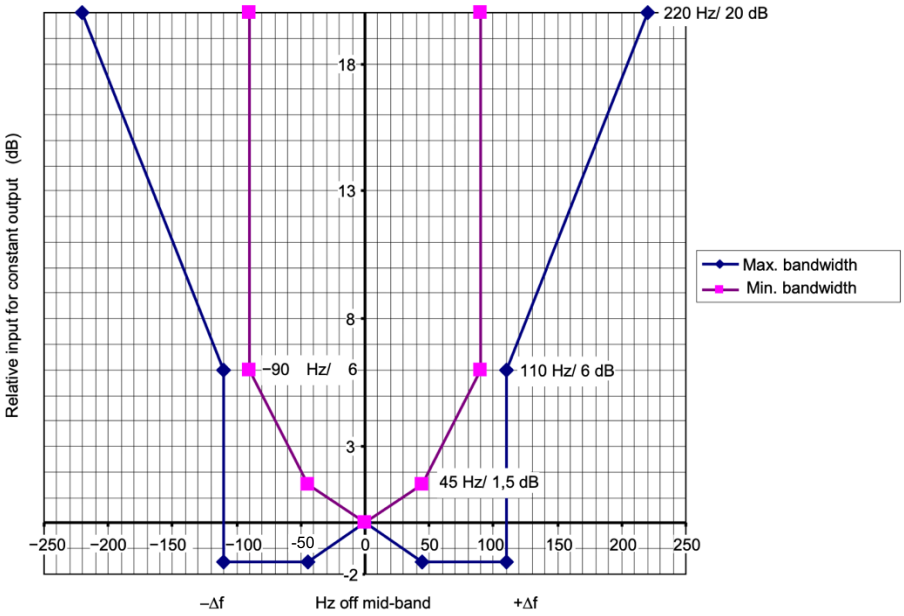

Figure 3: Limits of overall selectivity – Pass-band (Band A) [6]

However, the normative Annex A of CISPR 16-1-1 defines the bandwidths that meters compliant with this standard should have in the frequency response at two different amplitude levels. These bandwidths are set out in section A.2 of the annex as mentioned earlier, which can be calculated using the following mathematical expressions [6]:

$$B_3 = \frac{\left[\sqrt{2} \cdot \sqrt[4]{\sqrt{2}-1}\right] \cdot w_0}{\pi} = 0.361 \cdot w_0 \qquad \text{(Eq.1)}$$

$$B_6 = \frac{\sqrt{2} \cdot w_0}{\pi} = 0.450 \cdot w_0 \qquad \text{(Eq.2)}$$

where:

- B_3 is the bandwidth of overall selectivity at −3 dB,
- B_6 is the bandwidth of overall selectivity at −6 dB,
- w_0 is the angular frequency.

The mentioned bandwidths could be fulfilled using a Lanczos kernel window function with one pair of side-lobes[1].

[1] The Lanczos kernel has been proposed by Siemens AG. Its 3dB and 6dB bandwidths align closely with the theoretical frequency response specified in normative CISPR 16-1-1 Annex A

$$w'[n] = \operatorname{sinc}\left(2\left(\frac{2n}{N-1} - 1\right)\right)\operatorname{sinc}\left(\frac{2n}{N-1} - 1\right) \quad \text{(Eq.3)}$$

where:

- $w'[n]$ is the Lanczos kernel window function,
- N is the number of samples of the discretised window.

After getting the signal's spectrogram, or the envelopes of the spectra, the detectors should be applied to obtain the processed spectrum of the measured emissions. For band A (9 kHz to 150 kHz), CISPR 16-1-1 defines four different detectors: Peak, Average, RMS-Average and Quasi-Peak detectors. The last one is the most important of all detectors in this work, since the Compatibility Levels (CL) for band A and LV grids, under IEC 61000-2-2, are set according to QP meter. This detector is based on a mechanical meter consisting of a Quasi-Peak voltmeter (based on a RC, or Resistor-Capacitor, circuit) followed by a critically damped meter. Both analogue circuits could be digitally simulated using the bilinear approximation. The informative Annex H of CISPR 16-1-1 defines the behaviour of the Quasi-Peak voltmeter providing the time constants for the charging and discharging processes for the electronic passive elements that compose this circuit.

Nevertheless, as Annex H is not a normative annex, manufacturers can choose the value of the parameters indicated in this standard section. Despite that, this annex sets the electrical charge time constant of the RC circuit (τ_c) to 45 ms and the electrical discharge time constant (τ_d) to 500 ms. In the same annex, a mechanical time constant of 160 ms for the critically damped meter is proposed. Once these two electrical circuits have filtered the signal, the output of the detector are the weighted envelopes.

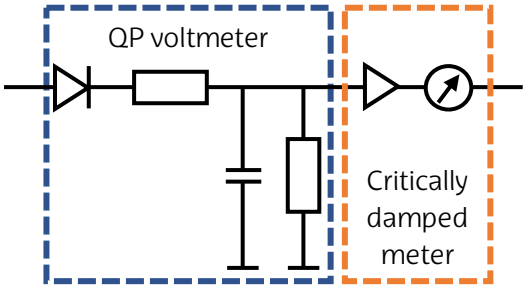

Figure 4: Schematic of Quasi-Peak detector

Finally, the Quasi-Peak values of this detector are the maximum of the weigthed envelopes for each frequency component.

As indicated above, certain aspects and parameters of CISPR 16-1-1 configuration are not strictly fixed, in which tolerances are allowed; mainly, the overlap between spectra to compute the STFT, the spectral shape of windows, and the parameters that define the behaviour of Quasi-Peak detector. Moreover, ±2 dB of uncertainties (– 20% to +26% of uncertainties) in measurements are allowed in the standard. However, as fixed values for these parameters are not given in the standard, or they are given in informative sections (not mandatory), manufacturers could select a different configuration. The reason behind the tolerances is the 'black box' approach used to define the CISPR 16-1-1 methods. Moreover, the normative section of CISPR 16-1-1 defines a calibration process that all implementations of this measurement method must pass, which is based on the analysis of detectors behaviour (i.e., charging and discharging processes of QP voltmeter-RC circuit) using signals of different pulse repetition frequency as input voltage.

Although this calibration test should ensure that all the calibrated implementations have the same behaviour and provide similar spectrum results, it is known that widely differing CISPR 16-1-1 configurations pass the calibration [10]. Therefore, the calibration test defined in the standard does not solve the reproducibility issue of the EMI meters, since methods with different configurations can pass calibration even if their behaviour is not similar.

6.1.1. CISPR TR 16-3 - Technical Report

The CISPR TR 16-3 is the informative technical report of CISPR 16 series in which technical suggestions are proposed to apply the normative standards of the same series. In this document, a guidance to FTT-based receivers (digital implementations) of CISPR 16-1-1 method is provided. However, as CISPR TR 16-3 is not normative, manufacturers of EMI meters do not have to follow the proposals of this report. Nevertheless, this technical guidance may be useful to have a clearer idea of the preferences of standardization working groups to implement FTT-based receivers [9].

In this document, five main proposals for EMI meters complying with CISPR 16-1-1 are made, which could be helpful for the digital implementation of CISPR 16-1-1 band A receivers. The first suggestion is to use DFT (Discrete Fourier Transforms) to compute the spectra of the analysed voltage signal. For the windowing of the signals, when the STFT is applied, three more suggestions are made: To use Gaussian or Kaiser windows, which should strictly have a resolution bandwidth of 200 Hz (B_6) at –6 dB, and the overlap between adjacent windows has to be, at least, of a 90%. Lastly, to avoid the 'picket fence effect' phenomenon, in which the spectral shape of emissions is lost when their frequency does not match the centre frequency of the frequency bins of the DFTs, CISPR TR 16-3 suggests using a FSS (Frequency Step Size) four times lower that B_6. In the case of the band A, the value of the FSS would be 50 Hz. To obtain spectra with a FSS of 50 Hz (spaced between frequency components of the spectra), a 20 ms window has to be applied in the STFT, since the temporal window length is the inverse of the frequency step in the spectrum.

Additionally, CISPR TR 16-3 defines the Gaussian window function that strictly has a bandwidth of 200 Hz at –6 dB [9][2]:

$$w[n]' = \frac{1}{g_c \cdot (N \cdot T_s) \cdot N} e^{(-1/2)\cdot\left[(\pi/\sqrt{2\cdot ln2})\cdot B_{IF}\cdot T_s \cdot n\right]^2}, \qquad n = -\frac{N}{2} \ldots 0 \ldots + \frac{N}{2} \qquad \text{(Eq.4)}$$

where:

- $w[n]'$ is the Gaussian window function,
- g_c is the coherent gain factor. $g_c = 1/N \cdot \sum_{n=0}^{N-1} w[n]'$,
- N is the number of samples of the window. $N = 20\ ms / T_s$,
- T_s is the sampling period of the analysed signal.
- B_{IF} is the IF filters bandwidth at -6 dB (B_6 parameter of CISPR 16-1-1). For the band A (9 kHz to 150 kHz): $B_{IF} = 200\ Hz$.

[2] Rohde&Schwarz use digital Gaussian filters in their CISPR 16 compliant EMI receivers.

6.2. IEC 61000-4-7 – Annex B

The IEC 61000-4-7 is an informative measurement method defined in the Annex B of the standard. This EMI measurement method was defined by the International Electrotechnical Commission (IEC) [11], [12].

This measurement method was initially created to measure the low frequency emissions, above the 40th harmonic of 50 Hz component (2 kHz), but lower than the limit for low frequency band (9 kHz). Moreover, the Compatibility Levels defined in IEC 61000-2-2 from 2 kHz to 9 kHz are set according to this method. Despite that, this method can be applied up to 150 kHz as suggested in Annex C of IEC 61000-4-30, which has already been proposed and carried out in some scientific studies, until a method for this band (9 kHz-150 kHz) is defined. [7], [13].

The implementation of this EMI method could be done as follows:

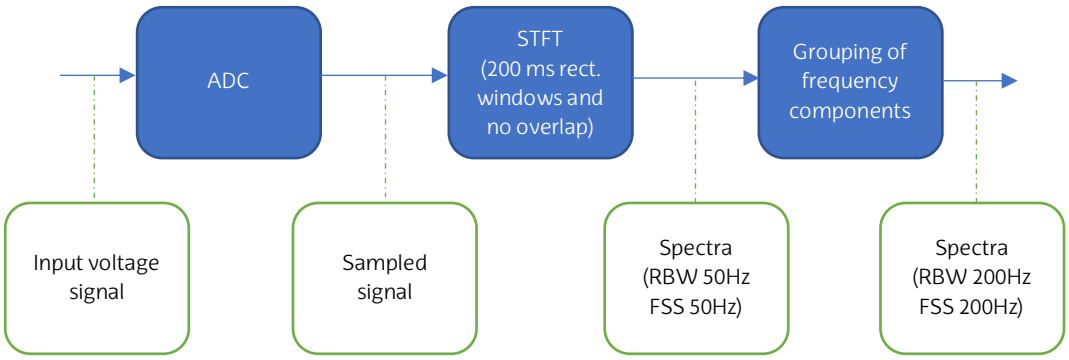

Figure 5: Schematic of IEC 61000-4-7 Annex B measurement method

As described in the previous subsection, before applying this EMI measurement method, the input analogue voltage signal has to be sampled following the Nyquist-Shannon theorem.

Once the signal is digitized, the spectra of the signal are computed applying the STFT. These operations are calculated for temporal periods of 200 ms (10 periods of the 50 Hz component), in which a rectangular window is applied without any overlap between them. As there is no overlap between windows, this is a 'gapless' method; therefore, the measurement must be continuous and gaps between windows are not allowed. Upon the signal has been windowed and STFT have been computed, the spectral output values, the frequency components, have a FSS and a RBW (Resolution Bandwidth) of 5 Hz; since the resolution bandwidth of rectangular windows is defined as the inverse of the time length of them. Nevertheless, these frequency domain values have to have a resolution bandwidth of 200 Hz to be comparable with other EMI measurement method. In order to get the mentioned RBW, 40 frequency components are grouped in the spectrum. To group the frequency components the Root Sum Square (RSS) operation is applied:

$$Y_{B,b} = \sqrt{\sum_{f=b-95\ Hz}^{b+100\ Hz} Y_{Cf}^2} \qquad \text{(Eq.5)}$$

where:

- $Y_{B,b}$ are the grouped values of the STFT with a resolution bandwidth and a frequency step size of 200 Hz,

- b are the frequency bins of the resulting spectra. *b=2.1 kHz, 2.3 kHz, … 149.9 kHz,*
- Y_{Cf} are the output values of the STFT with a RBW and a FSS of 5 Hz,
- f are the frequency components of the output values of the STFT. *f=2.05 kHz, 2.10 kHz, … 149.95 kHz.*

Finally, the resultant spectra could be integrated in a unique spectrum in order to evaluate the waveforms of the measured signals. To carry out this calculations a maximum, minimum or RMS detector could be applied in the time domain of $Y_{B,b}$ for each frequency bin.

6.3. IEC 61000-4-30 – Annex C

The IEC 61000-4-30 is an informative EMI measurement method that is described in the Annex C of this standard, which was deployed by the International Electrotechnical Commission [13].

The aim of this EMI method is to obtain *in situ*, in LV grid measurements, an estimation of the spectrum of the emissions without the complexity of the previously described methods (CISPR 16-1-1 and IEC 61000-4-7), as they have a high computational cost and demand a large amount of memory resources to compute the spectrum of waveforms. Thus, the requirements of this method are not as strict as in other methods. Moreover, to avoid unnecessary calculation, measurements with gaps are allowed, since the aim of this method is to obtain an estimated spectrum.

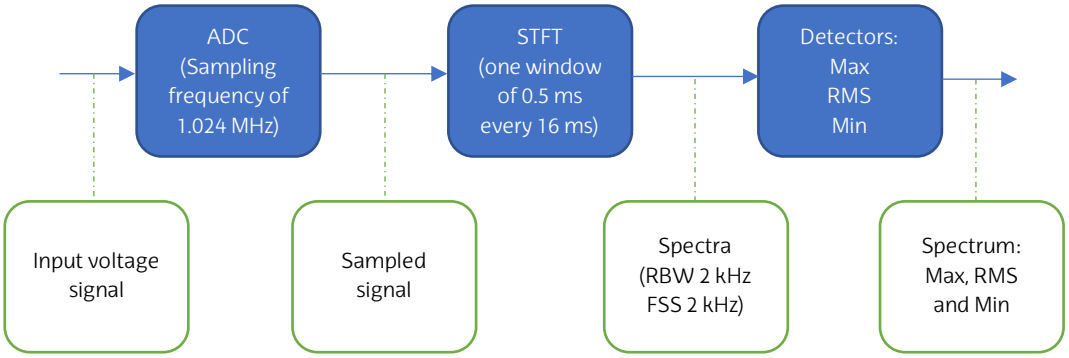

Figure 6: Schematic of IEC 61000-4-30 Annex C measurement method

The input required by the method is a sampled voltage signal, with a sampling frequency of 1.024 MHz. Once the analogue voltage is sampled, a 0.5 ms rectangular window is used to calculate the DFTs, with a 512 samples output. As mentioned before, in order to reduce the needed requirements to execute this method, gaps are allowed in the measurements; thus, the spectra only have to be computed in one-time slot every 32 intervals, which is the same as calculating one spectrum with 0.5 ms length window every 16 ms. After getting the spectra, the first 4 and the last 437 frequency components should be discarded; and the resulting 71 frequency domain samples, which contain the emissions between 8 kHz and 150 kHz, have a resolution bandwidth and a frequency step size of 2 kHz. Since these spectral values do not have a RBW of 200 Hz, the results obtained are not comparable with other EMI methods' results neither with the Compatibility Levels.

Lastly, three detectors could be applied to the obtained spectra in order to get a unique spectrum of the *in situ* measured emissions: maximum, root mean square and minimum.

6.4. Subsampling Approach

The Subsampling Approach is a research EMI measurement method described in the literature, the working principle of which is described in [14]. By the Shannon–Nyquist theorem, a sampling rate of at least 300 kHz is required to measure emissions up to 150 kHz. The subsampling approach is proposed to enable the use of existing power quality instruments limited to lower sampling rates [14]. An analogue filter bank decomposes the input signal into ten bandwidths of 15 kHz, which requires a minimum sampling rate of only 30 kHz. The ten bandlimited, subsampled signals are processed by calculating the DFT of consecutive rectangular 5-ms windows with a correction of the baseband frequencies to reflect the original components of the respective bands.

6.5. Compressive Sensing

In this Master's Thesis, two experimental methods based on compressive sensing, which have been published in scientific journals, will be analysed.

The underlying assumption of compressive sensing is the sparsity of emissions in the frequency domain, meaning that they are well described by a small subset of the 740 frequency bins from 2 to 150 kHz. This subset of components is estimated from 2 kHz bins, and the remaining components are assumed to be zero. A key advantage of compressive sensing is the possibility to decrease the frequency step from 2 kHz to 200 Hz while maintaining a window length of 0.5 ms.

6.5.1. OMP Compressive Sensing

A method that uses orthogonal matching pursuit (OMP) as a compressive sensing algorithm has been proposed [15]. The method first processes the input signal with a DFT of consecutive rectangular 0.5 ms windows to obtain 2 kHz bins. The compressive sensing is based on a multiple measurement vector model to reduce computation time, whereby a sparse estimation is computed simultaneously for a 200 ms block of 400 spectra. For all 400 spectra, the same number of 200 Hz frequency bins is estimated, i.e., the same sparsity is assumed, and it must be estimated in advance.

6.5.2. Bayesian Compressive Sensing

In the same way as OMP compressive sensing, this method has no gaps between 0.5 ms measurement windows and also uses a multiple measurement vector model but aims to improve accuracy over OMP by employing sparse Bayesian learning, which determines the joint sparsity automatically [16]. The parameters of the likelihood function and convergence threshold of the iterative algorithm have been set as specified in [16].

6.6. Wavelet approach

Finally, this project will analyse the Wavelet approach research EMI method described in [17].

An alternative to a DFT-based method is wavelet packet decomposition (WPD) of the digitized signal [17]. The WPD recursively filters and downsamples the input signal until a bandwidth of 200 Hz is achieved across the spectrum from 2 to 150 kHz. The filters are as flat as possible, designed to capture 100% of the energy of the frequencies in each bin. The result is a critically sampled signal for each frequency bin, and the amplitude value per measurement interval is calculated by taking the root-mean-square (rms) of the samples. The measurement interval is a rectangular window with a length of ten cycles synchronized to the power system frequency.

7. Description of the requirements

In order to achieve the objectives set out in *Section 3.1*, certain requirements have to be defined. These must be met by the digital implementation of CISPR 16-1-1 and the new NIE measurement method, whose results shall be comparable to those of CISPR 16-1-1. For this purpose, certain requirements will be set, following the requests, recommendations, and suggestions of the State of the Art described in this document. Nevertheless, the requirements that have to fulfil both EMI methods are going to be different. On the one hand, the purpose of the digital CISPR 16-1-1 is to deploy a fixed implementation of this normative method that can avoid the uncertainty issues due to the wide tolerances defined in the standard, but without addressing the reduction of the computational and storage requirements. On the other hand, the aim of one of the new EMI method is to define a method with 75% less computational cost and memory resources and an error in accuracy bellow the 10%, compared with the results provided by the digital implementation of CISPR 16-1-1.

7.1. Requirements for the digital implementation of CISPR 16-1-1

The requirements to be met by the digital implementation of the CISPR 16-1-1 standard will focus on the parameters need to define a specific behaviour of this measurement method, which must meet the tolerances allowed by the normative sections of the CISPR 16-1-1 standard. The fixed parameters were chosen following the guidance of the informative annexes of the same standard and the suggestions of CIRPR TR 16-3 for Fast Fourier Transform (FFT) based meters. These requirements are listed below:

a. Window function: Two different windows functions could be chosen to compute the windowed DFTs. The first option is a window that meets the information of A.2 section of CISPR 16-1-1. The other window function is defined in the Technical Report of CISPR 16 series (CISPR TR 16-3), and based on a Gaussian filter. An example of the first option was implemented by Siemens AG and provided to the consortium of the SupraEMI project, and the second option is used in the Rohde&Schwarz manufacture's meters.

b. Frequency step size: In order to avoid the 'picket fence effect', and following the guidance of CISPR TR 16-3, a 50 Hz frequency step size is selected, which implies that there will be samples in the spectrum every 50 Hz.

c. Temporal window's length: Since the window length is the inverse of the frequency step size a value of 20 ms is used.

d. Overlap: To ensure that all the impulsive waveforms are considered by the EMI method, a high grade of overlap between DFT windows has to be used. CISPR TR 16-3 proposes at least an overlap of the 90%. Nevertheless, in order to guarantee higher accuracy, the 95% of overlap might be also used. Therefore, both values (90% and 95%) could be used in CISPR 16-1-1 implementations.

e. QP detector's parameters: As mentioned in *Chapter 6.1*, the behaviour of the Quasi-Peak detector is based on the performance of an RC circuit and a critically damped meter. In the non-normative Annex H of CISPR 16-1-1 the electrical time constants that govern both analogue circuits are proposed; therefore, these values will be used in the digital implementation of this method.

Parameter	Value
Detector electrical charge time constant (RC circuit)	45 ms
Detector electrical discharge time constant (RC circuit)	500 ms
Mechanical time constant of critically damped indicating instrument	160 ms

Table 1: Time constants of QP detector [6]

7.2. Requirements for the new EMI measurement method

In order to fulfil the objectives of this project, certain requirements for the new EMI method have to be defined. Nonetheless, these requirements are primarily aimed at reducing the computational complexity and memory resources of the new method by 75%, compared to CISPR 16-1-1, ensuring at the same time that the difference in results between the two methods is equal to or less than 10%. Hence, some requirements will be less demanding than for CISPR 16-1-1. The requirements are the following:

a. Temporal window's length: A similar window length than the digital implementation of CISPR 16-1-1 is selected: 20 ms.

b. Overlap: In order to reduce the number of DFT operations, the overlap between consecutive FFT windows will be 0%.

c. Gaps in measurements: The new method has to perform continuous measurements to capture all the waveforms' energy; therefore, no gaps are allowed in this method. Moreover, this NIE measurement method will be gapless.

d. Window function: Since the overlap is defined to be 0% and all the energy of the emissions in LV grid have to be recorded and analysed, a rectangular window function has to be used.

e. Measurement time: The results of the new method shall be provided in aggregation periods, as defined in the IEC 61000-4-30 standard: 3 seconds, 10 minutes and 2 hours [13].

f. Frequency step size: In order to reduce the required memory resources, the number of the frequency samples to be stored are reduced , to a frequency step size of 100 Hz.

g. Data to be saved: So as to analyse, in a post-processing stage, the time evolution and the characteristics of the waveforms detected in the LV grid, the method must store in memory the spectrogram for at least one of the aggregation times defined in section *e* of this list.

8. Methodology

In this section, the methodology used to deploy new EMI measurement methods and calculate the results are explained. Therefore, all the necessary steps needed for those purposes are described in this chapter. In addition, this section presents the mathematical model developed in this work for the comparison of existing EMI measurement methods in standards and literature.

The mathematical model to compare exiting EMI methods is based on generating synthetic signals from Additive White Gaussian Noise (AWGN) and polar coding, in which the Power Spectral Density (PSD) is known. This model has been accepted for publication in the scientific journal *"Comparison of Measurement Methods for 2-150-kHz Conducted Emissions in Power Networks"* [7]. Nonetheless, the procedure to generate these synthetic signals and their corresponding theoretical levels is explained in detail in this section.

The Approximated Quasi-Peak (AppQP) is one of the new EMI method developed in this Master's Thesis, whose implementation is described in *13*. In the current section, the method's bases and the methodology followed to obtain this empirical method are described

8.1. Synthetic signals for the comparison of the existing EMI measurement methods

A pivotal role in comparing measurement methods is played by the test signals employed in the analysis of those methods. Some previous studies were based on simple single-frequency tones of constant or variable amplitude [18], [19], which is appropriate for assessing the amplitude accuracy of specific frequencies in laboratory conditions, but far from being a faithful representation of the distortion that can be found in the power networks. More complex signals, including representative grid recordings have been utilized [19], [20], but these cannot be used to calculate the accuracy of the methods, since their true frequency content is unknown.

The present study aims at a deeper and wider analysis, employing specifically designed test signals with theoretical amplitude reference values that are representative of the frequency content of the grid. For this purpose, a set of synthesized test signals has been developed, where centre frequency, bandwidth and amplitude of emissions can be adjusted to be similar to grid recordings. The test signals are defined in terms of PSD, from which reference levels for spectral amplitudes can be calculated according to the required bandwidth. In this way, the following features of the candidate methods can be studied: amplitude accuracy for signals of different bandwidth (from single-frequency to broadband signals), frequency resolution (both frequency accuracy and discrimination of signals close in frequency), and impact of method basis (DFT-based, wavelet approach, subsampling or compressive sensing). The development of these complex and configurable signals is based on the identification and characterization of the types of emission in the low voltage (LV) grid [21], [22].

For the generation of synthetic signals, two different methods are proposed, which are complementary. The NIE waveforms caused by the equipment and goods connected to the LV grid are created through AWGN-based signals, which are filtered out to achieve the desired spectral shape. The emissions of Power Line Communications (PLC) transmissions, which are generated by the smart meters installed in the grid, are synthetically created from polar coding, since these communications are based on Orthogonal Frequency Division Multiplexing (OFDM).

Once the synthetic signals are created, the outputs of both methods can be combined by summing the two types of signals in the time domain, and also their corresponding theoretical PSD values.

8.1.1. Principles of AWGN-based synthetic signals

This method to create synthetic signals takes advantage of certain characteristics of AWGN. These types of waveforms have an intrinsic random amplitude variability, in time and in frequency; however, all the power in the spectrum is distributed homogenously. Therefore, the level of the spectra of these emissions is constant. Afterwards, the amplitude of the noise can be modulated with a sinewave, or the modulus of a sinewave, in the time domain to achieve periodic variability. To generate the desired spectral shape of the, first, a filter is designed with the desired spectral shape for the waveform. Subsequently, the Gaussian noise is filtered, acquiring the required pattern in the frequency domain. This is possible since energy in Gaussian noise is distributed quasi-constantly over the whole spectrum; hence, when the AWGN is filtered it takes the spectral shape of the impulse response of the filter.

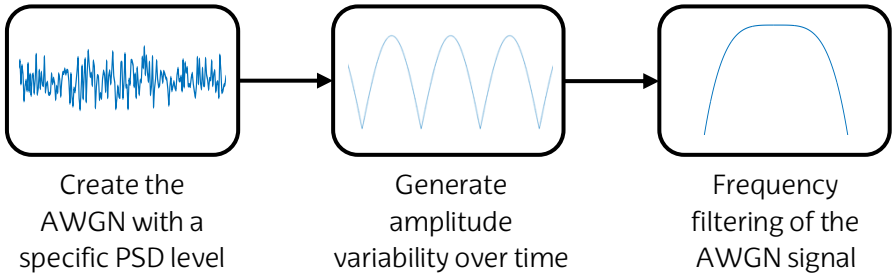

Figure 7: Overview of the method to generate synthetic signals from AWGN

To compute the theoretical spectrum of the signals created with this method, firstly, the level of AWGN must be calculated. As mentioned above, the power is distributed quasi-homogenously along the entire spectrum. Moreover, the sampling frequency (f_s) sets the band-limit of the waveforms, as described in Nyquist-Shannon sampling theorem, where all the power of the signals is confined. Hence, reference values (theoretical values) of PSD ($G_x(f)$) are calculated as follows:

$$G_x(f) = \frac{P_{AWGN}}{2 \cdot f_{max}} = \frac{P_{AWGN}}{f_s}, \qquad -f_{max} \leq f \leq f_{max} \qquad \text{(Eq.6)}$$

where:

- $G_x(f)$ is the reference value of PSD for AWGN-based signals,
- f is the frequency axis of waveforms spectrum,
- P_{AWGN} is the power of the AWGN signal,
- f_{max} is the maximum frequency of a sampled signal, where $f_{max}=f_s/2$,
- f_s is the sampling frequency of the signal.

Nonetheless, if the power of the AWGN has to be chosen to have a specific amplitude in the spectrum, the following formula can be applied.

$$P_{AWGN} = 10^{(A_s - 120 + 20 \cdot \log_{10}(\sqrt{Z}))/10} \quad \text{(Eq.7)}$$

where:

- P_{AWGN} is the power of the AWGN signal,
- A_s is the amplitude (in dBµV) of the noise in the spectrum,
- Z is the impedance of system, which must be 50Ω.

The Gaussian noise is shaped in the form of emissions similar to those in LV grid by filters specifically designed to that purpose. These are used to filter the original AWGN signal and obtain the desired spectral shape that replicates the emissions. The frequency responses of the resultant filters ($H_{filter}(f)$) are used to obtain the reference values of the LV-like signal.

If the signal requires a more significant amplitude variability over the time, signal's amplitude can be varied with a modulating signal, for example, with a sinewave or the modulus of the sinewave functions. The reference values are obtained by multiplying the PSD of the filtered signal by the square of the effective amplitude of the modulating signal.

$$G_y(f) = G_x(f) \cdot \left|H_{filter}(f)\right|^2 \cdot A_{eff}^2 \quad \text{(Eq.8)}$$

where:

- $G_y(f)$ is the reference value of the PSD of the resulting signal,
- $G_x(f)$ is the reference value of PSD of the original AWGN signals,
- H_{filter} is the frequency response of the filter,
- A_{eff} is the effective amplitude of the modulating signal in the time domain.

This procedure has been implemented in a MATLAB function, which requires the inputs listed below:

1. Parameters to generate the AWGN:
    a. Amplitude of the waveform in the spectrum: The required spectral amplitude of the original AWGN signal for a resolution bandwidth of 200 Hz (in dBµV).
    b. Duration of the signal: Duration of the signal to be produced (in s).
    c. Sampling frequency: The sampling frequency of the resulting signal (in MHz).
2. Parameter to generate the amplitude variability over time:
    a. Amplitude variability: The variability in amplitude over time that the resulting signal must have (in %).
    b. Amplitude variability type: The variability is modelled with the sinewave or modulus of sinewave functions.

c. Amplitude variability period: The period of variability that the function modulating the AWGN must have (in s).

3. Parameter of the filter to generate the spectral shape of the emission:

   a. Impulse response type: The type of impulse response the filter should have (FIR or IIR).

   b. Filter's design method: The method used to design the filter (Butterworth, Chebyshev, Elliptical, ...)

   c. Central frequency of the filter: Centre frequency of the filter (in kHz).

   d. Passband of the filter: Bandwidth at –3 dB that the filter must have (in Hz).

   e. Stopband: The bandwidth that the filter should have inside the stop band (in kHz).

   f. Stopband attenuation: Minimum attenuation to be guaranteed outside the stopband (in dB).

This function, which generates synthetic signals from AWGN, returns the following parameters:

1. The signal in the time domain:

   a. An array containing the signal: It returns an array containing the synthetic signal, in the time domain, in volts; as the values measured in the LV grid.

   b. Sampling period: The period between samples of the synthetic signal (in s).

2. The expected PSD result in the frequency domain:

   a. An array containing the reference values: This array contains the theoretical values of the PSD (in dBµV).

   b. An array with the frequency axis: This variable contains the frequency values associated with the reference values (in kHz).

8.1.2. Principles of synthetic signals based on polar coding

The second method for generating synthetic signals is based on polar coding, whose PSD is known [23]. The frequency response of polar coding is a sinc function, and its centre frequency is given by the carrier signal. Furthermore, the width of the main lobe of this function, in the

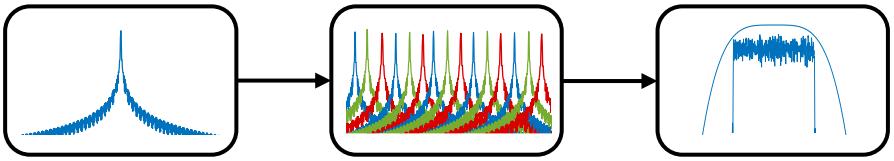

Figure 8: Overview of the method to generate synthetic PLC bursts from polar coding

frequency domain, is inversely proportional to the width of the pulse in the time domain. Multiple sincs have to be generated in order to create the required subcarriers of PRIME (PoweRline Intelligent Metering Evolution) PLC communication technology's OFMD schema. Afterwards, all the subcarriers must be combined and the resulting signal bandpass filtered, so as to remove spurious emissions outside the communication band.

To generate this type of signal, a pseudo-random sequence of bits is created and encoded using the polar coding. Thus, the generated sequence is composed of negative and positive amplitude values of equal magnitud. Once the polar code is applied, the signal is multiplied by a carrier which defines the centre frequency of the PSD. The reference values for these signals are given by the polar code:

$$G_x(f) = \frac{1}{4 \cdot T_p \cdot Z} \cdot \left| A_p \cdot T_p \cdot sinc\left(T_p \cdot (f - f_c)\right)\right|^2 \quad \text{(Eq.9)}$$

where:

- $G_x(f)$ is the reference value of PSD for signals based on polar coding,
- f is the frequency axis of waveforms spectrum,
- T_p the temporal length of each pulse of the polar code,
- Z is the impedance of system, which must be 50Ω,
- A_p is the absolute amplitude of the polar coding pulses,
- f_c is the carrier frequency.

However, if the amplitude of the pulses has to be chosen so that the sinc in the spectrum has a specific amplitude, the following formula can be applied.

$$A_p = 10^{(A_s - 120 + 20 \cdot \log_{10}(\sqrt{Z}))/10} \cdot \frac{4}{T_p \cdot RBW} \quad \text{(Eq.10)}$$

where:

- A_p is the absolute amplitude of the polar coding pulses in the temporal domain,
- A_s is the maximum amplitude (in dBμV) of the sinc in the spectrum,
- Z is the impedance of system, which must be 50Ω,
- T_p the temporal length of each pulse of the polar code,
- RBW is the resolution bandwidth of the method used to measure the emission.

Based on the signals generated from the polar code, PLC bursts are generated following the guidelines of the PRIME PLC standards, regulated in [24]. The information needed to create PRIME PLC bursts is as follows:

PRIME v.1.3.6 configuration	
Start frequency	41.992 kHz
Final frequency	88.867 kHz
Number of subcarriers	97 (96 data + 1 pilot)
Subcarrier spacing	488.28125 Hz
Symbol duration	2240 μs

Table 2: Information of PRIME v.1.3.6 configuration [24]

To achieve this, each subcarrier of the OFDM modulation that composes the PLC emissions will be generated with the procedure described above. The PSD's reference values corresponding to the PLC bursts will be calculated by combining the reference values of each subcarrier. Finally, the complete OFDM signal is filtered to remove the side lobes of the subcarriers. The resulting reference values of PSD can be calculated as follows:

$$G_y(f) = \sum_{i=1}^{N} G_{x,i}(f) \cdot \left|H_{filter}(f)\right|^2 \quad \text{(Eq.11)}$$

where:

- $G_y(f)$ is the reference value of the PSD of the resulting signal,
- $G_{x,i}(f)$ is the reference value of PSD of each subcarrier of OFDM schema,
- N is the number of subcarriers in PRIME PLC. $N=97$,
- H_{filter} is the frequency response of the filter.

This method to generate synthetic PLC bursts, as the AWGN-based procedure described previously, has been implemented in a MATLAB function. This code requires the following inputs in order to generate the synthetic signals:

1. Parameters to generate each burst of PRIME PLC:
    a. Amplitude of the burst in the spectrum: The required spectral amplitude of the PLC bust for a resolution bandwidth of 200 Hz (in dBμV).
    b. Duration of the burst: Duration of the PRIME PLC burst (in s).
    c. Sampling frequency: The sampling frequency of the resulting signal (in MHz).
    d. Central frequency of the emission: The frequency where the emission has to be centred (in kHz).
2. Parameter of the filter to remove the sidelobes generated by the OFDM:
    a. Impulse response type: The type of impulse response the filter should have (FIR or IIR).
    b. Filter's design method: The method used to design the filter (Butterworth, Chebyshev, Elliptical, ...)

c. Central frequency of the filter: Centre frequency of the filter (in kHz).

d. Passband of the filter: Bandwidth at −3 dB that the filter must have (in kHz).

e. Stopband: The bandwidth that the filter should have inside the stop band (in kHz).

f. Stopband attenuation: Minimum attenuation to be guaranteed outside the stopband (in dB).

This function, which generates synthetic PLC bursts signals, returns the following parameters:

1. The signal in the time domain

   a. An array containing the signal: It returns an array containing the synthetic signal, in the time domain, in volts; as the values measured in the LV grid.

   b. Sampling period: The period between samples of the synthetic signal (in s).

2. The expected PSD result in the frequency domain:

   a. An array containing the reference values: This array contains the theoretical values of the PSD (in dBµV).

   b. An array with the frequency axis: This variable contains the frequency values associated with the reference values (in kHz).

8.1.3. Creation of a synthetic signal to assess spectral accuracy

As mentioned before, in this Master's Thesis a comparison of existing measurement methods has been carried out. In order to evaluate the frequency accuracy of these methods, a synthetic signal containing only AWGN-based emissions has been generated. The signal described below, whose name is 'Intern-Syn', is composed of 8 different emissions.

A base waveform has been defined to generate this synthetic signal,, which will be repeated 8 times over the spectrum with different amplitudes and frequencies. The name of this base waveform is 'Tonal-1' and the parameters to generate it are as follows:

Parameters to generate the waveform 'Tonal-1'		
Parameters for the AWGN	Duration of the signal	5.00 s
	Sampling frequency	1.00 MHz
Parameters for the amplitude modulation	Amplitude modulation	90.00 %
	Modulation type	Modulus of sinewave function
	Period of variability	10.00 ms
Characteristics of the filter	Impulse response type	IIR - Bandpass
	Design method	Butterworth
	Passband	0.14 kHz
	Stopband	0.30 kHz
	Attenuation of the passband	10 dB

Table 3: Parameters to generate the waveform 'Tonal-1'

Once the base waveform has been described, the level and centre frequency of all emissions are defined.

'Interm-Syn' signal		
Waveform	Central frequency (kHz)	Level for 200 Hz BW (dBµV)
Tonal-1	33.85	69.00
Tonal-1	34.15	70.00
Tonal-1	34.55	65.50
Tonal-1	34.85	60.00
Tonal-1	40.15	60.00
Tonal-1	41.95	62.00
Tonal-1	43.35	64.00
Tonal-1	44.55	60.00

Table 4: Composition of 'Interm-Sym' signal

All the emissions described above are combined in the 'Interm-Sym' signal. The reference values of the PSD are as follows:

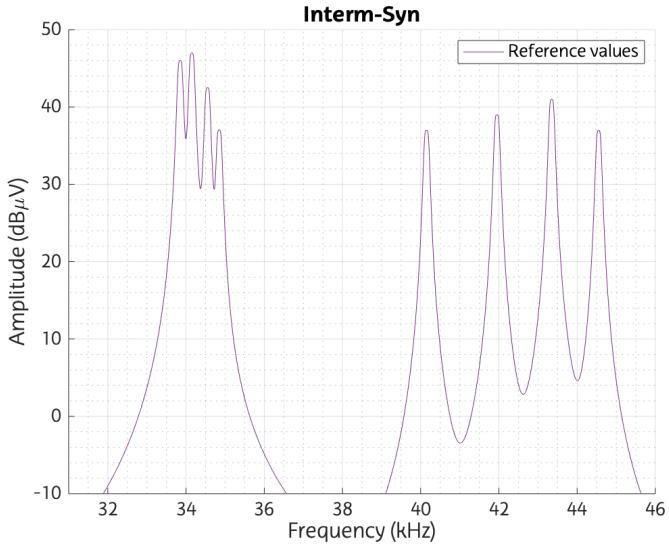

Figure 9: Reference values of 'Interm-Syn' signal for a unit bandwidth (1 Hz)

8.1.4. Generation of a synthetic signal from field measurements

In order to make a more detailed study of the existing measurement methods, a more complex signal has been created. This synthetic signal is based on a recording in the LV grid, in which the individual emissions have been reproduced and combined into a unique synthetic test signal. Among the waveforms included in the synthetic signal are: coloured noise, narrowband Non-Intentional Emissions, broadband NIEs and power line communication bursts.

The recording to be reproduced was labelled as 'AXRX4F3', which was measured by the TSR research group In the LV grid. The signal has the following spectrogram and spectrum, which were used to characterise its emissions and replicate them in the synthetic signal.

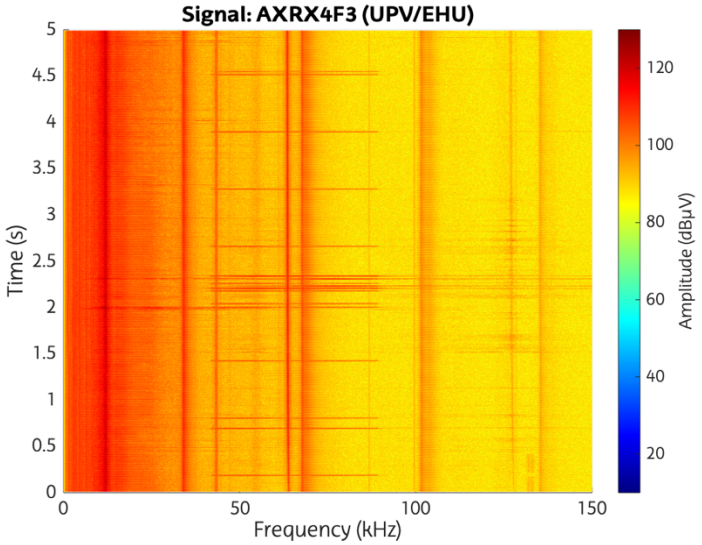

Figure 10: Spectrogram of 'AXRX4F3' signal recorded by TSR (UPV/EHU)

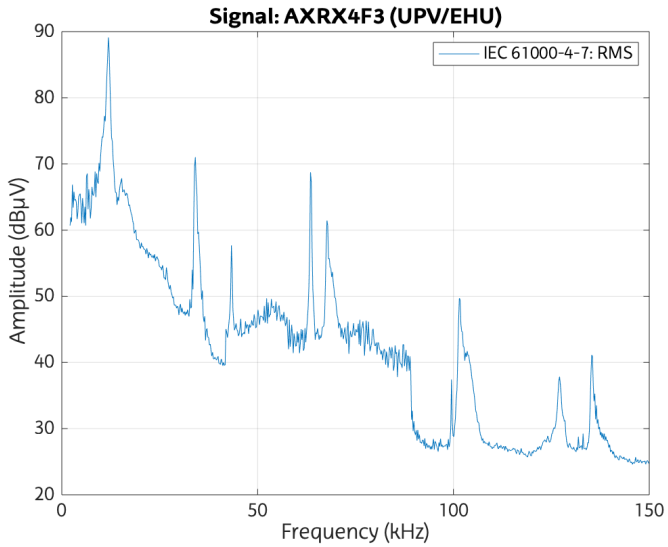

Figure 11: Spectrum computed with IEC 61000-4-7 (RMS detector) for 'AXRX4F3' signal recorded by TSR (UPV/EHU)

The corresponding synthetic composed signal was labelled as 'AXRX4F3-Syn', a name that refers to the signal recorded in the LV grid to be replicated. Although both signals have a similar spectrum and spectrogram, the PSD reference values of the synthetic signal are known. This aspect will allow the assessment of the accuracy of existing measurement methods.

As with the simple synthetic signal 'Interm-Syn', for the complex synthetic signal 'AXRX4F3-Syn' being described in this section, the characteristics of the base emissions that will make up the resulting signal are described.

The tonal emissions and harmonics of the grid to be contained in the synthetic signal shall be generated from AWGN. Four base emissions have been identified, one of which is 'Tonal-1' described in *Table 3*. The characteristics needed to generate them are described below.

Parameters to generate the waveform 'Tonal-2'		
Parameters for the AWGN	Duration of the signal	5.00 s
	Sampling frequency	1.00 MHz
Parameters for the amplitude modulation	Amplitude modulation	90.00 %
	Modulation type	Modulus of sinewave function
	Period of variability	10.00 ms
Characteristics of the filter	Impulse response type	IIR - Bandpass
	Design method	Butterworth
	Passband	0.30 kHz
	Stopband	1.00 kHz
	Attenuation of the passband	10 dB

Table 5: Parameters to generate the waveform 'Tonal-2'

Parameters to generate the waveform 'Tonal-3'		
Parameters for the AWGN	Duration of the signal	5.00 s
	Sampling frequency	1.00 MHz
Parameters for the amplitude modulation	Amplitude modulation	90.00 %
	Modulation type	Modulus of sinewave function
	Period of variability	35.00 ms
Characteristics of the filter	Impulse response type	IIR - Bandpass
	Design method	Butterworth
	Passband	1.00 kHz
	Stopband	2.00 kHz
	Attenuation of the passband	10 dB

Table 6: Parameters to generate the waveform 'Tonal-3'

Parameters to generate the waveform 'Tonal-4'		
Parameters for the AWGN	Duration of the signal	5.00 s
	Sampling frequency	1.00 MHz
Parameters for the amplitude modulation	Amplitude modulation	90.00 %
	Modulation type	Sinewave function
	Period of variability	240.00 ms
Characteristics of the filter	Impulse response type	IIR - Bandpass
	Design method	Butterworth
	Passband	2.00 kHz
	Stopband	6.00 kHz
	Attenuation of the passband	10 dB

Table 7: Parameters to generate the waveform 'Tonal-4'

The basic waveforms mentioned above are grouped into different harmonics and tones, in order to reproduce the patterns of the original signal 'AXRX4F3'. Four groups of waveforms were defined, and their characteristics are described below.

'Harmonics-1' waveforms group		
Waveform	Central frequency (kHz)	Level for 200 Hz BW (dBµV)
Tonal-1	33.85	69.00
Tonal-2	67.70	61.00
Tonal-2	101.55	50.00
Tonal-2	135.40	42.00

Table 8: Composition of 'Harmonics-1' waveforms group

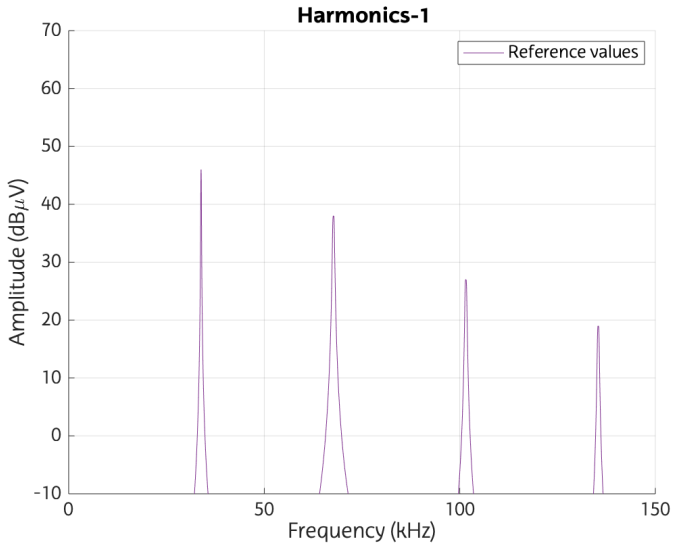

Figure 12: Reference values of 'Harmonics-1' waveforms group for a unit bandwidth (1 Hz)

'Harmonics-2' waveforms group		
Waveform	Central frequency (kHz)	Level for 200 Hz BW (dBµV)
Tonal-2	34.15	70.00
Tonal-2	68.30	56.00
Tonal-2	102.45	42.50
Tonal-2	136.60	33.5

Table 9: Composition of 'Harmonics-2' waveforms group

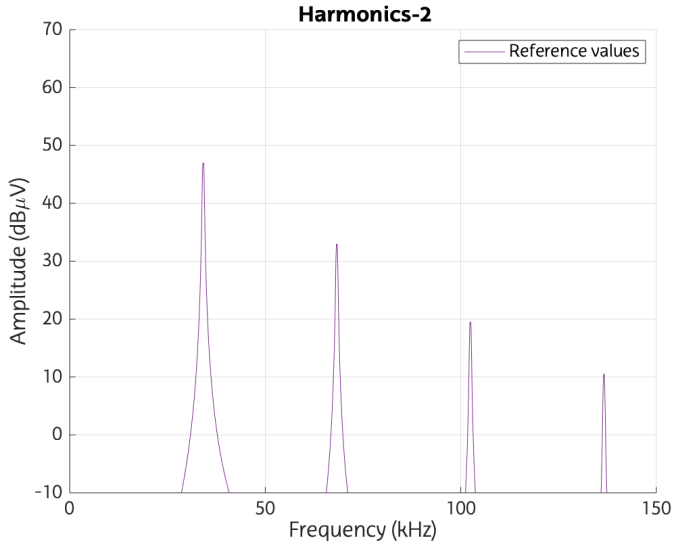

Figure 13: Reference values of 'Harmonics-2' waveforms group for a unit bandwidth (1 Hz)

'Harmonics-3' waveforms group		
Waveform	Central frequency (kHz)	Level for 200 Hz BW (dBµV)
Tonal-2	34.55	65.50
Tonal-4	69.10	54.00
Tonal-4	103.65	42.00

Table 10: Composition of 'Harmonics-3' waveforms group

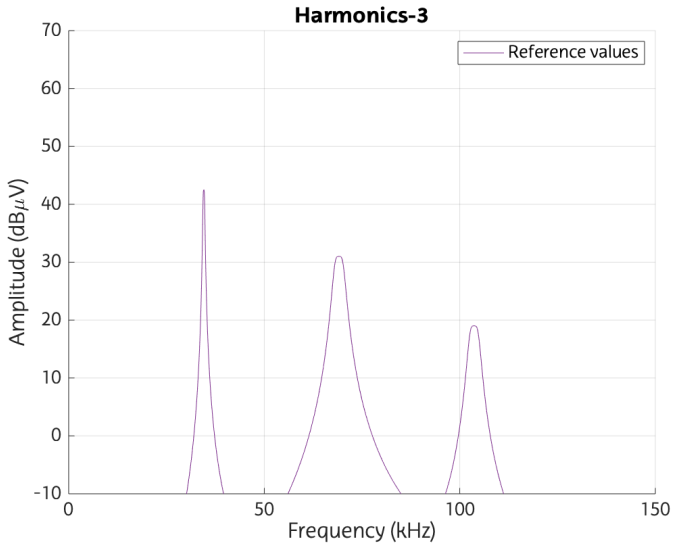

Figure 14: Reference values of 'Harmonics-3' waveforms group for a unit bandwidth (1 Hz)

'Tones' waveforms group		
Waveform	Central frequency (kHz)	Level for 200 Hz BW (dBµV)
Tonal-1	11.93	89.00
Tonal-3	34.85	60.00
Tonal-1	41.95	46.00
Tonal-2	43.35	58.00
Tonal-1	63.57	70.00
Tonal-2	102.25	45.00
Tonal-2	136.05	36.00

Table 11: Composition of 'Tones' waveforms group

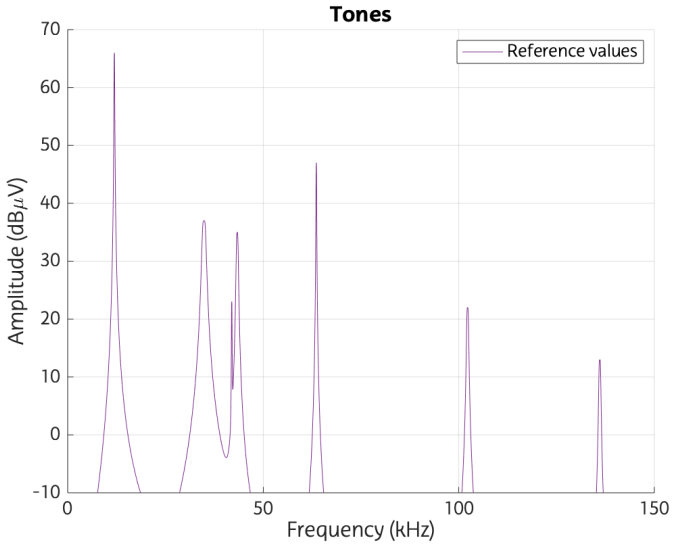

Figure 15: Reference values of 'Tones' waveforms group for a unit bandwidth (1 Hz)

The same technique (AWGN-based waveforms) is used to generate the noise floor of the signal. However, this emission is generated by two waveforms, one of which is unfiltered. This is because the coloured noise is not an emission concentrated in a single band, since it must cover the whole spectrum, and it does not require additional amplitude modulation over time. The parameters for generating this emission are as follows.

Parameters to generate the 'Coloured Noise'			
First waveform	Parameters for the AWGN	Duration of the signal	5.00 s
		Sampling frequency	1.00 MHz
		Power of the AWGN	-4.00 dBm
	Characteristics of the filter	Impulse response type	IIR - Lowpass
		Design method	Butterworth
		Passband	6.50 kHz
		Order of the filter	2
Second waveform	Parameters for the AWGN	Duration of the signal	5.00 s
		Sampling frequency	1.00 MHz
		Power of the AWGN	-54.00 dBm

Table 12: Parameters to generate the 'Coloured Noise'

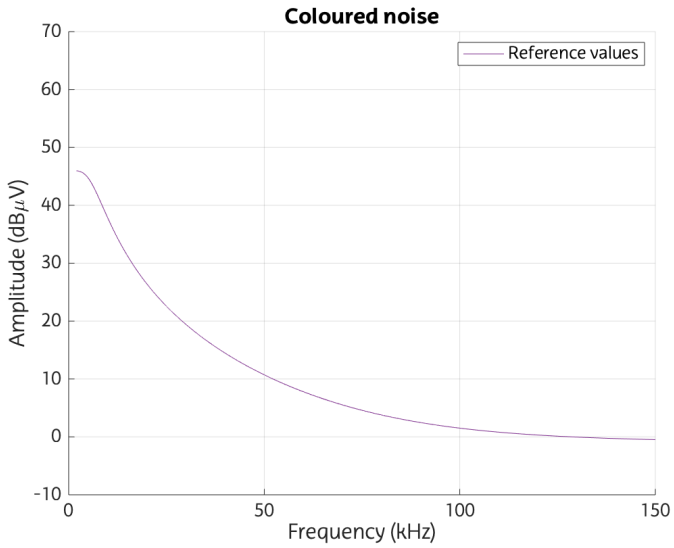

Figure 16: Reference values of 'Coloured Noise' for a unit bandwidth (1 Hz)

To conclude the description of the waveforms composing the 'AXRX4F3-Syn' complex synthetic signal, the emissions corresponding to the PLC bursts are described. These waveforms, unlike the previous ones, are generated by polar coding . Therefore, the reference values of the PSD of these synthetic signals can be assessed in a similar way. In order to generate them, apart from knowing the characteristics of the PRIME PLC transmissions (described in *8.1.2*), the duration of the bursts and the amplitude of each subcarrier within OFDM scheme must also be known.

PLC bursts in 'AXRX4F3-Syn'				
PLC burst number	Start time (ms)	Final time (ms)	Number of symbols	Subcarrier level for 200 Hz BW (dBμV)
1	177.99	195.92	8	48.80
2	685.99	703.92	8	53.19
3	797.89	813.58	7	48.45
4	1413.99	1434.16	9	50.05
5	1993.99	2014.16	9	49.39
6	2033.99	2051.92	8	49.51
7	2169.99	21901.68	9	52.43
8	2197.99	22181.68	9	60.29
9	2221.99	22421.68	9	61.24
10	2251.99	2269.92	8	45.04
11	2297.99	2318.16	9	60.79
12	2329.99	2350.16	9	56.80
13	2651.99	2669.92	8	50.42
14	3269.99	3287.92	8	48.65
15	3887.99	3905.92	8	48.90
16	4505.99	4526.16	9	49.63
17	4539.99	4555.68	7	44.68

Table 13: Parameters to generate the PLC bursts in 'AXRX4F3-Syn'

Once the PLC bursts have been generated, they must be filtered to remove the side lobes from the emissions and not interfere with adjacent frequencies, as commercial devices do.

Parameters to filter PLC bursts		
Characteristics of the filter	Impulse response type	IIR - Bandpass
	Design method	Butterworth
	Central frequency (kHz)	65.67 kHz
	Passband	51.56 kHz
	Order of the filter	20

Table 14: Parameters to filter PLC bursts

The reference values of the PLC emissions after filtering are as follows:

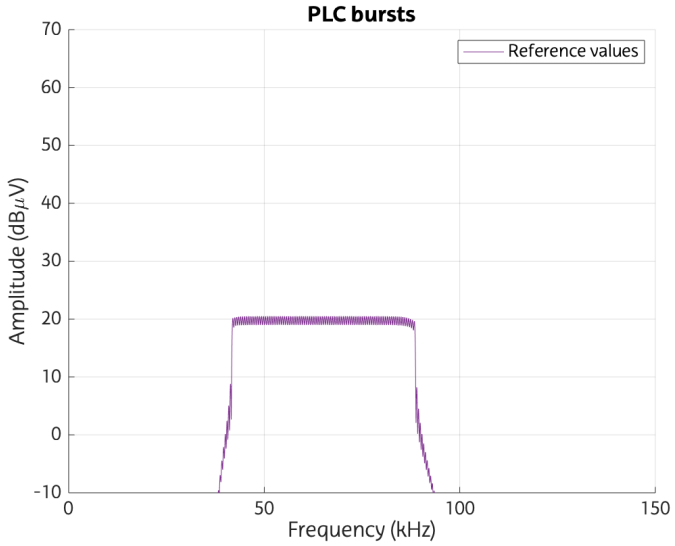

Figure 17: Reference values of 'PLC bursts' for a unit bandwidth (1 Hz)

After generating all the emissions, and their corresponding reference values, these can be combined to create the 'AXRX4F3-Syn' signal. This signal will be used in the following sections to evaluate existing measurement methods.

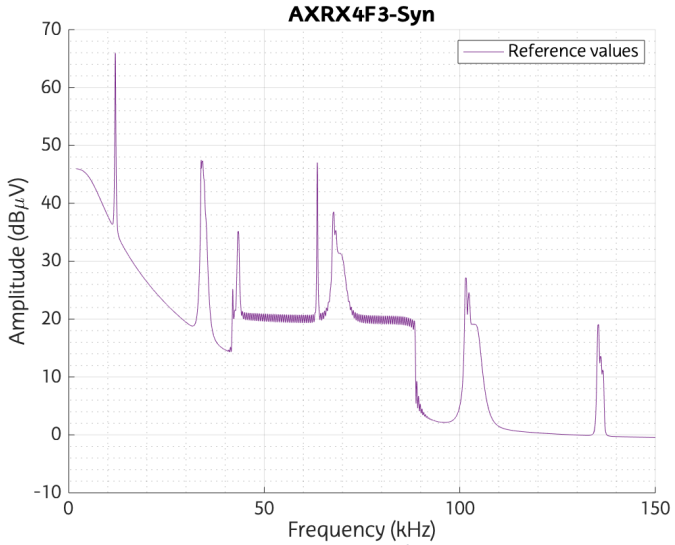

Figure 19: Reference values of 'AXRX4F3-Syn' signal for a unit bandwidth (1 Hz)

As mentioned at the beginning of this subsection, the complex synthetic signal tries to reproduce the emissions of 'AXRX4F3', measured in the LV grid. In order to analyse the time evolution of both signals, and to compare the synthetic signal to measured recording (see *Figure 10* , 'AXRX4F3'), the spectrogram of the synthetic signal is shown below.

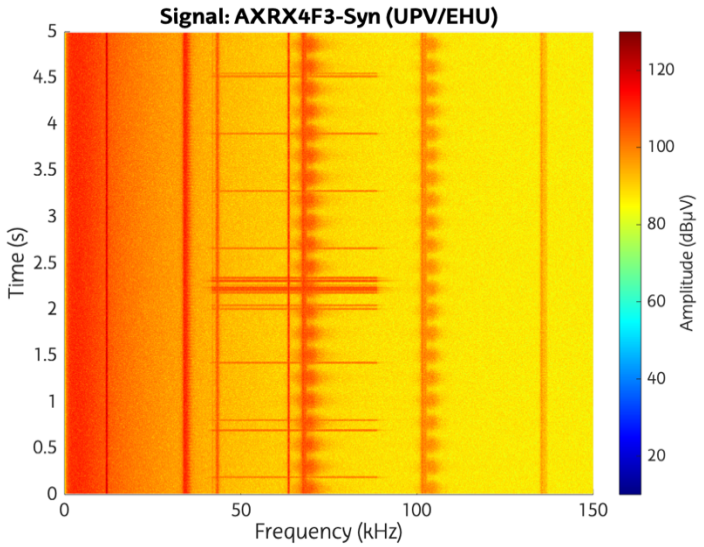

Figure 18: Spectrogram of 'AXRX4F3-Syn'

8.2. Procedure for the comparison between exiting EMI methods

This section describes the procedure and parameters used for the evaluation and comparison of existing EMI measurement methods. These parameters will be based on the results obtained by the methods described in the state of the art of this project (*Section 6*) and on the reference values of the synthetic signals described in the previous subsection. The parameters described below will be used to compare the results of the methods with the theoretical spectral values that these methods should provide, if they were ideal. This is very relevant, as it allows a common reference to be set for all meters that is not biased by any method.

As mentioned above, this work, developed in collaboration with members of the European SupraEMI project, was published in [7]. The the parameters mentioned below were selected or defined by other partners of this project (NPL and TUD).

8.2.1. Reference values

In this study, candidate methods are compared against reference levels that reflect the thermal impact of emissions over a given bandwidth. Reference values for β bandwidth are calculated as

$$R_f = \sqrt{\sum_{x=f-\beta/2+1}^{f+\beta/2} G(x)^2} \quad \text{(Eq.12)}$$

where:

- R_f are the reference values,
- β is the bandwidth of reference values,
- $G(x)$ are the reference values for a unit bandwidth (1 Hz),
- x is the centre frequency of the bandwidth.

By this definition, R_f represents 100% of the signal power in the frequency range [f−β/2+1,f+β/2], corresponding to a flat frequency response over the bandwidth β. All reference values in this study have been calculated using β = 200 Hz in line with the bandwidth of compatibility levels.

8.2.2. Amplitude and frequency

Each method results in amplitudes for frequency components in the range 2–150 kHz reported at regular time intervals. Let variable $U_{b,i}$ be the amplitude value reported for frequency bin b and time interval i. As a representative quantity over the duration of a test signal, the amplitude values $U_{b,i}$ of each frequency bin are aggregated over the number of time intervals N into RMS values U_b.

The measurement accuracy for narrowband emissions is assessed by calculating the error in amplitude and frequency of the aggregated RMS values identified by each method for characteristic emissions defined in the synthetic signals with known reference values. The error in frequency $E_{f,P}$ is defined as:

$$E_{f,P} = f_{b,P} - f_P \quad \text{(Eq.13)}$$

where:

- $E_{f,P}$ is the error in frequency detection of the analysed emission,
- $f_{b,P}$ is the frequency of the respective bin provided by the method where the emission is detected,
- f_P is the frequency value where the emission is located in the reference values.

The percentage error in peak amplitude $E_{U,P}$ is defined as:

$$E_{U,P} = (U_{b,P}/U_P - 1) \cdot 100 \quad \text{(Eq.14)}$$

where:

- $U_{b,P}$ is the error in peak amplitude detection of the analysed emission,
- $U_{b,P}$ is the peak amplitude result identified by a given method,
- U_P is the reference value for the peak amplitude of a given characteristic narrowband emission.

If the magnitude of $E_{f,P}$ does not exceed 50% of the frequency step of a method, then the correct frequency bin has been identified for the peak emission.

8.2.3. Integral value

Integral values are a useful additional measurement quantity for assessing the total power of emissions over a frequency range. Given M adjacent frequency bins with centre frequencies f_m, $m = 1, 2, 3, ..., M$, the integral value $T_{f1, fM}$ is calculated as [18]:

$$T_{f_1,f_M} = \sqrt{\sum_{m=1}^{M} U_{fm}^2} \quad \text{(Eq.15)}$$

where:

- $T_{f1, fM}$ is the integral value between f_1 and f_M frequencies,
- U_{fm} is the RMS amplitude result for the frequency bin centred in f_m.

Let $\tau_{f1\,fM}$ be the integral value calculated from the reference level R_f of a synthetic test signal, calculated as:

$$\tau_{f_1,f_M} = \sqrt{\sum_{m=1}^{M} R_{fm}^2} \quad \text{(Eq.16)}$$

where:

- $\tau_{f1\,fM}$ is the integral value between f_1 and f_M frequencies calculated from the reference level,
- R_f are the reference values.

Then, the percentage error in the integral value is:

$$E_T = \left(T_{f_1,f_M}/\tau_{f_1,f_M} - 1\right) \cdot 100 \quad \text{(Eq.17)}$$

where:

- $T_{f1, fM}$ is the integral value between f_1 and f_M frequencies,
- $\tau_{f1\,fM}$ is the integral value between f_1 and f_M frequencies calculated from the reference level.

For the CISPR 16-1-1 method, the calculation of integral values is not suitable without additional compensation for the difference in effective bandwidth relative to the reference level. The method for this compensation is still an ongoing research topic, and no specific assessment procedure ha been defined; therefore, no integral values are reported for the CISPR 16 method in this article.

8.3. Input signals for AppQP

The AppQP method is an empirical EMI method, whose detector's configuration has been mathematically defined based on the behaviour of the waveforms of LV grid. This characterization has been performed over 30 LV grid signal and the validation of the method over 29 recording, which are going to be explained in this subsection. The signals used in this analysis were recorded by TSR research group (UPV/EHU), 56 of them, and TUD University, the other 3 signals.

The measurement system used by TSR was composed of a voltage probe that provides galvanic isolation and protection against transient overvoltages, an oscilloscope for high-resolution sampling (16-bit, 8.92-MHz sampling rate) and a laptop to configure, automatize, and record the measurements [22]. The measurement was recorded with a bandpass filter to remove frequencies outside the range 2–150 kHz. The details of the uncertainty of the measurement system are described in [22] and [25].

The signals provided by TUD were shared within the SupraEMI project, so the details of the measurement system are not known. However, the shared signals have a duration of 3 seconds and a sampling rate of 1 MHz. These signals contain the 50 Hz component present in the LV grids; therefore, digital filtering was applied with a Zero-phase elliptical high pass filter between 2 kHz and 150 kHz [26].

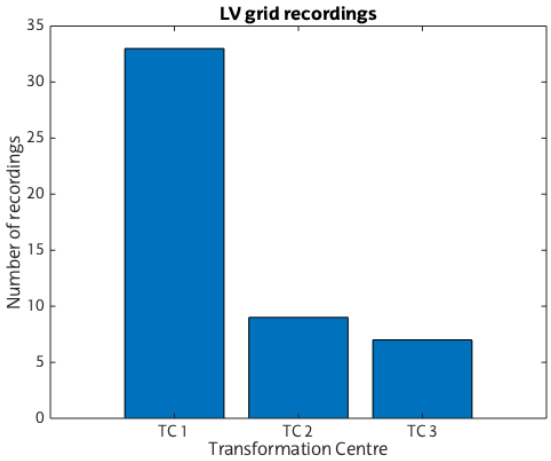

Figure 20: Distribution of LV grid recording according to the location where they were measured

Recordings could be distinguished into three categories: LV grid measurements, Photovoltaic (PV) inverter signals recorded directly at the Point Of Connection (POC) and Electric Vehicle (EV) charger measurements at the POC. However, the LV grid signals could also be grouped in three main sections, depending on the localization of the Transformation Centre (TC).

8.3.1. Distribution of signals to design and validate the AppQP

To design and validate the AppQP method, two groups of signals were defined, in which 50 recordings were randomly grouped. Later, a set of additional recordings with the rest of 9 signals was used for further validation.

The first group, the 'model group', is composed of 30 recordings and its objective is to define the model of the new EMI method. These 30 signals were measured by TSR research group in four different locations, where three of those locations were LV grid measurement points, and the other one was recorded on a POC of a PV inverter.

The second group, the 'LV grid validation group', is composed of 20 signals registered in the same LV grid locations than those used for the 'model group'. However, in this group there is no recording of PV inverters.

The third group, 'PV and EV validation group', is used to do a further validation of the method, which has 9 signals directly measured in the POC of PV inverters and EV chargers. The purpose of grouping the validation signals into two distinct categories is to evaluate the behaviour of different types of grid waveforms. The signals directly measured at the POC of PV inverters and EV chargers are of higher amplitude, narrower in frequency and with lower variability in amplitude over time; while the grid emissions are of lower amplitude, wider in the spectrum and of higher variability over time.

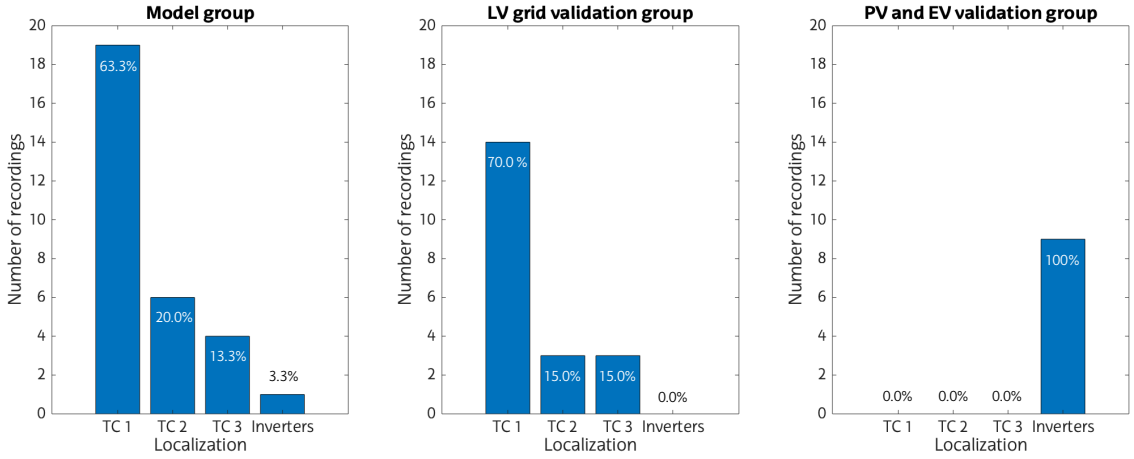

Figure 21: Distribution of recordings in the three signal groups

As depicted in the figure above, the recorded LV grid signals have been proportionally distributed into the 'model group' and 'LV grid validation group' according to the TC at which they were measured. Although they were randomly distributed in these groups, monitoring that these two groups of signals have the same proportionality is crucial, as the AppQP should not be biased by misclassification of the input data. This supervision has not been carried out with the signals from PV inverters and EV chargers due to the small number of available recordings and the variety of measurement points used, 7 to be precise.

8.4. Procedure to calculate the accuracy of AppQP

Before describing any results of the AppQP method, the procedure to calculate the statistic assessing accuracy should be explained to understand the outcome of the performed analysis correctly.

To focus the analysis on the behaviour of the AppQP method with LV grid waveforms, frequency bins where only electromagnetic noise is present are discarded for the performed study. This selection of frequency bins has been made following the criteria described in *Section 10.2*.

In this analysis, ten statistics have been computed to calculate the accuracy of AppQP:

1. Average absolute difference: It is the average of the differences, in mV, between the spectra of CISPR 16-1-1 QP and AppQP. The mathematical expression to calculate this parameter is as follows:

$$Average\ abs.diff. = mean\left(U_{QP}[f_b] - U_{AppQP}[f_b]\right) = mean\left(\Delta_{QP,AppQP}[f_b]\right)(mV) \quad \text{(Eq.18)}$$

   where:

   - $U_{AppQP}[f_b]$ is the Approximated Quasi-Peak spectrum,
   - $U_{QP}[f_c]$ is the Quasi-Peak spectrum of the digital implementation of CISPR 16-1-1,
   - $\Delta_{QP,AppQP}[f_b]$ is the absolute difference, in 3 seconds, between CISPR 16-1-1 Quasi-Peak spectrum and AppQP spectrum.
   - f_b are the frequency bins, f_b = 2.1 kHz, 2.2 kHz, 2.3 kHz … 149.9 kHz

2. Median absolute difference: It is the median of the differences, in mV, between the spectra of CISPR 16-1-1 QP and AppQP.

$$Median\ abs.diff. = median\left(\Delta_{QP,AppQP}[f_b]\right)\ (mV) \quad \text{(Eq.19)}$$

3. Standard deviation of absolute difference: It is the standard deviation of the differences, in mV, between the spectra of CISPR 16-1-1 QP and AppQP.

$$Std.dev.abs.diff. = std.dev.\left(\Delta_{QP,AppQP}[f_b]\right)\ (mV) \quad \text{(Eq.20)}$$

4. Average relative difference: It is the average relative differences, in percentage, between the spectra of CISPR 16-1-1 QP and AppQP.

$$Average\ rel.diff. = mean\left(\frac{\Delta_{QP,AppQP}[f_b]}{U_{QP}[f_b]} \cdot 100\right)\ (\%) \quad \text{(Eq.21)}$$

5. Median relative difference: It is the median relative differences, in percentage, between the spectra of CISPR 16-1-1 QP and AppQP.

$$Median\ rel.diff. = median\left(\frac{\Delta_{QP,AppQP}[f_b]}{U_{QP}[f_b]} \cdot 100\right)\ (\%) \quad \text{(Eq.22)}$$

6. Standard deviation of relative difference: It is the standard deviation of relative differences, in percentage, between the spectra of CISPR 16-1-1 QP and AppQP.

$$Std.dev.rel.diff. = std.dev.\left(\frac{\Delta_{QP,AppQP}[f_b]}{U_{QP}[f_b]} \cdot 100\right)\ (\%) \quad \text{(Eq.23)}$$

7. Average relative difference from absolute values: It is the average relative value of the modulus of differences between the spectra of CISPR 16-1-1 QP and AppQP.

$$Average\ rel.diff.form\ abs.values = mean\left(\left|\frac{\Delta_{QP,AppQP}[f_b]}{U_{QP}[f_b]}\right| \cdot 100\right)\ (\%) \qquad \text{(Eq.24)}$$

8. Median relative difference from absolute values: It is the median relative value of the modulus of differences between the spectra of CISPR 16-1-1 QP and AppQP.

$$Median\ rel.diff.form\ abs.values = median\left(\left|\frac{\Delta_{QP,AppQP}[f_b]}{U_{QP}[f_b]}\right| \cdot 100\right)\ (\%) \qquad \text{(Eq.25)}$$

9. Percentage of differences within ±2% of Compatibility Levels: The percentage of the frequency bins with absolute differences between AppQP and CISPR 16-1-1 Quasi-Peak spectra within the ±2% of the corresponding Compatibility Levels (regulated in IEC 61000-2-2 for differential mode) in frequency.

$$Diff.\pm 2\%\ of\ CL = \frac{n}{N} \cdot 100\ (\%), \qquad \begin{cases} n = card\left(\left|\Delta_{QP,AppQP}[f_b]\right| < 2\%\ CL[f_b]\right) \\ N = card\left(\forall\ \Delta_{QP,AppQP}[f_b]\right) \end{cases}^{3} \qquad \text{(Eq.26)}$$

10. Percentage of differences with in ±10% of Compatibility Levels: This parameter follows the same methodology as the previous one; however, the differences are evaluated with respect to the ±10% of the corresponding Compatibility Levels in frequency.

$$Diff.\pm 10\%\ of\ CL = \frac{n}{N} \cdot 100\ (\%), \qquad \begin{cases} n = card\left(\left|\Delta_{QP,AppQP}[f_b]\right| < 10\%\ CL[f_b]\right) \\ N = card\left(\forall\ \Delta_{QP,AppQP}[f_b]\right) \end{cases} \qquad \text{(Eq.27)}$$

It is important to mention that in statistics in which the absolute value or the square is not applied to $\Delta_{QP,AppQP}[f_b]$, exactly in *1*, *2*, *4* and *5*, the results will have the corresponding sign. This is important, as it gives information about whether the measurement is being overestimated or underestimated. For an application that tries to calculate emissions in the network approximately, as is the case of the AppQP, it is important that the measured values are conservative and, therefore, the waveforms are overestimated. This is because these methods aim to compare the spectrum results with the CL, and if the conservative results are below these limits, it can be ensured that the exact values of the emissions will remain below the limits. Therefore, it should be noted that if the above-mentioned statistics (*1*, *2*, *4* and *5*) have a negative sign, the AppQP will be conservative, as the values of the AppQP method are higher than the CISPR 16-1-1 spectrum. In contrast, if these same statistics give positive values, the results will not be conservative.

To explain graphically how the statitstics are calculated, an additional description with figures of the parameters listed above is given. This explanation will be based on a specific waveform of a signal used to evaluate AppQP method's accuracy.

First of all, the spectra of the signal are obtained by applying CISPR 16-1-1 and Approximated Quasi-Peak methods described in sections *11* and *13*, respectively.

[3] The operation 'card' expresses the cardinality of a set, i.e., the number of elements of a set.

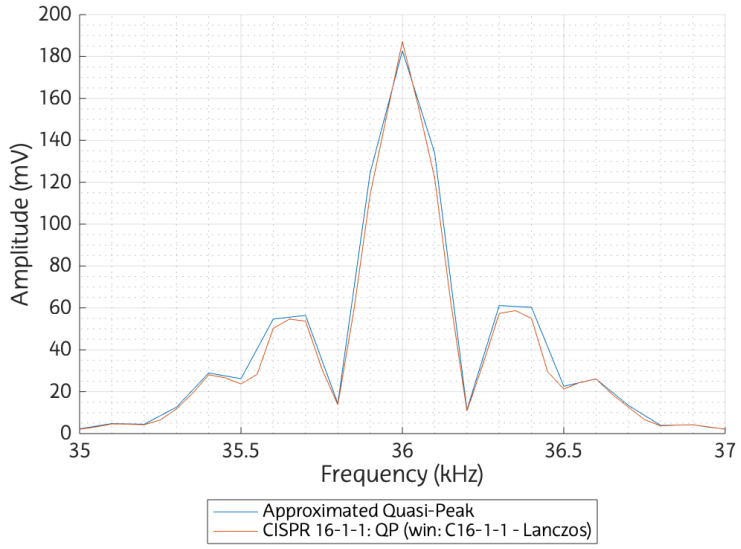

Figure 22: Spectra of a waveform, recorded directly in the POC of a PV inverter, computed with AppQP and CISPR 16-1-1 methods described in sections 11, 12 and 13.

Once both spectra are calculated, the absolute difference between the methods are assesses for all the frequency bins. Since AppQP and the proposed digital implementation of CISPR 16-1-1 have different frequency step size (100 Hz and 50 Hz, respectively), the differences are only computed for the frequencies where AppQP provides results, that is *2.1 kHz, 2.2 kHz, 2.3 kHz … 149.9 kHz*. Nevertheless, those frequency bins must have a level above the noise threshold defined in *Section 10.2*. Hence the same criterion has to be applied to discard frequency samples. Besides, the absolute difference is helpful to calculate the magnitude of the divergence between both methods.

The absolute difference between AppQP and CISPR 16-1-1 is shown in the following graph:

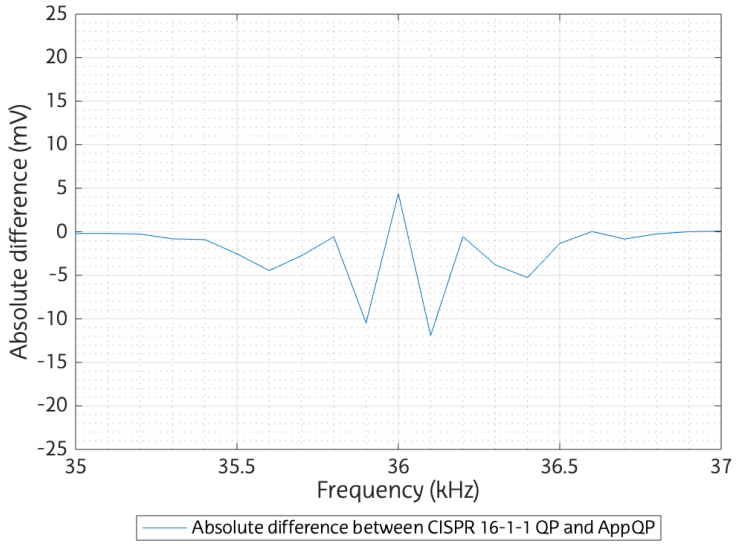

Figure 23: Absolute difference between AppQP and CISPR 16-1-1 spectra

After computing the absolute difference, the relative difference may be calculated. This parameter could be obtained by dividing the absolute difference by CISPR 16-1-1 QP values in each frequency bin. With this parameter, it is possible to know the difference in percentage between the two methods concerning the CISPR 16-1-1 spectrum, which has been used as a reference to define the AppQP.

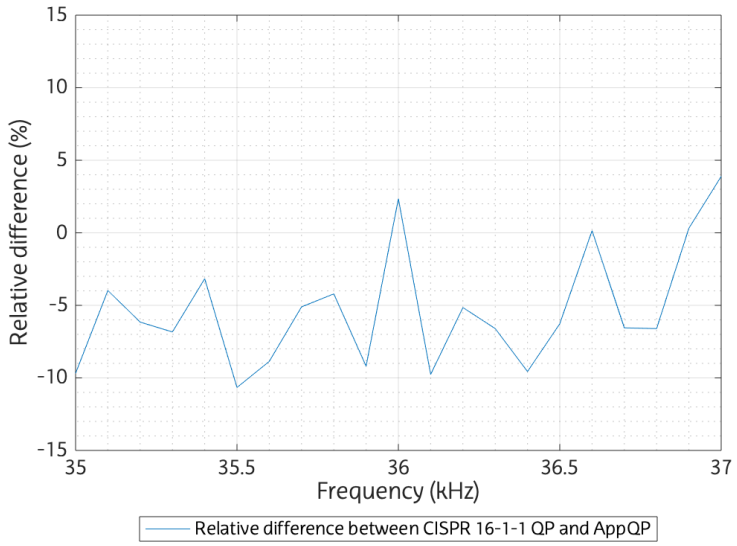

Figure 24: Relative difference between AppQP and CISPR 16-1-1 spectra

Then, the relative difference from absolute values is calculated computing the modulus of the relative difference. This data could be useful when 'average' or 'median' mathematical operations are applied, since the given information is not distorted by the positive or negative sign of each datum.

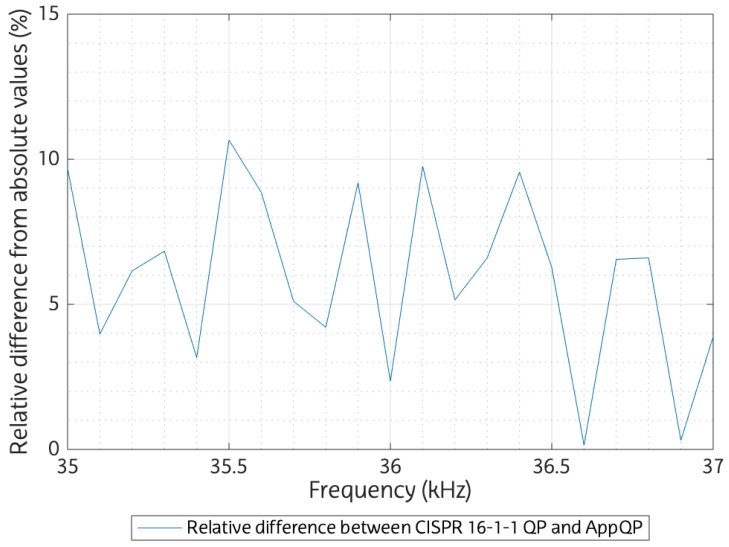

Figure 25: Relative difference from absolute values of AppQP and CISPR 16-1-1 spectra

The next stage calculates the percentage of frequency bins with a difference within ±2% and ±10% of the corresponding Compatibility Levels regulated in IEC 61000-2-2. These emissions limits are not constant over the whole band from 2 kHz to 150 kHz. This allows a study with asymmetric thresholds, which will be more permissive at low frequencies (where the higher amplitude waveforms are found) and more restrictive at high frequencies (where low-level

emissions occur) [3]–[5]. Furthermore, this analysis is useful to evaluate the percentage of frequency bins that have a difference higher than an extreme value, a parameter that is very necessary to bound the accuracy of the EMI method.

The Compatibility Levels from 2 kHz to 150 kHz are as follows:

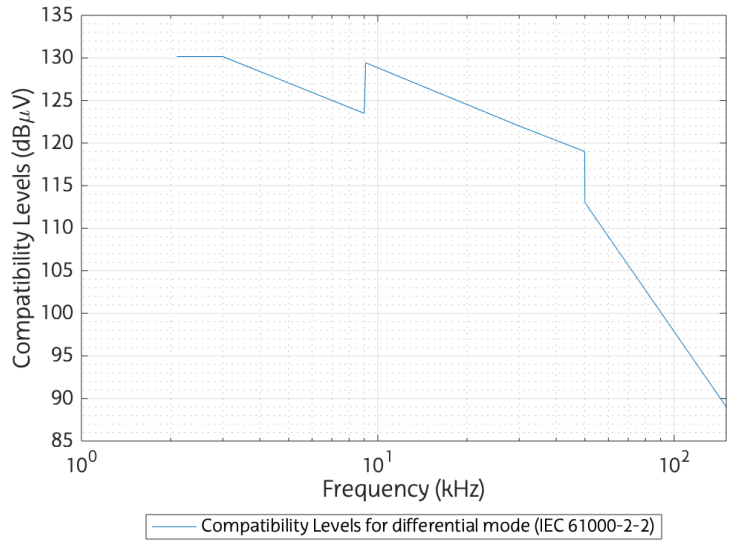

Figure 26: Compatibility levels for differential mode regulated in IEC 61000-2-2 [3]–[5]

The ±2% and ±10% of Compatibility Levels for the same frequency range, with horizontal and vertical axis in linear scale, will be:

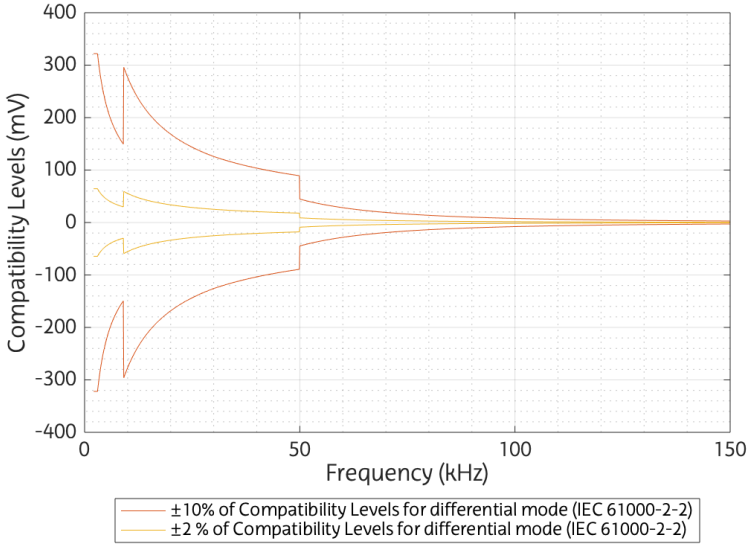

Figure 27: ±2% and ±10% Compatibility Levels for differential mode regulated in IEC 61000-2-2

If these thresholds are used in the example shown in *Figure 22–Figure 25*, it is possible to evaluate how many frequency bins of that particular waveform have differences within a specific percentage of CL.

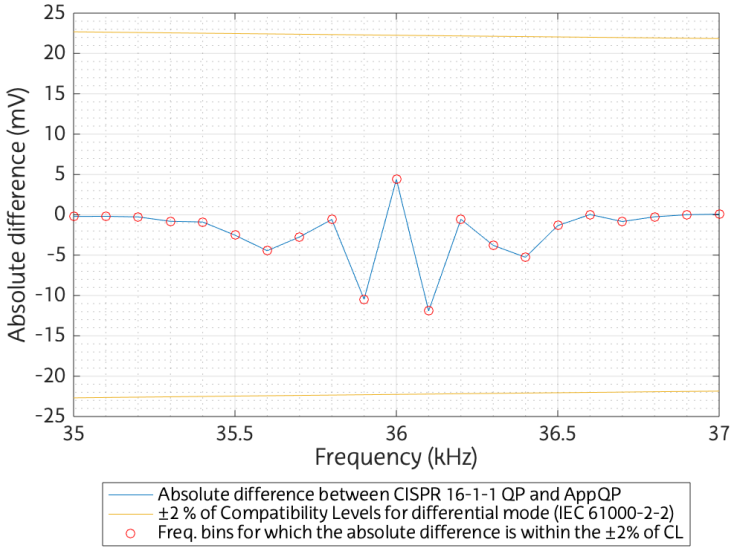

Figure 28: Frequency bins for which the absolute difference is within the ±2% of CL

As could be seen in the previous figure, all the differences of frequency bins are within ±2% of the corresponding Compatibility Level in frequency (and therefore within the 10 % as well). Thus, in the particular case of the analysed emission, the percentage of frequency bins with a difference within ±2% and ±10% of Compatibility Levels is 100%.

8.4.1. Accuracy criteria for the validation of the AppQP

Since a statistical analysis is being carried out to assess the accuracy of the Approximate Quasi-Peak method, certain criteria have to be defined to evaluate the results and to set a threshold above which the proposed method is valid. As mentioned in previous sections, the proposed EMI measurement method has to be previously approved by the SupraEMI consortium in order to be proposed in the IEC77A/WG9 regulatory working group. For this reason, the metrology experts involved in the European project imposed certain criteria for the validation of the method, such as the difference between the QP and AppQP spectrum must be below 10%.

Three criteria, for three specific statistics, have been defined to set the minimum accuracy that any new EMI method must meet:

a. Median relative difference from absolute values: The value of this parameter must be below 10% to ensure that the uncertainty of the new measuring method is comparable to the digital implementation of CISPR 16-1-1. Nevertheless, it is suggested that this value should be less than or close to 5%.

b. Percentage of differences within ±2% of Compatibility Levels: As the differences between the AppQP and CISPR 16-1-1 spectra should remain as small as possible, the value of this parameter should be close to 100% and higher than 95%.

c. Percentage of differences within ±10% of Compatibility Levels: Since this parameter is based on the same concept as the previous one, the limits also apply here. Therefore, the value of this parameter should be close to 100% and must be higher than 95%.

9. Comparison of accuracy for existing EMI methods

The two synthetic test signals introduced in *Section 8.1* have been processed by the methods selected in the state of the art of this project to obtain the metrics defined in *Section 8.2*. This chapter provides a quantitative and qualitative analysis of the results in order to compare the methods with respect to different types of characteristic emissions. First, the accuracy of the methods is assessed using the synthetically generated simple signal, known as 'Interm-Syn'. Thereafter, the complex synthetic signal 'AXRX4F3-Syn' is used to evaluate the performance of the methods with waveforms similar to those recorded in the LV grid. In addition, both signals have associated reference values, which provide the theoretical value of the amplitude in the spectrum, essential to carry out the study shown in this section.

It must be noted that the reported errors in digital CISPR 16 RMS values and IEC 61000-4-30 RMS amplitudes arise from the difference in bandwidth definitions to the reference level, rather than intrinsic deficiencies of the algorithms. Since Quasi-Peak values are a different measurement quantity, error values with respect to RMS reference levels are not a useful metric and are, thus, not included in the tables in this section. However, to illustrate the differences compared with RMS amplitudes, Quasi-Peak values have been included in graphical results. The plotted results of the methods for a single signal have been divided between two figures for visual clarity. The values for the error in frequency of peak amplitudes are only reported if they exceed 50% the frequency step of the method, i.e., greater than 25 Hz for digital CISPR 16, 1 kHz for IEC 61000-4-30, and 100 Hz for other methods.

As stated in previous sections, this comparison results from the joint work carried out by the members of the European SupraEMI project, which was published in [7]. The contribution from this Master's Thesis in obtaining results for this evaluation consisted of the definition and development of the synthetic signals, and the assessment of the results for the IC 61000-4-7 and IEC 61000-4-30 methods. Researchers from the NPL and TUD were in charge of obtaining the rest of the methods' results.

9.1. 'AXRX4F3': the measured grid signal

This section of the comparison analyses the results of the signal recorded in the LV grid 'AXRX4F3', whose emissions were characterised and used to generate the complex synthetic signal 'AXRX4F3-Syn'. As this signal does not contain reference values, the results are given on the absolute values of the amplitude and frequency on the spectrum.

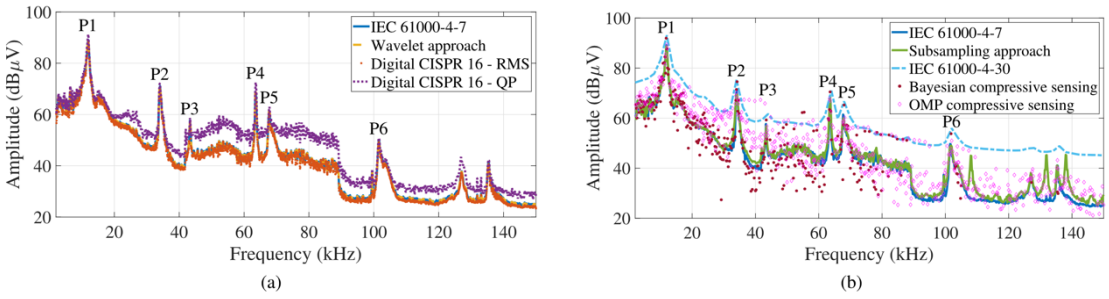

Figure 29: Spectral amplitude results for the measured grid signal ('AXRX4F3') [7]

	Frequency and amplitude							
	f_{P1} (Hz)	$E_{U,P1}$ (dBµV)	f_{P2} (Hz)	$E_{U,P2}$ (dBµV)	f_{P3} (Hz)	$E_{U,P3}$ (dBµV)	f_{P4} (Hz)	$E_{U,P4}$ (dBµV)
IEC 61000-4-7	11.90	89.1	34.10	71.0	43.30	57.7	63.50	68.7
Wavelet approach	11.90	89.2	34.10	71.1	43.30	57.8	63.50	68.7
Digital CISPR 16 - RMS	11.90	88.6	34.05	70.5	43.40	57.1	63.60	68.7
Subsampling approach	12.00	88.7	34.20	69.5	43.40	56.8	63.60	68.7
IEC 61000-4-30	12.00	93.1	34.00	75.3	44.00	61.7	64.00	71.0
Bayesian compressive sensing	11.80	91.9	34.20	74.6	43.40	59.2	63.60	70.5
OMP compressive sensing	12.00	89.3	34.00	70.3	41.60	67.3	63.40	67.7
Range	0.20	4.5	0.20	5.8	2.40	10.5	0.60	3.3

	Frequency and amplitude				Integral values	
	f_{P5} (Hz)	$E_{U,P5}$ (dBµV)	f_{P6} (Hz)	$E_{U,P6}$ (dBµV)	40-90 kHz E_T (dBµV)	2-150 kHz E_T (dBµV)
IEC 61000-4-7	67.70	61.4	101.50	49.7	74.4	94.5
Wavelet approach	67.70	61.5	101.50	49.7	74.5	94.6
Digital CISPR 16 - RMS	67.80	60.9	101.60	49.2	-	-
Subsampling approach	67.80	59.9	101.80	49.0	74.6	94.6
IEC 61000-4-30	68.00	66.7	102.00	55.9	74.9	94.2
Bayesian compressive sensing	68.00	65.2	101.80	53.8	75.3	95.6
OMP compressive sensing	68.20	60.2	102.00	51.0	77.0	95.1
Range	0.50	6.8	0.50	6.9	2.6	1.4

Table 15: Error in results for the measured grid signal ('AXRX4F3') [7]

Figure 29 shows the plots of the rms amplitude values for the measured grid signal for all methods, as well as quasi-peak values calculated using the digital CISPR 16 method. It can be seen in *Figure 29 (a)* that the plots of rms results overlap for the IEC 61000-4-7 method, wavelet approach, and digital CISPR 16, while the quasi-peak values are consistently higher. Eight peaks of narrowband emission can be clearly distinguished from a decreasing noise level and broadband emission in the PLC region from 40 to 90 kHz. The graphs in *Figure 29 (b)* show a broader range of emission levels and shapes of the amplitude spectrum. Results from the IEC 61000-4-30 method are consistently higher, and the peaks are less distinct from noise as each 2-kHz bin reports the root sum square of ten 200 Hz bins. The subsampling approach results in similar values as the methods in *Figure 29 (a),* with some additional peaks above 108 kHz. The Bayesian compressive sensing gives a very sparse signal representation, particularly above 90 kHz. Around 80 kHz, it can be seen that, for some frequency components, compressive sensing was not effective in decreasing frequency step from 2 kHz to 200 Hz, as the amplitude values coincide with the levels of the IEC 61000-4-30 method.

Table 15 lists the results for peak amplitude and frequency values identified by the different methods for six of the characteristic narrowband emissions. It can be observed that there is

strong agreement in the frequency value of the first two peaks, with a range of only 200 Hz, while there is more discrepancy in the frequency values of other peaks, mainly due to the IEC 61000-4-30 and compressive sensing methods. The difference in peak amplitude values between methods ranges from 3.3 to 10.5µV, which corresponds to 40%–300% between the reported peak values. The variation in the calculated integral values is lower with 2.6 dBµV for the PLC region and 1.4 dBµV for the total signal power over 2–150 kHz.

Since there is no reference value for the recorded grid signal, no conclusions can be made about the absolute accuracy of the methods. In order to investigate the source of the relative differences in results between methods, the accuracy is assessed in the following sections using synthetically generated signals with known frequency content.

9.2. 'Interm-Syn': simple synthetic test signal

The identification of the shape of the spectrum is relevant for the characterization of the type and source of emissions, while the priority for compliance assessment is to identify the worst emissions, corresponding to the highest emission level. *Figure 30* shows the plots of the amplitude results, including the indications of the highest peak in both frequency ranges. Errors in frequency and amplitude of the highest peak in each frequency range are given in *Table 16* to assess how well the worst emissions are identified.

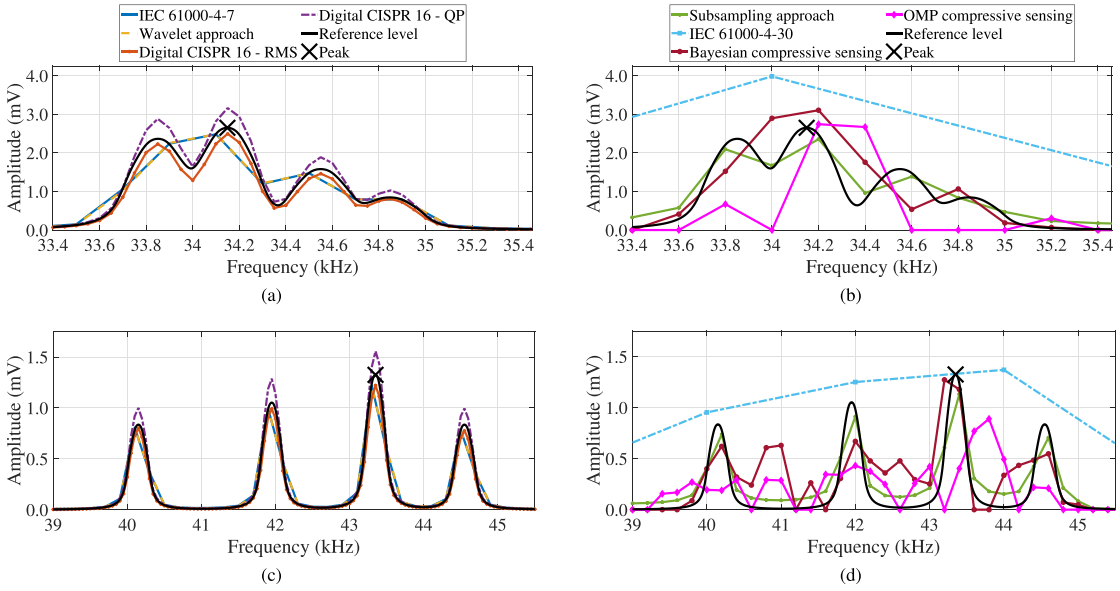

Figure 30: Spectral amplitude results for the synthetic signal with several narrowband emissions ('Interm-Syn') [7]

Frequency range	33-36 kHz		39-46 kHz	
Error in peak values	$E_{f,P}$ (Hz)	$E_{U,P}$ (%)	$E_{f,P}$ (Hz)	$E_{U,P}$ (%)
IEC 61000-4-7	-	−6.3	-	−7.9
Wavelet approach	-	−6.4	-	−8.6
Digital CISPR 16 - RMS	-	−5.9	-	−7.8
Subsampling approach	-	−11.1	-	−14.6
IEC 61000-4-30	-	50.3	-	3.4
Bayesian compressive sensing	-	17.2	−150	−4.0
OMP compressive sensing	-	3.5	450	−32.8
Reference	34 149	-	43 350	-

Table 16: Error in results for narrowband emissions ('Interm-Syn') [7]

Considering the set of emissions with narrow spacing in the range 33–36 kHz, *Figure 30 (a)* shows that the digital CISPR 16 method traces the spectral shape of the reference level most accurately due to its smaller frequency step, indicating four spectral peaks. For the more widely separated emissions in the range 39–46 kHz, all methods in *Figure 30 (c)* and the subsampling approach in *Figure 30 (d)* match the four spectral peaks of the reference spectrum.

Table 16 shows that IEC 61000-4-7, wavelet approach, and digital CISPR 16 method are within 10% of the peak reference values, while the subsampling approach has greater deviations. The IEC 61000-4-30 and compressive sensing methods have deviations within 10% only for one peak value.

Figure 30 (b) and *(d)* shows that the IEC 61000-4-30 method does not resolve the emissions, while the compressive sensing methods result in spectra with different shapes from the reference level in terms of number, width, and location of identified emissions.

9.3. 'AXRX4F3-Syn': complex synthetic test signal

The results for the simple synthetic test signals ('Interm-Syn') have revealed various emission characteristics that cause the accuracy of the methods to deviate from the calibration scenario. Test signal 'AXRX4F3-Syn' has been designed to assess the performance of the methods in a grid measurement scenario.

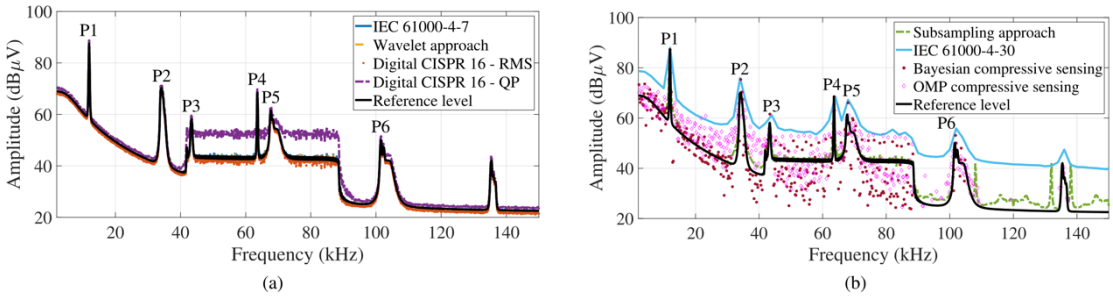

Figure 31: Spectral amplitude results for the synthetic grid signal ('AXRX4F3') [7]

	Error in frequency and amplitude							
	$E_{f,P1}$ (Hz)	$E_{U,P1}$ (%)	$E_{f,P2}$ (Hz)	$E_{U,P2}$ (%)	$E_{f,P3}$ (Hz)	$E_{U,P3}$ (%)	$E_{f,P4}$ (Hz)	$E_{U,P4}$ (%)
IEC 61000-4-7	-	−1.1	-	−3.7	-	1.3	-	−10.5
Wavelet approach	-	−1.2	-	−3.8	-	1.0	-	−11.1
Digital CISPR 16 - RMS	-	−6.3	-	−12.2	-	−9.5	-	−5.9
Subsampling approach	-	−19.0	-	−3.9	-	−4.9	-	−7.3
IEC 61000-4-30	-	5.8	-	91.4	-	41.6	-	0.5
Bayesian compressive sensing	-	−2.9	-	80.0	-	48.5	-	0.5
OMP compressive sensing	-	−20.6	205	−4.0	-	−20.4	-	−28.8
Reference	11 930	-	34 195	-	43 353	-	63 570	-

	Error in frequency and amplitude				Error in integral values	
	$E_{f,P5}$ (Hz)	$E_{U,P5}$ (%)	$E_{f,P6}$ (Hz)	$E_{U,P6}$ (%)	40-90 kHz E_T (%)	2-150 kHz E_T (%)
IEC 61000-4-7	-	0.7	-	0.0	0.5	0.8
Wavelet approach	-	0.7	-	0.2	0.6	0.9
Digital CISPR 16 - RMS	-	−9.6	-	−8.2	-	-
Subsampling approach	-	−6.0	-	−1.9	1.6	0.6
IEC 61000-4-30	-	95.2	-	93.6	2.4	2.9
Bayesian compressive sensing	284	69.9	245	41.0	−4.2	1.3
OMP compressive sensing	484	−3.9	445	−2.5	8.8	4.9
Reference	67 716	-	101 555	-	-	-

Table 17: Error in results for the synthetic grid signal ('AXRX4F3-Syn') [7]

Figure 31 shows the plots of the spectral amplitude results for the synthetic grid signal. Similar to the results of the grid recording in *Figure 31*, it can be observed that the amplitude spectra of the IEC 61000-4-7 method and wavelet approach overlap, with the digital CISPR 16 RMS values slightly lower and Quasi-Peak values higher. Further similarities to measured signal results are the sparsity of the Bayesian compressive sensing above 90 kHz and the amplitude values for the compressive sensing methods that have not been resolved effectively to the 200 Hz level. However, the use of a synthetic signal has the advantage of known reference levels, which means that reliable conclusions about the accuracy of the results can be drawn.

It can be seen clearly that the compressive sensing methods trace the reference spectrum less closely. The amplitude spectrum given by the subsampling approach matches the reference level, although above 108 kHz some additional narrowband emissions can be observed.

Table 17 gives errors in frequency and amplitude values identified for the highest peak narrowband emissions, as well as errors in integral values for the PLC range and over 2–150 kHz. The error values confirm that the IEC 61000-4-7 method and the wavelet approach are closest to the reference level for all but one of the peak amplitude values, and the frequency values are

accurate to within the 200-Hz step between centre frequencies. The subsampling method gives the results between 3.9% and 19% below the reference peak amplitudes but the smallest deviation of 0.6% from the integral value over the whole frequency range. The performance of the compressive sensing methods is mixed. For some narrowband emissions, the methods successfully decrease the frequency step from 2 kHz to 200 Hz, thereby reducing the error in amplitude (e.g., $E_{U,P2}$, $E_{U,P5}$, and $E_{U,P6}$) compared with the IEC 61000-4-30 results. However, this performance is not consistent; for some peaks, the amplitude error is, in fact, increased. All methods give integral values of this synthetic grid signal within 10% of the reference values.

10. Conversion between RMS and QP spectra

An analysis of the behaviour of the IEC 61000-4-7 method adapted to CISPR Band A, or RMS-A method, described in *Section 12*, and the differences in the results of this method with respect to the selected implementation of CISPR 16-1-1 (described in *Section 11*), has been done. The aim of this study is to link the temporal evolution of waveforms measured in the LV grid with respect the difference between the final results of RMS-A and CISPR 16-1-1 Quasi-Peak.

10.1. Relation between RMS and QP spectra

The AppQP is an empirical EMI measurement method, whose detector has been designed using 30 LV grid recordings, in which a statistical study of the differences between QP values of CISPR 16-1-1 and maximum spectrum of RMS-A method has been performed. Moreover, the Approximated Quasi-Peak has been designed to reproduce the results of a particular digital implementation of CISPR 16-1-1; since the coefficients of the AppQP's method can be change for every implementation of CISPR 16-1-1.

The performed study has shown that there is a linear relation between the differences of CISPR 16-1-1 QP ($U_{QP,3s}[f_c]$) and maximum values of RMS-A method ($U_{max3s}[f_b]$), and the temporal distribution in the spectrogram of this last method ($U[f_b,k]$), in 3 seconds intervals. This temporal distribution is computed using two percentiles (100^{th} and 96^{th}), within the 3 seconds interval under analysis. In the following figure, this linear tendency is shown:

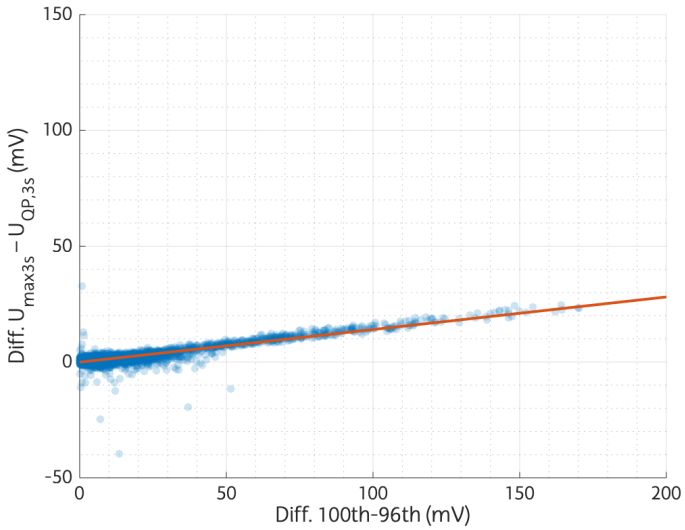

Figure 32: Linear relation between CISPR 16-1-1 QP values and 4-4-7 results and the temporal distribution of emissions over 50 signals ('Model group' and 'LV grid validation group')

The linear tendency shown in *Figure 32* could be used as a conversion procedure to obtain maximum values of RMS-A method having CISPR 16-1-1 QP results, and vice versa. Nonetheless, the strong point of this conversion procedure is to get CISPR 16-1-1 QP results with applying the RMS-A method, as this last method has a lower computational complexity. This linear tendency is the principle behind the Approximated Quasi-Peak method, which is defined by the parameters of the straight line of this linear tendency. Moreover, the coefficients of the AppQP measurement method are the coefficients of the straight line of this linear tendency.

10.2. Conversion from QP values to RMS values

Based on the principle described in the previous subsection, the linear relationship between the QP and RMS spectra defined by the parameters of the tendency line, a conversion procedure between the two spectra can be calculated.

To compute the coefficients of conversion procedure, first of all, the spectrum of the 30 signals of the 'model group' (see *Section 8.3.1*) has to be calculated. For that propose, CISPR 16-1-1 and RMS-A methods are applied in 3 seconds long periods of LV grid recodings, so as to obtain QP values ($U_{QP,3s}[f_c]$) and the conservative spectrum ($U_{max3s}[f_b]$), respectively. In addition, during the execution of RMS-A method, the spectrogram of unaggregated spectra ($U[f_b,k]$) is stored (the procedure to compute these parameters is explained in *Section 13*).

Nevertheless, as the intention of this EMI method is to estimate the Quasi-Peak spectra adapting its behaviour to detect correctly waveforms, the frequency bins that contain only noise has to be discarded. For this purpose, a threshold level of 0.5637 mV has been defined, to discard the noise values below this level in the calculations to obtain the coefficients. The noise threshold value has been defined as the 2% of the lowest CL of IEC 61000-2-2, in the frequency range between 2 kHz and 150 kHz. The minimum of Compatibility Levels in this range corresponds to 150 kHz value, whose corresponding CL limit is 89 dBµV.

$$Noise\ threshold = 2\% \cdot 10^{89\ dB\mu V/20} \cdot 10^3 = 0.5637\ mV \qquad \text{(Eq.28)}$$

The procedure in which the noise threshold is applied, and in which the frequency bins below that level are discarded, is related to the maximum spectrum of RMS-A method. Thus, the frequency bins that do not exceed that level in $U_{max3s}[f_b]$ are excluded from the analysis. In adittion, spectral samples at the same frequencies in the other stored spectra must be discarded, $U_{QP,3s}[f_c]$ (CISPR 16-1-1) and $U[f_b,k]$ (RMS-A).

Once the spectra are calculated, and noise frequency samples are discarded, the final spectra of CISPR 16-1-1 and RMS-A methods are subtracted in order to calculate the differences between values of both methods. The differences in results are only calculated for the frequencies where both methods provide results: since CISPR 16-1-1 provide results every 50 Hz (*2.05 kHz, 2.10 kHz, 2.15 kHz, … , 149.90 kHz, 149.95 kHz*) and RMS-A method every 100 Hz (*2.1 kHz, 2.2 kHz, … , 149.8 kHz, 149.9 kHz*), the frequency axis of this last method is used to compute the differences.

$$\Delta_{QP,max3s}[f_b] = U_{max3s}[f_b] - U_{QP,3s}[f_b](mV) \qquad \text{(Eq.29)}$$

where:

- $\Delta_{QP,max3s}[f_b]$ is the difference, in 3 seconds, between RMS-A method maximum spectrum and CISPR 16-1-1 Quasi-Peak spectrum,
- f_b are the frequency samples of the differences between both methods. f_b = *2.1 kHz, 2.2 kHz, … , 149.8 kHz, 149.9 kHz,*
- $U_{max3s}[f_b]$ is the maximum spectra of IEC 61000-4-7 for 3 seconds long measurement interval,
- $U_{QP,3s}[f_b]$ is the Quasi-Peak spectra of CISPR 16-1-1 for 3 seconds long measurement interval.

After calculating the difference between both methods' results, the temporal behaviour of emissions is performed. This study has to be done using the data stored in the spectrogram of unaggregated spectra of RMS-A method ($U[f_b,k]$), as explained in *Chapter 13*. The temporal distribution of waveforms is computed calculating $P_{100}[f_b]$ and $P_{96}[f_b]$, the 100th and 96th percentiles, respectively, along the temporal axis of the mentioned spectrogram for each frequency bin. The temporal distributions statistic is calculated as follows:

$$\Delta P[f_b] = P_{100}[f_b] - P_{96}[f_b]\ (mV) \quad \text{(Eq.30)}$$

where:

- $\Delta P[f_b]$ is the temporal distribution's statistic for 3 seconds long measurement intervals,
- f_b are the frequency samples. f_b = *2.1 kHz, 2.2 kHz, … , 149.8 kHz, 149.9 kHz,*
- $P_{100}[f_b]$ is the 100th percentile of $U[f_b,k]$ spectrogram along the temporal axis: $P_{100}(U_{fb}[k])$,
- $P_{96}[f_b]$ is the 100th percentile of $U[f_b,k]$ spectrogram along the temporal axis: $P_{96}(U_{fb}[k])$.

The conversion coefficients could be computed by performing the linear regression between $\Delta_{QP,max3s}$ and the subtraction of P_{100} and P_{96}. These coefficients are equal to the slope, *a*, and the y-intercept, *b*, of the straight line obtained after applying the linear regression.

$$a = \frac{\sum_{f_b=2.1\ kHz}^{149.9\ kHz} \Delta_{QP,max3s}[f_b] - b \cdot \sum_{f_b=2.1\ kHz}^{149.9\ kHz} \Delta P[f_b]}{n} \quad \text{(Eq.31)}$$

$$b = \frac{\sum_{f_b=2.1\ kHz}^{149.9\ kHz} \Delta P[f_b] \cdot \Delta_{QP,max3s}[f_b] - \frac{\sum_{f_b=2.1\ kHz}^{149.9\ kHz} \Delta P[f_b] \cdot \sum_{f_b=2.1\ kHz}^{149.9\ kHz} \Delta_{QP,max3s}[f_b]}{n}}{\sum_{f_b=2.1\ kHz}^{149.9\ kHz} \Delta P^2[f_b] - \frac{\left[\sum_{f_b=2.1\ kHz}^{149.9\ kHz} \Delta P[f_b]\right]^2}{n}} \quad \text{(Eq.32)}$$

where:

- *a* is the slope of the straight line of linear regression,
- *b* is the y-intercept of the straight line of linear regression,
- $\Delta P[f_b]$ is the temporal distribution's statistic for 3 seconds long measurement interval,
- $\Delta_{QP,max3s}[f_b]$ is the difference, in 3 seconds, between RMS-A method maximum spectrum and CISPR 16-1-1 Quasi-Peak spectrum,
- f_b are the frequency samples. f_b = *2.1 kHz, 2.2 kHz, … , 149.8 kHz, 149.9 kHz.*

The mathematical expression to perform the conversion from RMS values of RMS-A method to QP spectrum of CISPR 16-1-1 is:

$$\Delta U_{f_b,3s} = a \cdot \Delta P_{f_b} - b\ (mV) \quad \text{(Eq.33)}$$

where:

- $\Delta U_{fb,3s}$ is the conversion for each frequency bin,

- ΔP_{fb} is the temporal distribution's statistic for 3 seconds long measurement interval.
- a is the first coefficient conversion procedure (slope of the linear regression),
- b is the second coefficient of conversion procedure (y-intercept of the linear regression).

10.3. Percentiles relating QP and RMS spectra

As it has been explained, the Approximated Quasi-Peak is based on the statistical analysis of the emissions in the LV grid. The aim of this system is to model the amplitude variability of waveform with a combination of two percentiles; in order to statistically characterize each frequency bin of the recordings' spectra. These two percentile values (100^{th} and 96^{th}) were selected after considering a set ofdifferent alternatives.

In the analysis of the temporal variability of the waveforms, and also in the selection of most representative percentiles, the 30 LV grid recordings for the AppQP model (see *8.3*) have been used in this study. To choose the best percentile combination for the conversion factor's statistic variable, the goodness of fit of different linear regressions (calculated as described in *10.2*) has been computed using different percentiles combinations on each of them. In this study, the RMSE (Root Mean Square Error) has been used to evaluate the goodness of fit of linear regressions, a mathematical tool that provides the standard deviation of the data with respect to the calculated trend line.

$$RMSE = \sqrt{\frac{\sum(y_{tren\ line} - y_{data})^2}{N}} \qquad \text{(Eq.34)}$$

where:

- $RMSE$ is the Root Mean Square Error of trend line,
- $y_{trend\ line}$ are the values of the trend line; the predicted values,
- y_{data} are the values of LV grid recordings; dependant values of regressions,
- N is the number of available values to calculate the RMSE.

In addition, this analysis has also been used to choose the best configuration of CISPR 16-1-1 that best fits the Approximated Quasi-Peak methodology. It is important to mention that the parameters governing the AppQP detector change when the input data used in the linear regression change; i.e., CISPR 16-1-1 QP values. Moreover, the results of the AppQP method in the validation procedure are evaluated with respect to the specific CISPR 16-1-1 implementation defined in a previous section. Therefore, it is important to select the percentile combination and the CISPR 16-1-1 implementation that generates the lowest possible RMSE value.

In order to obtain select the best percentile combination and the CISPR 16-1-1 implementation that best fits the AppQP methodology, 34 percentile combination and 4 implementations of CISPR 16-1-1 have been chosen. The latter has been selected following the requirements explained in *Section 7.1*. Thus, two different windows are used: CISPR 16-1-1 (Lanczos kernel window function) and CISPR TR 16-3 (Gaussian window). Regarding overlaps, also two values are used: 90% (time step of 2 ms) and 95% (time step of 1 ms).

In the following figure the results of the RMSE of linear regressions for the mentioned percentiles and CISPR 16-1-1 implementations are shown:

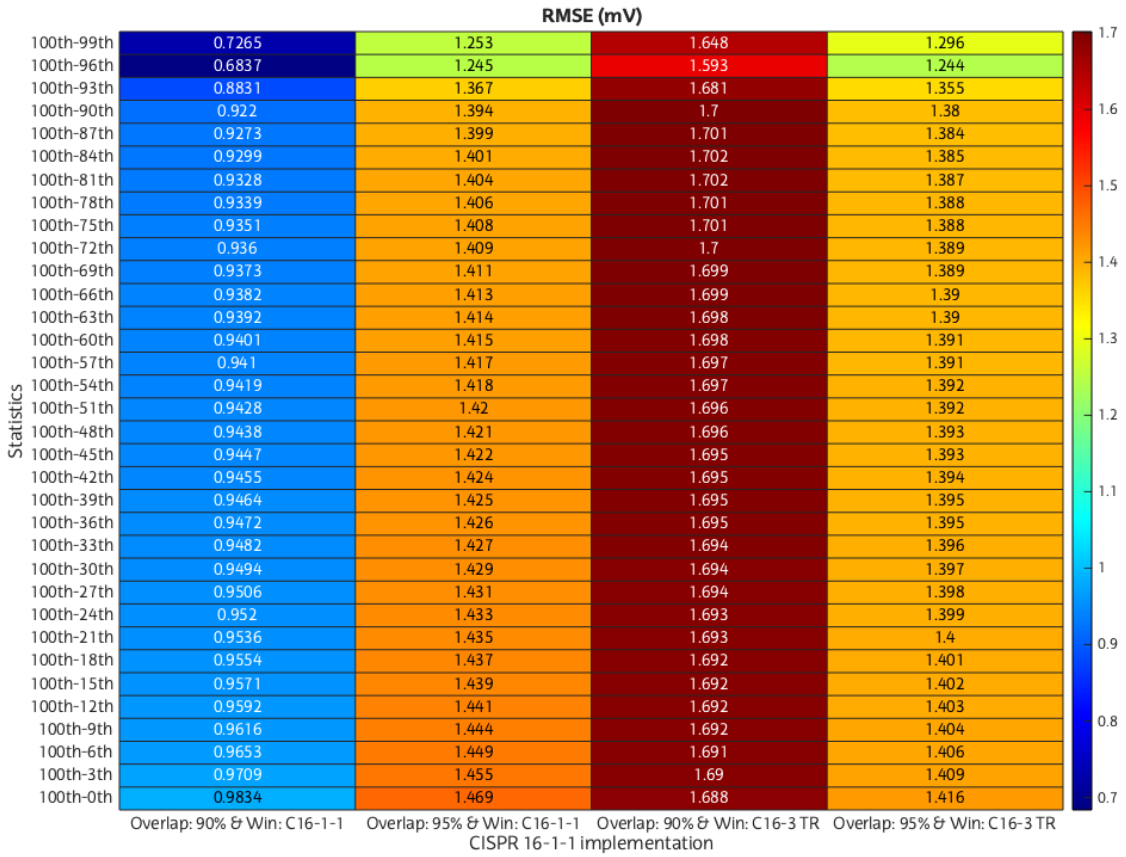

Figure 33: Root Mean Square Error (RMSE) of the linear regression for 34 combination of percentiles and 4 implementations of CISPR 16-1-1 for 'model group' recordings

As illustrated by the results in the figure above, the lowest RMSE is provided by the CISPR 16-1-1 implementation with the window described in the same standard, the Lanczos kernel window, and an overlap of a 90% (2 ms of time step). Moreover, the best statistic to model this configuration is the subtraction between 100^{th} and 96^{th} percentiles. Therefore, those parameters of the conversion factor and that particular implementation of CISPR 16-1-1 have been selected to develop the Approximated Quasi-Peak EMI measurement method.

11. Digital implementation of CISPR 16-1-1

The first of the new EMI measurement methods proposed in this work is a specific digital implementation of CISPR 16-1-1 method. This implementation will be used as a reference to create and evaluate the new EMI measurement method developed in this Master's Thesis, the AppQP.

As mentioned in *Chapter 7.1* of project, where the requirements for the digital implementation of CISPR 16-1-1 were described, this implementation follows the technical guidance described in the standard CISPR 16-1-1 and CISPR TR 16-3 (Technical Report) [6], [9]. For this reason, the values of the parameters needed to define some parts of the method, such as IIR (Infinite Impulse Response) filters (QP mechanical voltmeter and critically damped meter) or the windows for DFTs, have been chosen considering all the information in both documents mentioned above, although CISPR TR 16-3 and some annexes of CISPR 16-1-1 are informative and not normative. Nonetheless, in this digital implementation of CISPR 16-1-1 not all possible implementations described in the requirements of *Section 7.1* have been included, since the results obtained in *10.3* have been taken into account.

The mathematical expressions that describe the behaviour of the digital implementation of CISPR 16-1-1 are as follows:

Denote the sampled input signal as $x[n]$. The STFT of $x[n]$ is defined as

$$Z[f_c, k] = \sum_{n=0}^{N-1} x[n-k]w[n]e^{-j2\pi fn} \qquad \text{(Eq.35)}$$

where:

- $Z[f_c,k]$ is a spectrogram, i.e. a time series of complex values for frequency components f at time instants $k \cdot T_e$,
- T_e is the time step between successive spectra $Z[f_c,k]$ and $Z[f_c,k+1]$, determined by the window overlap,
- f_c are the frequency components,
- $w[n]$ is the sampled time domain window function,
- N is the window length in samples.

In order to compute the correct amplitude of the waveforms in spectrum, a correction coefficient has to be applied. Define the RMS amplitudes of frequency components f_c as

$$z_{f_c}[k] = \left|Z_{f_c}[k]\right| \cdot \frac{2}{\sqrt{2} \cdot \sum_{n=1}^{N} w[n]} \qquad \text{(Eq.36)}$$

where:

- $z_{fc}[k]$ are the RMS values of the DFT,
- $Z_{fc}[k]$ is a spectrogram,
- $w[n]$ is the normalized discretised window function,

- N is the number of samples of the discretised window.

It is important to mention that the timestamp t_k of $z_{f_c}[k]$ should be the centre of the input window *x[n]*.

The parameters of the reference implementation are as follows:

the window length is 20 ms, i.e. $N = 0.02 \cdot f_s$, where f_s is the sampling frequency in samples per second. Hence, the frequency components are f_c = 9050 Hz, 9100 Hz, 9150 Hz, ..., 149 950 Hz, 150 000 Hz.

the overlap of successive windows is 90 %, i.e. time step T_e = 2 ms

w[n] is a discretized window function:

$$w[n] = \frac{w'[n]}{g_c} \quad \text{(Eq.37)}$$

$$g_c = \frac{1}{N}\sum_{n=0}^{N-1} w'[n] \quad \text{(Eq.38)}$$

where:

- *w[n]* is the normalized discretised window function,
- *w'[n]* is the discretised window function,
- g_c is the coherent gain factor of the window,
- N is the number of samples of the discretised window.

The discretised window function *w'[n]* is a Lanczos kernel window function with one pair of side-lobes, whose resolution bandwidth at –6 dB (B_6) is 200 Hz and which emulates the frequency response in CISPR 16-1-1 Annex A.2 (normative)[4].

$$w'[n] = \operatorname{sinc}\left(2\left(\frac{2n}{N-1} - 1\right)\right)\operatorname{sinc}\left(\frac{2n}{N-1} - 1\right) \quad \text{(Eq.39)}$$

where:

- *w'[n]* is the discretised window function,
- N is the number of samples of the discretised window.

[4] The Lanczos kernel has been proposed by Siemens AG. Its 3dB and 6dB bandwidths align closely with the theoretical frequency response specified in normative CISPR 16-1-1 Annex A

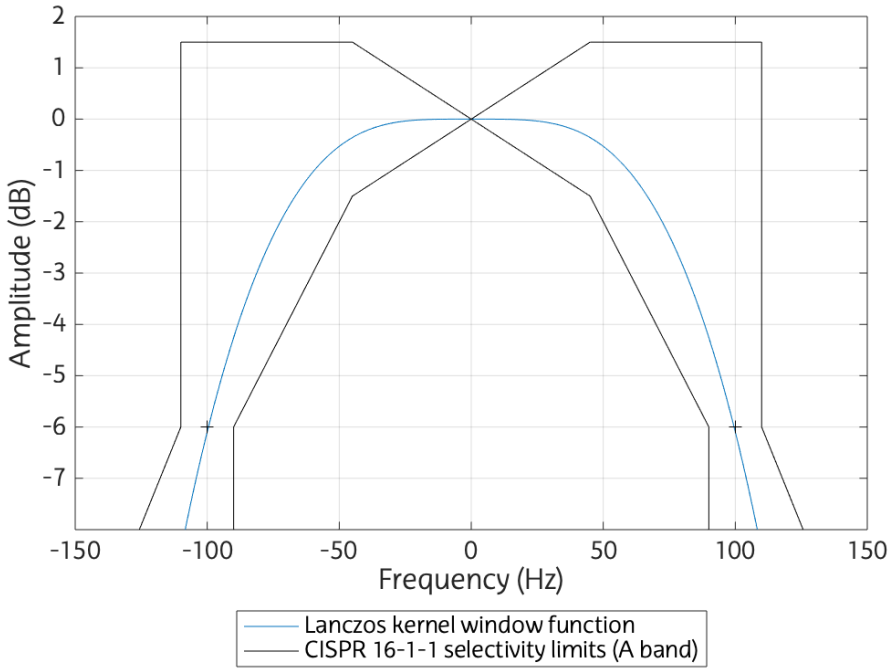

Figure 34: Frequency response of the Lanczos kernel window function

Once the DFT are computed, the $z_{fc}[k]$ have to be weighted by a digital implementation of the Quasi-Peak detector. As mentioned in *Section 6.1*, the digital Quasi-Peak detector must reproduce the physical behaviour of the electronic components it is composed of: a QP voltmeter and a critically damped meter. The first one is based on a RC circuit, implemented using a first-order linear system characterised by the electrical charging and discharging time constants. The second component of the QP detector, the critically damped meter, is deployed using a second-order linear system, whose behaviour is defined by the natural system frequency. The mentioned devices are digitally implemented using IIR filters.

Defined $u_{fc}[k]$ as the output voltage of the charging/discharging RC circuit (QP voltmeter), depending on voltage level $u_{fc}[k]$ compared to the input envelope value $z_{fc}[k]$, the charging and discharging process is modelled by a first-order IIR filter:

$$u_{f_c}[\mathrm{k}] = b_0 z_{f_c}[k] + b_1 z_{f_c}[k-1] - a_1 u_{f_c}[k-1] \qquad \text{(Eq.40)}$$

where:

- $u_{fc}[k]$ is the output voltage of the RC circuit,
- $z_{fc}[k]$ is the spectrogram of the input signal,
- b_0, b_1 and a_1 are the coefficients for the IIR filter.

If $u_{fc}[k-1] \leq z_{fc}[k]$, coefficients b_0, b_1, a_1 are set according a time constant $\tau_c = 45$ ms for charging, else if $u_{fc}[k-1] \leq z_{fc}[k]$, $b_0=0$ and b_1, a_1 are set according to a time constant $\tau_d = 500$ ms for discharging. These charging and discharging time constants have been defined according to the informative Annex H of CISPR 16-1-1. The mentioned parameters for CISPR Band A (9 kHz to 150 kHz) and a time step of 2 ms would be as shown in the following table:

Coefficients	Charging process	Discharging process
b_0	$2.1743 \cdot 10^{-2}$	0
b_1	$2.1743 \cdot 10^{-2}$	$1.9960 \cdot 10^{-3}$
a_1	$-9.5651 \cdot 10^{-1}$	$-9.9610 \cdot 10^{-1}$

Table 18: IIR filter coefficient values for the RC circuit

Nevertheless, these parameters could be calculated for any configuration and band of CISPR 16-1-1 using the bilinear approximation method, which is defined by the following equations:

The analogue cut-off frequency for the bilinear approximation parameters:

$$w_{cut-off} = 1/\tau, \quad \text{(Eq.41)}$$

where:

- $w_{cut-off}$ is the cut-off analogue frequency,
- τ is the electrical charge or discharge time constant of the RC filter.

Prewarped coefficient for the bilinear approximation:

$$s = \frac{1}{\tan\left(\frac{w_{cut-off} \cdot T_e}{2}\right)} \quad \text{(Eq.42)}$$

where:

- s is the prewarped coefficient,
- $w_{cut-off}$ is the cut off analogue frequency,
- T_e is the time step between spectra in the spectrogram.

The coefficients to calculate the output of RC circuits $u_{fc}[k]$ will be:

$$b_0 = b_1 = \frac{1}{1+s} \quad \text{(Eq.43)}$$

$$a_1 = \frac{1-s}{1+s} \quad \text{(Eq.44)}$$

where:

- b_0, b_1 and a_1 are the coefficients for the IIR filter.

The RC circuit output $u_f[k]$ is processed further with a second-order IIR filter to calculate the weighted signal envelope:

$$v_{f_c}[k] = b_{0,m}u_{f_c}[k] + b_{1,m}u_{f_c}[k-1] + b_{2,m}u_{f_c}[k-2] - a_{1,m}v_{f_c}[k-1] - a_{2,m}v_{f_c}[k-2] \quad \text{(Eq.45)}$$

where:

- $v_{fc}[k]$ is the output voltage of the critically damped meter,
- $u_{fc}[k]$ is the output voltage of the RC circuit,
- $b_{0,m}$, $b_{1,m}$, $b_{2,m}$, $a_{1,m}$ and $a_{2,m}$ are the coefficients for the IIR filter.

Coefficient values $b_{0,m}$, $b_{1,m}$, $b_{2,m}$, $a_{1,m}$ and $a_{2,m}$ are set according to an analogue angular cut-off frequency ω_n = 1/0.16 rad/s, according to informative Annex H of CISPR 16-1-1.For the A band and an overlap of 90% the mentioned coefficients would have the following values:

Coefficient	Value
$b_{0,m}$	$9.2506 \cdot 10^{-5}$
$b_{1,m}$	$1.8501 \cdot 10^{-4}$
$b_{2,m}$	$9.2506 \cdot 10^{-5}$
$a_{1,m}$	−1.9615
$a_{2,m}$	$9.6190 \cdot 10^{-1}$

Table 19: IIR filter coefficient values for the critically damped mechanical meter

However, these parameters could be calculated for any configuration and band of CISPR 16-1-1 applying bilinear transform:

The correction factor for the IIR filter is:

$$c = (2^{0.5} - 1)^{-\frac{1}{2}} \quad \text{(Eq.46)}$$

where:

- c is the correction factor of the IIR filter.

The corrected analogue cut-off frequency for the critically damped meter is:

$$f_n = \frac{w_n}{2 \cdot \pi} \cdot c \quad \text{(Eq.47)}$$

where:

- f_n is the analogue cut-off frequency,
- c is the correction factor of the IIR filter,
- w_n the analogue angular cut-off frequency.

The digital angular cut-off frequency:

$$w_0 = \tan(\pi \cdot f_n \cdot T_e) \quad \text{(Eq.48)}$$

where:

- w_0 is the digital angular cut-off frequency,

- f_n is the corrected analogue cut-off frequency,
- T_e is the time step between spectra in the spectrogram.

The second-order IIR filter coefficients, which are calculated from the bilinear transform and are used in the calculation of the critically damped detector output $v_f[k]$, will be:

$$b_{0,m} = b_{2,m} = \frac{w_0^2}{w_0^2 + 2 \cdot w_0 + 1} \quad \text{(Eq.49)}$$

$$b_{1,m} = 2 \cdot b_{0,m} \quad \text{(Eq.50)}$$

$$a_{1,m} = -2 \cdot b_{0,m} \cdot \left(\frac{1}{w_0^2} - 1\right) \quad \text{(Eq.51)}$$

$$a_{2,m} = -\left(1 - \left(b_{0,m} + b_{1,m} + b_{2,m} - a_{1,m}\right)\right) \quad \text{(Eq.52)}$$

where:

- $b_{0,m}$, $b_{1,m}$, $b_{2,m}$, $a_{1,m}$ and $a_{2,m}$ are the coefficients for the IIR filter.
- w_0 is the digital angular cut-off frequency.

Finally, the QP values are obtained computing the maximum value of the weighed envelope per frequency bin.

$$U_{QP}[f_c] = \max_k(v[f_c, k]) \quad \text{(Eq.53)}$$

where:

- $U_{QP}[f_c]$ is the Quasi-Peak spectrum,
- $v[f_c,k]$ is the output voltage of the critically damped meter.

12. RMS-A: IEC 61000-4-7 method adapted to CISPR Band A

This new EMI method, the RMS-A method, is based on IEC 61000-4-7 – Annex B informative method, in which some changes have been performed, to consider requirements of higher frequencies emissions. The schematic in *Figure 35* shows a diagram of the operation of this EMI method.

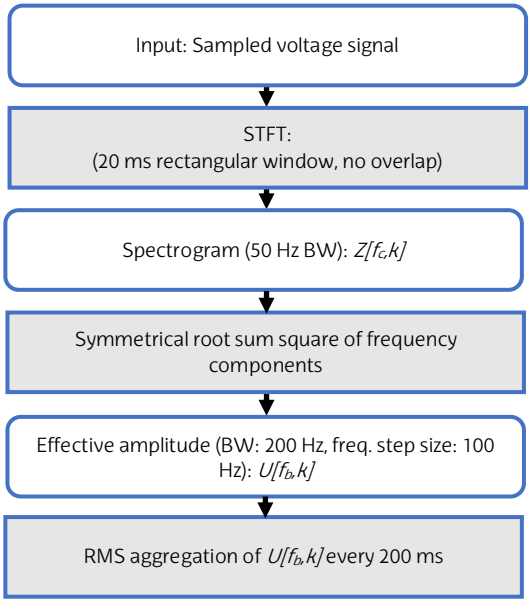

Figure 35: Schematic overview of the RMS-A method

The informative method described in Annex B of IEC 61000-4-7 standard has been adapted to the particularities of the CISPR Band A (9 kHz – 150 kHz) and the requirements of waveforms of this band. In addition, this method is the basis for the AppQP method (see *Section 13*), whose results must be comparable to QP detector, as defined in CISPR16-1-1. These requirements determine some relevant aspects in the evolution of the IEC 61000-4-7 method.

- A sorter window length is proposed. In this method a 20 ms rectangular windows, instead of 200 ms, are used to compute the STFT (Short-Time Fourier Transform) of the input signal, whose output frequency components would have a ResBW and a FSS of 50 Hz. For this reason, the spectrum samples are grouped into 200 Hz bins, in order to obtain values with a RBW of 200 Hz.

- A symmetrical grouping of frequency components of the STFT is proposed, with the aim of obtaining a proper assignment of the waveforms in frequency.

- To avoid the 'picket fence effect', a 100 Hz frequency step between adjacent frequency bins is proposed.

- RMS aggregation of spectra every 200ms is proposed, in order to ensure that this new method for the 9 kHz – 150 kHz range is aligned to the IEC 61000-4-7 for the range 2 kHz – 9 kHz..

The mathematical expressions to obtain the spectra of the emissions with the RMS-A method are the following:

The rectangular window used to compute STFT is defined as:

$$w[n] = 1, \qquad 1 < n < N \tag{Eq.54}$$

where:

- $w[n]$ is the sampled time domain window function,
- N is the window length in samples, $N = f_s \cdot T_w$,
- T_w is the window length, $T_w = 20\ ms$,
- f_s is the sampling frequency of the input signal.

The STFT is applied as

$$Z[f_c, k] = \sum_{n=0}^{N-1} x[n-k] \cdot w[n] \cdot e^{-j2\pi f_c n} \tag{Eq.55}$$

where:

- $Z[f_c,k]$ is a spectrogram, i.e. a time series of complex values for frequency components f_c at time instants $k \cdot T_e$,
- $x[n]$ is the digitized input signal in the temporal domain.
- T_e is the time step between successive spectra $Z[f_c,k]$ and $Z[f_c,k+1]$, determined by the window length (T_w), as there is no overlap between windows,
- f_c are the frequency components with a frequency step size of 50Hz, $f_c = 2.00\ kHz, 2.05\ kHz, 2.10\ kHz \ldots 150.00\ kHz$.

In order to compute the correct amplitude of the waveforms in spectrum, a correction coefficient has to be applied.

$$z_{f_c}[k] = \left|Z_{f_c}[k]\right| \cdot \frac{2}{\sqrt{2} \cdot \sum_{n=1}^{N} w[n]} \tag{Eq.56}$$

where:

- $z_{fc}[k]$ are the RMS values of the DFT,
- $Z_{fc}[k]$ is a spectrogram,
- $w[n]$ is the window function,
- N is the number of samples of the window.

The amplitude values in $z[f_c,k]$ are grouped to obtain bands of 200 Hz resolution bandwidth, for coherence with IEC 61000-2-2 and IEC 61000-4-7. Grouping is applied by means of a symmetrical RSS (Root Sum Square) of adjacent frequency components of $z[f_c,k]$. This grouping procedure is applied each 100 Hz, from 2.1 kHz to 149.9 kHz.

$$U_k[f_b] = \sqrt{\frac{1}{2} \cdot z_k^2[f_b - 100\ Hz] + \sum_{f=f_b-50\ Hz}^{50\ Hz} z_k^2[f] + \frac{1}{2} \cdot z_k^2[f_b + 100\ Hz]} \quad \text{(Eq.57)}$$

where:

- $U_k[f_b]$ is the STFT data grouped every 100 Hz with a resolution bandwidth of 200 Hz,
- f_b are the frequency bins distanced 100 Hz, f_b = 2.1 kHz, 2.2 kHz, 2.3 kHz ... 149.9 kHz.

Grouped RMS measurement values per frequency bins are aggregated over time every 200 ms:

$$U_{f_b,rms}[i] = \sqrt{\frac{1}{M} \cdot \sum_{k=i-100\ \text{ms}}^{i+90\ \text{ms}} U_{f_b}^2[k]} \quad \text{(Eq.58)}$$

where:

- $U_{fb,rms}[i]$ is the RMS value aggregated every 200 ms,
- i are the time instants of $U_{fb,rms}[i]$, i = *0.1 s, 0.3 s, 0.5 s ... 2.9 s*
- M is the number of samples that have to be aggregated. M = *200 ms / 20 ms = 10*

13. Approximated Quasi-Peak

The Approximated Quasi-Peak, or AppQP, is the new EMI measuring method to obtain the spectrum of Non-Intentional Emissions measured in the Low-Voltage grid. This method, which has been created and described within this work, has been designed thanks to the participation of TSR research group in the SupraEMI consortium.

It is important to mention that all the results shown in this section have been presented in numerous SupraEMI project meetings, which have been endorsed by the experts of the European consortium in charge of proposing new EMI method standards. Therefore, the results that will be shown in the following subsections have been reviewed and accepted by professionals of accredited research solvency in the field in which this Master's Thesis is framed.

In addition, part of the results has been defended in three meetings of the international working group IEC SC77A WG9 of International Electrotechnical Commission (IEC), which is in charge of the redefinition of Annex C of IEC 61000-4-30 standard and the proposal of a new method for the frequency range 2 kHz – 150 kHz.

13.1. AppQP: Description of the measurement method

The AppQP is a novel NIE measument method based on the statistical variability of the signal over time, instead of the specifications that define the response of a specific electronic circuit. This approach is linked to the digital implementation of CISPR 16-1-1 described in *Section 11*; therefore, the results obtained with AppQP are comparable with those from the digital implementation of CISPR 16-1-1.

This new EMI method is based on RMS-A method described in *Section 12*. In order to calculate the Approximated Quasi-Peak results, the conservative spectrum of the RMS-A method has to be computed, which is obtained using the maximum detector on the spectra, and the conversion factor of AppQP is subtracted. This parameter is calculated for each frequency bin of the spectrum, performing a statistical analysis based on two percentiles over the time samples of the spectrogram linked to them.

The AppQP is an empirical EMI method, which has been designed using different LV grid signals, as it is explained in *Section 8.3*, to characterise the level of high amplitude emissions properly.

This empirical approach is because only frequency bins with a level above 0.5637 mV (maximum spectrum of RMS-A method) are considered in this method, as explained in *Section 10.1.*

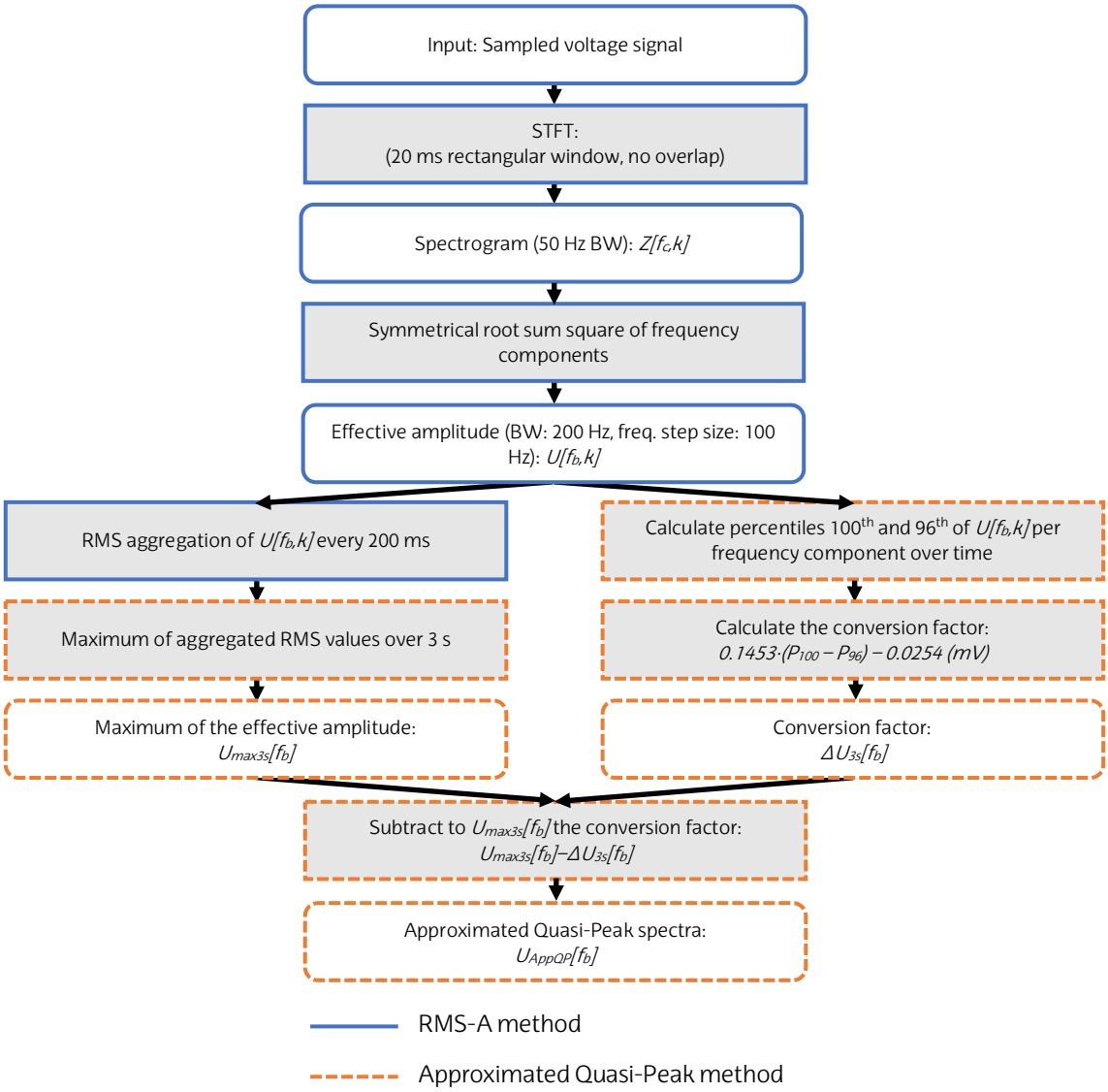

Figure 36: Schematic overview of the Approximated Quasi-Peak method

Once the spectra are obtained applying the RMS-A method, the Approximated Quasi-Peak procedure would be used. The method is based on the subtraction of a fraction of the maximum of the aggregated spectra, $U_{rms}[f_b,k]$, which depends on the statistical variation of the signal. This quantity is calculated as a conversion factor of the unaggregated spectra, $U[f_b,k,]$ in 3 seconds. This calculation is based on the subtraction of two percentiles (100th and 96th, respectively) of the unaggregated spectra, whose resultant values have to be multiplied by two conversion coefficients.

The mathematical expressions which describe the behaviour governing the AppQP method are as follow:

To determine AppQP values, the maximum of the RMS values over 3 seconds is calculated as

$$U_{f_b,max_{3s}} = \max_i(U_{f_{b,,rms}}[i]) \qquad \text{(Eq.59)}$$

where:

- $U_{fb,max3s}$ is the maximum of grouped amplitudes per frequency bin,

- *i* are the time instants of $U_{fb,rms}[i]$. i = 0.1 s, 0.3 s, 0.5 s ... 2.9 s

Additionally, the conversion factor ΔU_{f_c} is calculated for each frequency bin every 100 Hz, based on the subtraction of 100th and 96th percentiles of the values of $U_k[f_b]$ for a 3s period. The values used in the following equation have been calculated following the procedure described in sections *10.2* and *10.3*.

$$\Delta U_{f_b,3s} = 0.1453 \cdot \left(P_{100}\left(U_{f_b}[k]\right) - P_{96}(U_{f_b}[k])\right) - 0.0254\ (mV) \quad \text{(Eq.60)}$$

where:

- $\Delta U_{fb,3s}$ is the conversion factor for each frequency bin,
- P_{100} and P_{96} are the 100th and 96th percentiles of $U_{fb}[k]$ over time, respectively.

The AppQP values are obtained by subtracting the conversion factor from the maximum of effective amplitudes of each frequency component:

$$U_{AppQP}[f_b] = U_{max_{3s}}[f_b] - \Delta U_{3s}[f_b] \quad \text{(Eq.61)}$$

where:

- $U_{AppQP}[f_b]$ is the Approximated Quasi-Peak spectrum,
- f_b are the frequency bins of $U_{AppQP}[f_b]$, f_b = 2.1 kHz, 2.2 kHz, 2.3 kHz ... 149.9 kHz
- $U_{max3s}[f_b]$ is the maximum of aggregated spectra of RMS-A method,
- $\Delta U_{3s}[f_b]$ is the conversion factor for each frequency bin.

As mentioned before, the results of AppQP are only going to be valid when the level of frequency bins of U_{max3s} have an amplitude higher than 0.5637 mV.

13.2. Validation of AppQP: statistical study to assess the accuracy of AppQP

In the following subsections, the results of the procedure to calculate the statistics assessing accuracy are explained. As described in *Section 3.2,* both the SupraEMI and IEC77A WG9 working groups are specialists in PQ metrology. Consequently, the professionals who compose these task forces demand a thorough and detailed statistical study to support the accuracy of the obtained results. A summary of the results of this validation procedure, already presented in SupraEMI consortium and IEC SC77A WG9 in several meetings, is described in the following paragraphs.

13.2.1. Results of statistics assessing accuracy for LV grid recordings

In this section, the accuracy of the results of the Approximated Quasi-Peak method for the entire frequency band (2 kHz to 150 kHz), tested with recordings measured in the LV grid, is explained.

As described in *8.3*, in the validation procedure of the AppQP method, 29 signals recorded in the LV grid are used. These recordings were divided into two specific groups, due to the characteristics of the waveforms of the recordings; for this reason, two validation procedures have been carried out. The first group, the 'LV grid validation group', is composed of 20 signals recorded in the LV grid, which are used in this section to assess accuracy.

Although in this analysis the whole spectrum from 2 kHz to 150 kHz has been studied, in this work all the frequency bins which contain only electromagnetic noise are discarded following the criteria described in *Section 10.1*. In this study, the parameters for assessing accuracy are those described in *Section 8.4*.

The statistics assessing accuracy for the spectrum of AppQP are computed. In this case, $U_{QP}[f_b]$ and $U_{AppQP}[f_b]$ are the spectra that are compared, and from which the accuracy statistics will be obtained.

Statistics assessing accuracy for Approximated Quasi-Peak method 'LV grid validation group'		
1.	Average relative difference	1.273 %
2.	Median relative difference	2.170 %
3.	Standard deviation of relative difference	11.227 %
4.	Average absolute difference	0.138 mV
5.	Median absolute difference	0.030 mV
6.	Standard deviation of absolute difference	0.679 mV
7.	Average relative difference from absolute values	8.414 %
8.	Median relative difference from absolute values	6.427 %
9.	Percentage of differences within ±2% of Compatibility Levels	100.000 %
10.	Percentage of differences within ±10% of Compatibility Levels	99.717 %

Table 20: Statistics assessing accuracy for Approximated Quasi-Peak method with 'LV grid validation group'

As illustrated in the above table, the AppQP has a good perfomance on the obtained spectra; since it provides results very close to those of the CISPR 16-1-1. Furthermore, the statistics evaluating the absolute differences are below a millivolt and the relative differences below 10%; therefore, the spectra obtained with both methods are very similar. Moreover, in the three statistics where a minimum threshold has been defined, the criterion has been fulfilled.

In order to develop a more detailed analysis of the Approximated Quasi-Peak method, the absolute differences for the frequency bins of each signal are calculated and shown in *Figure 37*. The difference for the whole set of the signals has been also calculated and displayed in the graph. In this plot, the distribution, in mV, of the differences between CISPR 16-1-1 method's QP and AppQP results is shown in a boxplot. This type of graph shows the distribution of the represented values, for each data set, by a box and whiskers. The box is limited by the 25^{th} and 75^{th} percentiles of the dataset, and the whiskers cover all values but the outliers [27]. This way of expressing the results gives an indication of how the AppQP results spread, and therefore, how accurate the developed EMI method is.

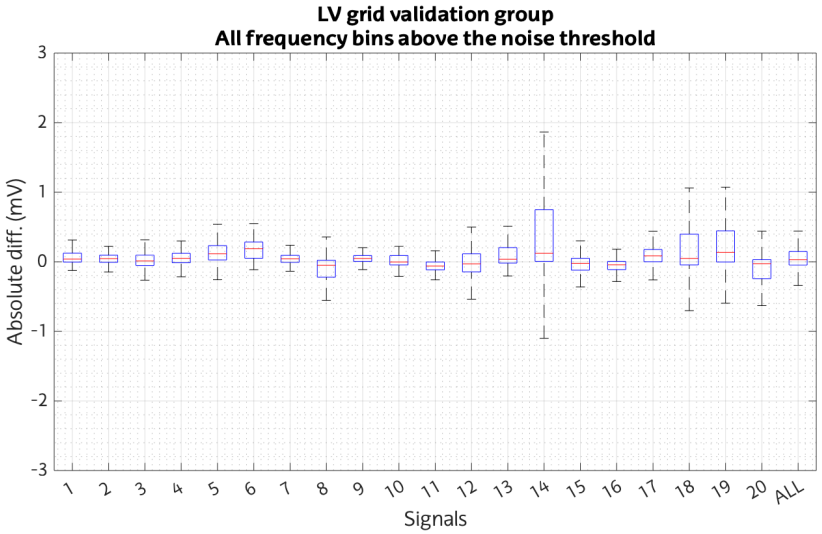

Figure 37: Boxplot of the absolute differences between AppQP and CISPR 16-1-1 QP for 'LV grid validation group' signals

As it can be seen in the figure above, the dispersion of the absolute differences in the 'LV grid validation group' has, in general, a positive sign. Therefore, the results obtained are not conservative, as the QP values of CISPR 16-1-1 are higher than those of the AppQP. Nevertheless, the obtained results are in the order of a few millivolts; thus, the deviation of the method is not very large.

13.2.1. Results of statistics assessing accuracy for PV and EV interter recordings

A similar study to the one carried out in the previous section is performed in this chapter. On this occasion, the remaining 9 signals for the validation phase not used previously are process to assess the accuracy of the AppQP method. These signals, labelled as 'PV and EV validation group', were directly measured in the POC of PV inverters and EV chargers. For this reason, the spectral nature of the waveforms may be different, and further validation is performed; moreover, as these devices are well-identified sources of high-level emissions, it is interesting to evaluate them separately.

The accuracy of the EMI measurement methods described in this Master's Thesis is calculated for all the frequency bins above the noise threshold of each group of signals. In the study described bellow, the statistics described in *Section 8.4* are used. The outcomes of the evaluation are shown in the following table.

Statistics assessing accuracy for Approximated Quasi-Peak method 'PV and EV validation group'		
1.	Average relative difference	– 14.203 %
2.	Median relative difference	– 4.865 %
3.	Standard deviation of relative difference	25.843 %
4.	Average absolute difference	– 0.291 mV
5.	Median absolute difference	– 0.069 mV
6.	Standard deviation of absolute difference	2.893 mV
7.	Average relative difference from absolute values	17.073 %
8.	Median relative difference from absolute values	7.153 %
9.	Percentage of differences within ±2% of Compatibility Levels	99.866 %
10.	Percentage of differences within ±10% of Compatibility Levels	98.287 %

Table 21: Statistics assessing accuracy for Approximated Quasi-Peak method with 'PV and EV validation group'

As shown in *Table 21*, the results of the AppQP method are similar to those obtained in the previous section, although the input signals are different. As the statistical results show, the differences between AppQP and CISPR 16-1-1 are very small, because the spectra of PV inverters and EV chargers are very similar. In addition, the statistics evaluating absolute differences are within a few millivolts and relative differences below 10%. Moreover, in all three statistics where a minimum threshold has been defined, the criterion has been met.

When comparing the results for both sets of signals, i.e. the results of this and the previous section, it is observed that the AppQP has different behaviour with different input signals containing distinct emission types. The results of the 'LV grid validation group' show that the results of the AppQP method for this input signals are not as good as for LV grid recordings. This is because Approximated Quasi-Peak is a method that relies on the temporal variability of the signals; if the emissions of these signals have little or no variability in amplitude over time, AppQP method's conversion factor does not apply large changes to the spectrum provided by the RMS-A . Nevertheless, the results obtained for the 1, 2, 4 and 5 statistics show that the results obtained are conservative. In this type of waveforms, it is important to overestimate the results, as these emissions are of very high amplitude and may be closer to the CL.

The dispersion of the absolute differences is shown below by means of a figure containing the boxplots of this parameter for each signal.

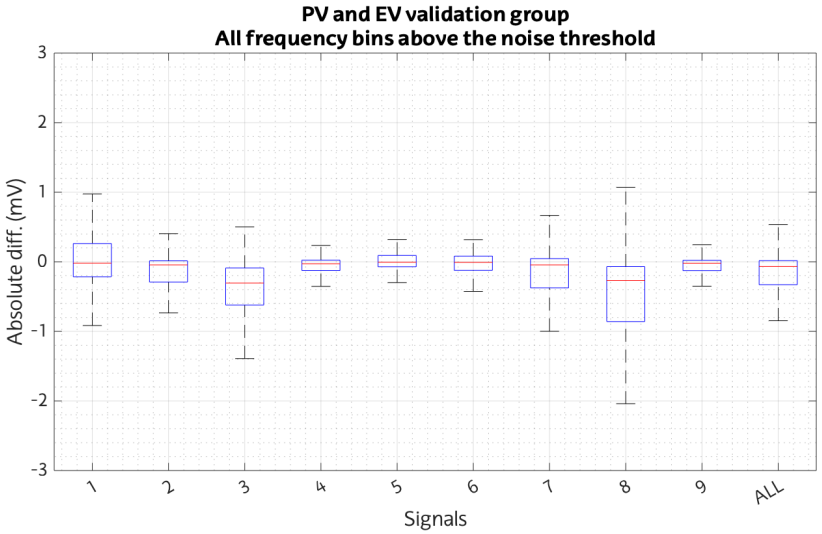

Figure 38: Boxplot of the absolute differences between AppQP and CISPR 16-1-1 QP for 'PV and EV validation group' signals

As expected, the results for the 'PV and EV validation group' signals are slightly higher than the results for LV gid signals, although they do not differ much for the other group of signals. On the contrary, the 'PV and EV validation group' gives a conservative result, since a large percentage of the boxes in the boxplots are on the negative side of the graph.

In summary, it can be concluded that the results for all frequency bins above the electromagnetic noise are within the set limits, and they demonstrate that the AppQP method is an accurate NIE measurement method.

13.2.2. Results of statistics assessing accuracy for 50 frequency bins per signal with highest level

As discussed in the previous sections, when developing an approximate method for EMI measurements it is important to deploy a method to obtain conservative results to ensure that these values are higher than the actual level when compared to the CL. This would mean that if the same waveform were measured with a more accurate method, such as CISPR 16-1-1, the results of the last method would provide a lower amplitude value. This section of the results will verify the behaviour of the method for the highest amplitude emissions; knowing that it is important for the method to be conservative in the higher-level emissions of each signal, since these will be the waveforms closest to overpassing the CL.

To study the behaviour of the AppQP for the highest emissions, the 50 frequency bins with higher levels of every recording are chosen. With these selected data, a similar statistical analysis to evaluate the accuracy is applied (see *Section 8.4*) and the accuracy criteria defined in *Section 8.4.1* of this validation procedure are maintained.

The statistics assessing accuracy for the 50 frequency bins with the highest levels per signal are as follow:

Statistics assessing accuracy for AppQP method -50 freq. bins with the highest level 'LV grid validation group'	
1. Average relative difference	3.127 %
2. Median relative difference	3.336 %
3. Standard deviation of relative difference	7.729 %
4. Average absolute difference	0.617 mV
5. Median absolute difference	0.204 mV
6. Standard deviation of absolute difference	1.743 mV
7. Average relative difference from absolute values	6.152 %
8. Median relative difference from absolute values	4.631 %
9. Percentage of differences within ±2% of Compatibility Levels	100.000 %
10. Percentage of differences within ±10% of Compatibility Levels	99.600 %

Table 22: Statistics assessing accuracy for 50 frequency bins with the highest level per signal in the Approximated Quasi-Peak method with 'LV grid validation group'

Statistics assessing accuracy for AppQP method - 50 freq. bins with the highest level 'PV and EV validation group'	
1. Average relative difference	– 6.273 %
2. Median relative difference	– 0.161 %
3. Standard deviation of relative difference	20.993 %
4. Average absolute difference	– 0.988 mV
5. Median absolute difference	-0.018 mV
6. Standard deviation of absolute difference	9.995 mV
7. Average relative difference from absolute values	10.906 %
8. Median relative difference from absolute values	5.167 %
9. Percentage of differences within ±2% of Compatibility Levels	99.333 %
10. Percentage of differences within ±10% of Compatibility Levels	96.222 %

Table 23: Statistics assessing accuracy for 50 frequency bins with the highest level per signal in the Approximated Quasi-Peak method with 'PV and EV validation group'

As shown in *Table 22* and *Table 23*, the precession results of AppQP method for the 50 frequency bins with the highest level are in the same order of magnitude as the results for all frequency bins above the noise threshold. However, certain parameters show the performance of the method for the highest emissions is not as good as for the overall, for example, the standard deviation of absolute difference or average absolute difference. On the contrary, other statistics demonstrate a better accuracy of the Approximated Quasi-Peak, such as average and median relative difference from absolute values or standard deviation of relative difference. Nevertheless, these

results were expected, since the absolute differences increase for the highest amplitudes, while the relative differences decrease due to be related to higher values . In contrast, all the uncertainty values are below the defined limits, following the criteria described in *8.4.1*.

The dispersion of the absolute differences of the Approximated Quasi-Peak values is shown in the form of boxplots in the graphs below (notice that vertical axis shows a different scale).

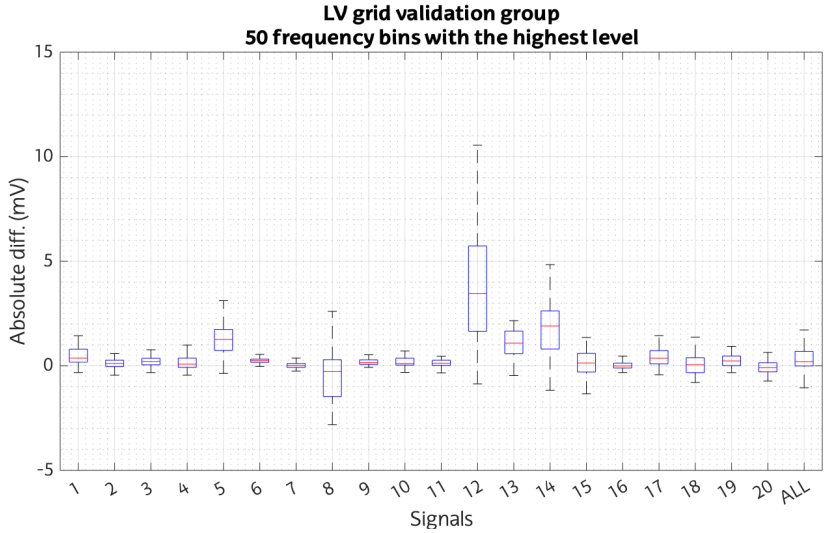

Figure 40: Boxplot of the absolute differences between AppQP and CISPR 16-1-1 QP for 50 frequency bins with the highest level for 'LV grid validation group' signals

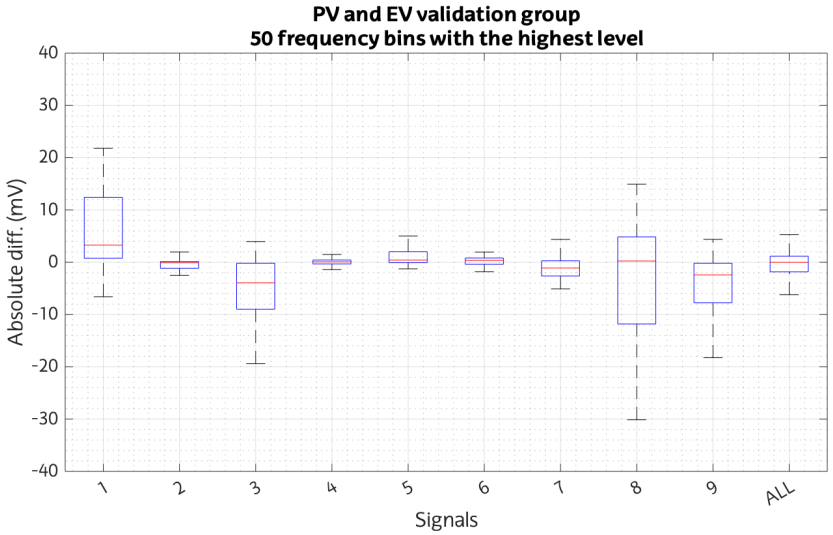

Figure 39: oxplot of the absolute differences between AppQP and CISPR 16-1-1 QP for 50 frequency bins with the highest level for 'PV and EV validation group' signals

As shown in the previous graphs, the dispersion of the differences between CISPR 16-1-1 and AppQP methods is higher in this study. The results of the new method depend on the type of waveforms that are analysed; since the differences for signals directly measured in the POC of PV inverters and EV chargers are higher. As explained before, this is due to the shape of these waveforms, of higher amplitudes and narrower bandwidths. As in the case of the 'PV and EV validation group', the results are placed at the bottom of the graph, indicating that the results are conservative. Nonetheless, the dispersion of values is in the range of a few millivolts.

To sum up, the results for the highest amplitude emissions are within the accuracy limits and are acceptable for an approximate NIE measurement method as AppQP.

13.3. Analysis of the sources of the differences between AppQP and CISPR 16-1-1 spectrum

In order to evaluate the performance of the proposed EMI measurement method, an analysis of certain cases where the spectrum differs from the reference method (the digital implementation of CISPR 16-1-1, described in *11*) has been developed. In this analysis, the differences in the results of both methods were analysed, identifying the causes and the effect of the processing procedures of the proposed method.

In this analysis, four different sources of differences have been identified and evaluated: rectangular window's leakage, picket fence effect, variation of amplitude within the 50 Hz period and waveforms with low amplitude variability over time. The main outcomes of this analysis are described in the following sections.

13.3.1. Rectangular window's leakage

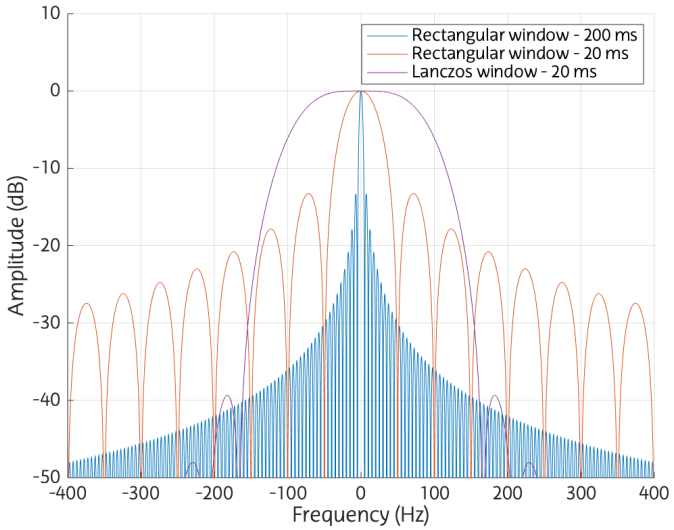

Figure 41: Spectral shape of rectangular windows and Lanczos window

As mentioned in *Section 13*, the RMS-A method, in which the AppQP is based on, uses 20 ms rectangular window to compute DFTs. This window generates high-frequency variations in the spectra of the analysed signal, since the spectrum of the rectangular window function has high amplitude sidelobes. Consequently, the effect of this characteristic is that the energy of each frequency bin is spread to the adjacent frequencies, and therefore, altering the power measured for each frequency bin, and increasing the error floor of the method. The shorter the temporal duration of the window, the higher the distortion in the spectrum of the analysed signal generated by the sidelobes of rectangular windows. For this reason, the resultant noise floor is higher with 20 ms windows (window length used by RMS-A and AppQP method), than with 200 ms windows (window length used by IEC 61000-4-7 method). This source of interference is an intrinsic characteristic of the rectangular window; therefore, it is unavoidable. In signal processing, this phenomenon is known as leakage [23], [28].

As shown in the figure above, the sidelobes of the 200 ms rectangular window are spectrally narrower, and its amplitude decrease with a smaller increase of frequency. The sidelobes of the

20 ms rectangular window are wider and their amplitude is higher than 200 ms ones. Regardless the window length, the rectangular window shows considerable sidelobes compared to the Lanczos window.

The leakage of the rectangular window has a particularly noticeable effect on narrowband waveforms of amplitude greater than the surrounding emissions. Nonetheless, in broadband emissions, or those that do not show a steep slope, the behaviour of this window is quite good.

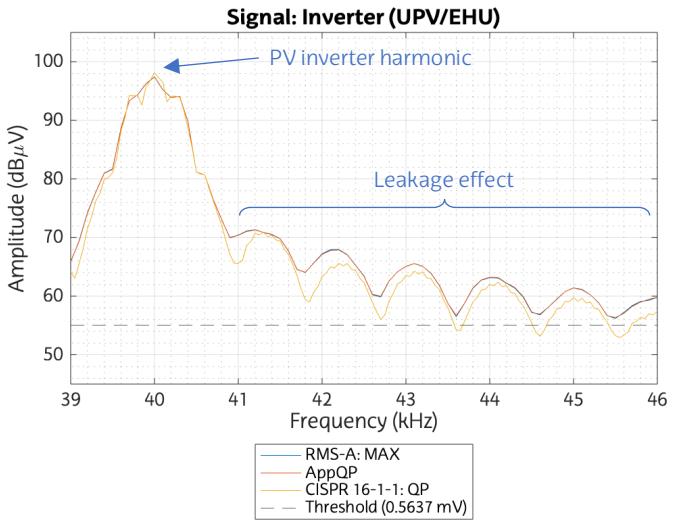

Figure 42: Effect of the leakage of the rectangular window on 'Inverter' signal

Figure 42 shows the effect that the leakage of the rectangular window generates on signals containing high amplitude waveforms surrounded by low amplitude emissions. The signal shown in *Figure 42* was recorded at the POC of a PV inverter. This device generates high-level harmonics of the switching frequency with very stable amplitude over time. In this figure, the harmonic frequency is 40 kHz, and waveforms above that frequency have amplitudes at least 30 dB lower, which in linear scale represents an amplitude 68% lower. In these waveforms, the leakage effect is noticable, since their amplitude is higher when measured with AppQP method than with the digital implementation of CISPR 16-1-1 method.

When these emissions are not of high amplitude and the slope of the emissions is not so steep, the behaviour of the AppQP (above the defined threshold) is in line with the QP results of CISPR 16-1-1, as can be seen in *Figure 43*.

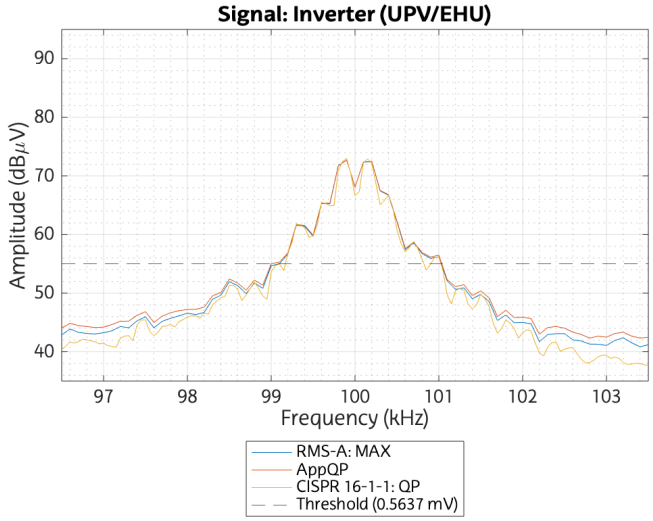

Figure 43: Waveform on 'Inverter' signal

13.3.2. Picket fence effect

The picket fence effect is a common phenomenon in signal processing, mainly with the use of DFT. As the FFT provides values distanced by the FSS, some spectral information can be missed, because only those frequencies related to the DFT provide information. This effect is especially noticeable in narrowband emissions, whose bandwidth is smaller than the FSS of the FFT. A graphical description of the picket fence effect can be seen in *Figure 45*: part of the spectral information (the red line behind the fence) is not be represented by the FFT (black dots in the figure). Furthermore, the linear interpolation obtained from the results of the FFT (green dashed line in the figure) does not match the real spectrum. As a result, fast variations in frequency that lie "behind the picket fence" are not detected, and they will not be included in the analyses derived from this result, which implies that some emissions can be underestimated.

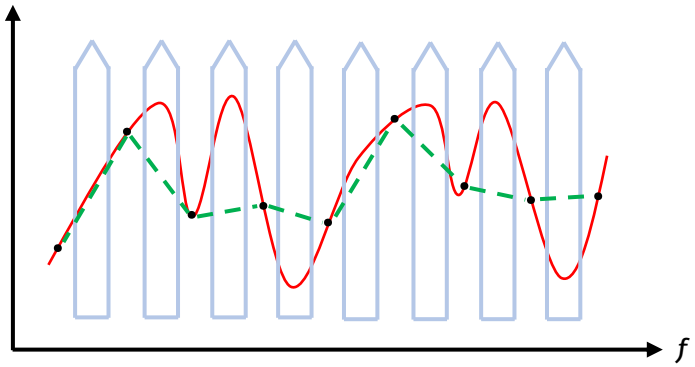

Figure 45: Graphical representation of the picket fence effect

The picket fence effect is remarkable in the comparison of the QP results of the AppQP method and digital CISPR 16-1-1, since they have different FFS (100 Hz and 50 Hz, respectively). This results in emissions that are identified by CISPR 16-1-1, but not detected by the AppQP method. As a representative example, in *Figure 44*, the picket fence effect is shown in the frequency bins adjacent to the centre frequency of the emission.

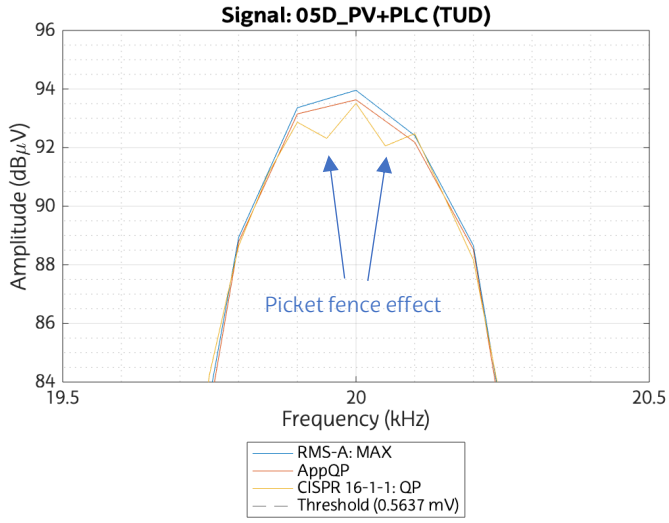

Figure 44: Picket fence effect on "05D_PV+PLC' signal

13.3.3. Variation of the amplitude within the 50 Hz cycle

There are many different types of emissions in the LV grid: impulsive emissions, broadband emissions, periodic emissions, coloured noise, etc [22]. Some of them are linked to the 50 Hz power signal, for example, varying their amplitude within the period of the 50 Hz sinewave. Thus, the amplitude variations of some of the emissions change within 20 ms of the 50 Hz electrical signal period (see *Figure 46*).

As mentioned in *Section 13*, the AppQP method uses 20 ms rectangular windows to calculate the DFT; therefore, the potential variability of the emissions within the 50 Hz period is integrated when calculating the spectrum. Furthermore, in this method, there is no overlap between adjacent windows. These two circumstances make AppQP method unable to detect variations within the 50 Hz cycle. On the contrary, the overlap used by CISPR 16-1-1 methods allows the detection of these sub-cycle variations. For this reason, there are certain waveforms where the AppQP method underestimates their amplitudes, while the CISPR 16-1-1 method gives higher

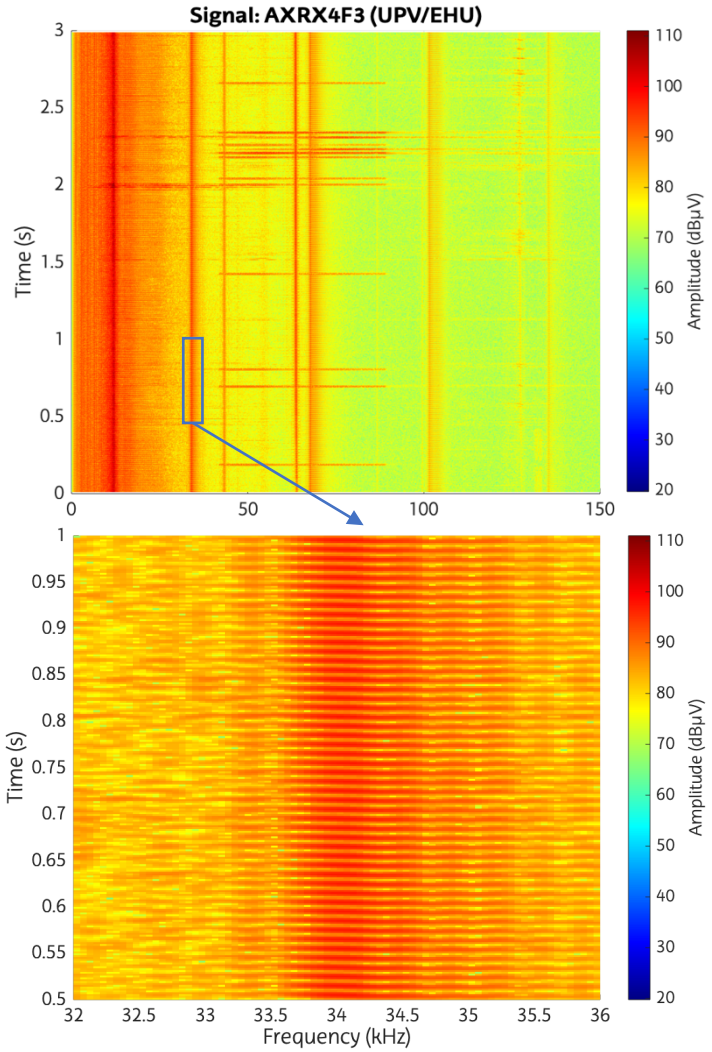

Figure 46: (Up) Spectrogram of the 'AXRX4F3' signal; (bottom) detail of the recording, where the cariations within the 20 ms mains period can be observed.

amplitude values. To illustrate this effect, the *Figure 46* shows a waveform with some variability within the 50 Hz cycle, and the *Figure 47* shows that the results provided by CISPR 16-1-1 method are of higher amplitude than those obtained by the AppQP method.

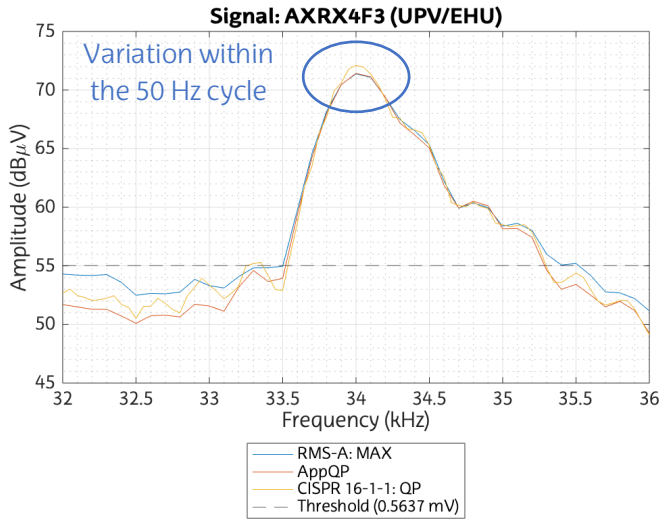

Figure 47: Effect of variation within the 50 Hz cycle on 'AXRX4F3' recording

13.3.4. Waveforms with low amplitude variability over time

As mentioned in *13.3.3*, there is a wide variety of emissions in the LV grid with very different characteristics. One of these types of emissions shows constant amplitude over time, which are very common in the harmonics of the switching frequencies generated by PV inverters and EV chargers.

As already described, the AppQP method is based on a statistical analysis of the amplitude variability of emissions over time, by a detector that applies a conversion factor based on this variability. Hence, in case that the emissions have no amplitude variability over time, the conversion factor does not apply any correction to the spectrum obtained with the RMS-A. This circumstance, combined with other sources of error (such as the leakage generated by the rectangular window), causes that the results provided by the AppQP method are higher than the results from the digital CISPR 16-1-1 method. This aspect can be observed in the following figure.

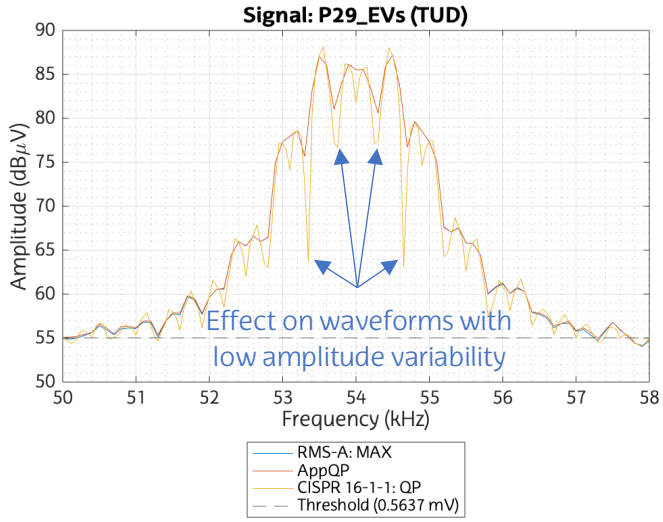

Figure 48: Harmonic with low amplitude variability on 'P29_EVs' signal

Nevertheless, the AppQP method performs well with waveforms with high amplitude variability over time. An example is the PLC transmission bursts, which do not have a constant amplitude over time, as they are present in the grid when the smart meters transmit data.

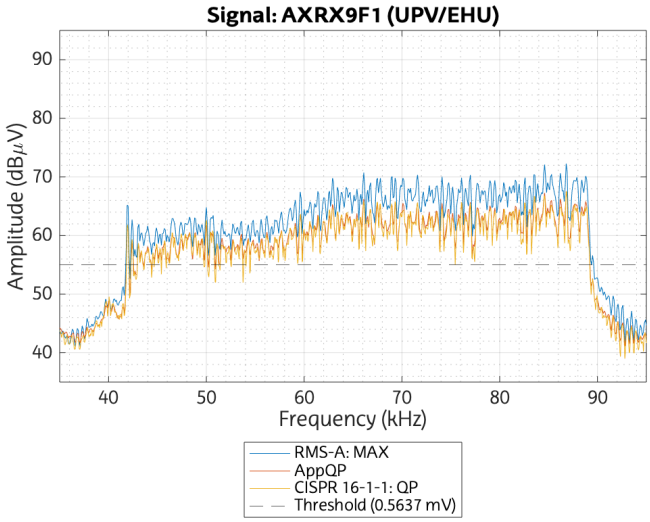

Figure 49: PLC PRIME emission on 'AXRX9F1' signal

13.4. Analysis of computational complexity and memory resources requirements

As described in sections *3.1* and *7.2*, the new EMI measurement method must meet certain requirements imposed by standardisation bodies. One of them is that the new EMI method must require 75% less computational complexity and memory resources than the digital implementation of CISPR 16-1-1. This section describes the analysis developed and the results obtained in these two aspects.

When assessing the computational cost of a measurement method that computes the spectrum of a signal, the operations that require the most machine cycles are the calculations related to the FFTs. For this reason, when comparing the different methods, the ratio between the number of FFTs needed to give the final result with both methods is the main parameter. In addition, the number of points in the FFTs is also considered, since longer FFTs need more clock cycles to be calculated. In the case under study, the comparison of the FFTs between the digital implementation of CISPR 16-1-1 (described in *11*) and the AppQP method (described in *13*) are calculated. In this case, the number of FFT points is the same in both EMI methods, as they use a 20 ms window.

Measurement method	Number of FFTs
Digital implementation of CISPR 16-1-1	1491
AppQP	150

Table 24: Number of FFTs in 3 seconds long signals with the digital implementation of CISPR 16-1-1 and AppQP

In *Table 24*, the number of FTTs required by digital CISPR 16-1-1 and AppQP methods is shown. As shown in the table, the AppQP method requires 90% fewer FFTs, due to the overlap defined in the digital implementation of CISPR 16-1-1.

The computational cost of a method can also be evaluated by measuring the execution time of the code implemented to apply such a method. As the methods above have been implemented in MATLAB, two metrics provided by this software tool can be used to evaluate the performance of the code. First, the 'Wall-clock time', shows the absolute time required to execute the code, without considering the time used by the computer's processor to execute other tasks [29], [30]. Second, the 'CPU time', counts the time CPU to execute the code, without taking into account the rest of the computer's processes; nonetheless, it counts the execution time on each CPU processor; therefore, if the CPU uses more than one processor, this time may be higher than the 'Wall-clock time' [31]. [5]

Measurement method	Wall-clock time	CPU time
Digital implementation of CISPR 16-1-1	6.60 s	9.83 s
AppQP	0.39 s	0.83 s

Table 25: Execution time for 3 seconds long signals with the digital implementation of CISPR 16-1-1 and the AppQP method.

As the table above shows, the AppQP requires a much shorter execution time to obtain the results. If 'Wall-clock time' is considered, it requires 94 % less time, and the comparison is made by 'CPU time', the performance is 91 % better.

The memory requirements of the above-mentioned methods are calculated for all the spectra generated within 3 seconds.

Measurement method	Required memory
Digital implementation of CISPR 16-1-1	203.23 MB
AppQP	1.77 MB

Table 26: Required memory for 3 seconds long signals with the digital implementation of CISPR 16-1-1 and AppQP

The results show that the AppQP method needs much fewer memory resources to store the spectrogram of the analysed signals: it needs 99 % fewer resources to store this data.

It can be concluded that the AppQP method fulfills the requirement of an improvement of 75% of efficiency in the performance. Therefore, it can be assured that the AppQP is a much more efficient NIE measurement method than the digital implementation of the CISPR 16-1-1 method.

[5] This analysis has been carried out on the following platform:

Commercial name: MacBook Pro 13" (Mid 2014); OS: macOS Big Sur – version 11.2.3; CPU: 2,6 GHz Intel Core i5 dual core; RAM: 8 GB 1600 MHz DDR3; Graphics: Intel Iris 1536 MB; MATLAB: R2019b (Update 8 - version 9.7.0.1286710)

The signal characteristics used in this analysis are as follows:

Sampling frequency: 1.48 MHz; Length: 3s; Number of samples: 4 464 286

14. Project planning

This section describes the tasks that have been carried out in order to complete this Master's Thesis.

This work was scheduled in five Work Packages for two academic years. The first Work Package (WP1) consists of the comparison of the existing normatived an research measuremet methods. However, the WP2 includes the design and generation of the synthetic test signals with similar characteristics to the signals present in the LV grid. In WP3 the definition of the new measurement method, the IEC 61000-4-7 method adapted to CISPR Band A or RMS-A, is deployed. Nonetheless, in WP4 the research of the relation between RMS and QP values and the development of new measurement methods, the AppQP, is performed. Meanwhile, in WP5 the digital implementation of CISPR 16-1-1 with fixed parametres, in which the reproducibility issues are solved, is deployed. Finally, WP6 is the work package where the project documentation has been created, a task that has lasted for the entire duration of the project.

Work package	Task tag	Begin date	End date	Description
WP1	T01	16/09/2019	15/10/2019	Bibliographic search of EMI measurement methods
	T02	16/10/2019	15/11/2019	Implementation of normative methods
	T03	18/11/2019	27/12/2019	First tests of the implemented methods with signals recorded in the LV grid
	T04	29/05/2020	30/06/2020	Processing of synthetic test signals for the comparison of EMI methods
WP2	T05	01/01/2020	28/01/2020	Bibliographic search and definition of the principles of synthetic signals.
	T06	29/01/2020	24/03/2020	Implementation of the code for synthetic signal generation.
	T07	25/03/2020	22/04/2020	Characterisation of the emissions of LV grid signals for the creation of synthetic signals.
	T08	23/04/2020	28/05/2020	Generation of synthetic test signals.
WP3	T09	01/09/2020	15/09/2020	Study of IEC 61000-4-7 standard
	T10	16/09/2020	15/10/2020	Development of RMS-A method
	T11	16/10/2020	26/11/2020	Implementation of RMS-A measurement method
WP4	T12	01/09/2020	31/10/2020	Study of the relationship of CISPR 16-1-1 QP values and RMS-A results.
	T13	02/11/2020	01/02/2021	Development of the RMS-QP conversion factor for IEC 61000-4-7.
	T14	02/02/2021	01/03/2021	Definition of AppQP method.
	T15	03/03/2021	31/03/2021	Validation of the AppQP and generation of method accuracy statistics.
WP5	T16	01/01/2021	10/02/2021	Bibliographic search of a FTT-based CISPR 16-1-1 implementations.
	T17	11/02/2021	15/03/2021	Definition of the digital implementation of CISPR 16-1-1 with fixed parameters.

WP6	T18	16/09/2019	12/06/2021	Documentation of research work
	T19	01/07/2020	31/08/2021	Writing the paper on measurement methods comparison.
	T20	01/04/2021	11/06/2021	Writing the Master's Thesis.

Table 27: Master's Thesis's tasks

The milestones related to the tasks described above are listed in the table below. It lists the milestones for the completion of the work packages and the most relevant publications/meetings of the project.

Milestone tag	Date	Milestone
M01	28/05/2020	Completion of work package WP1
M02	30/06/2020	Completion of work package WP2
M03	29/09/2020	IEC77A-WG9 meeting. First results of the relation between QP and RMS values are presented.
M04	11/11/2020	SupraEMI workshop. 'Characterisation of different types of emission in the range 2-150kHz. Presentation about the synthetic signals.'
M05	19/11/2020	Publication of the paper 'Comparison of Measurement Methods for 2–150-kHz Conducted Emissions in Power Networks'
M06	23/11/2020	Completion of work package WP3
M07	28/01/2021	IEC77A-WG9 meeting. The approach of the AppQP method is presented.
M08	15/03/2021	Completion of work package WP5
M09	31/03/2021	Completion of work package WP4
M10	19/04/2021	IEC77A-WG9 meeting. The complete AppQP method is presented.
M11	11/06/2021	Completion of work package WP6

Table 28: Master's Thesis's milestones

The tasks and milestones described above are shown in the Gantt chart below, in order to understand more visually the achievement of tasks over time.

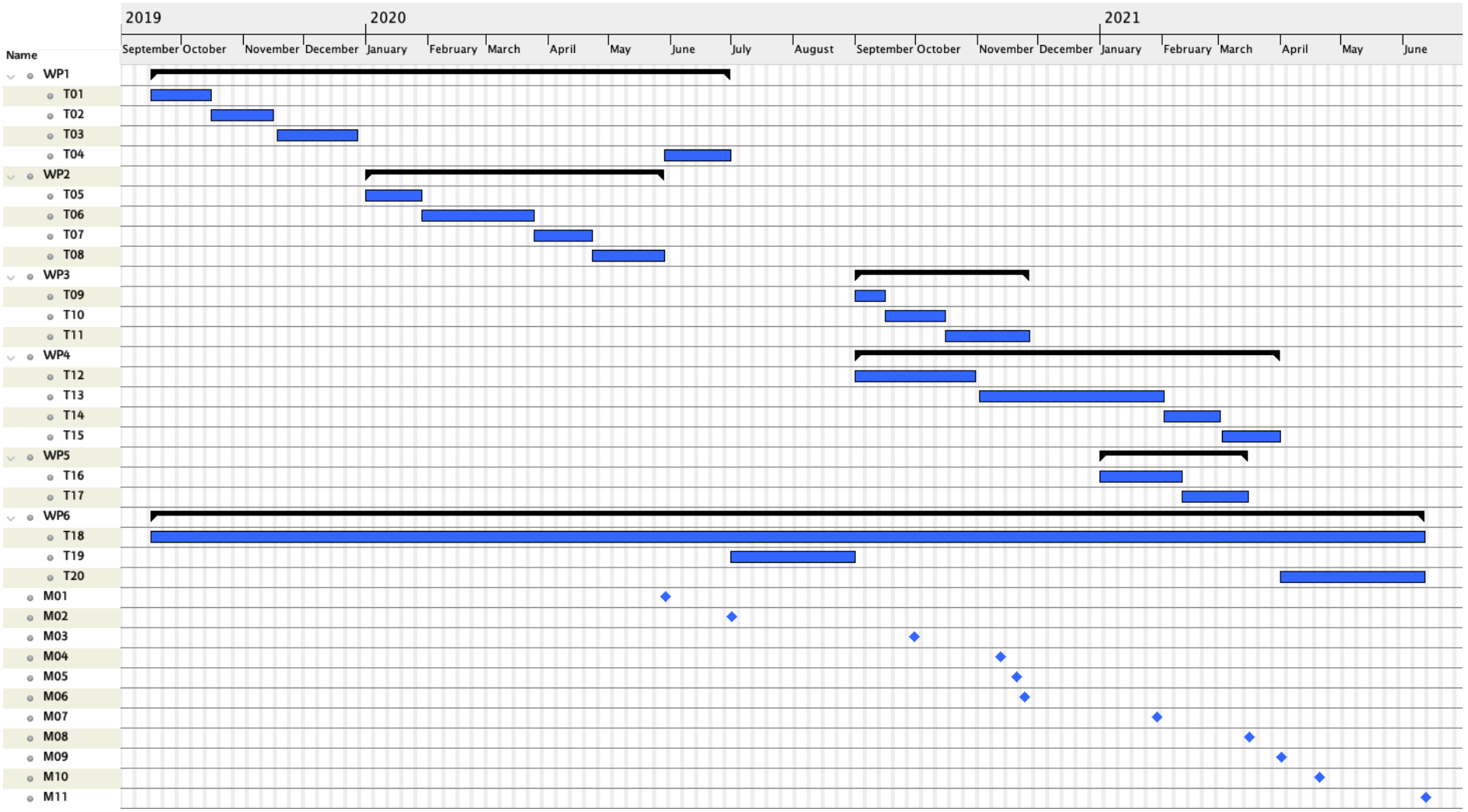

Figure 50: Master's Thesis' Gantt chart

15. Conclusions

This section presents the conclusions of the Master's Thesis. Therefore, this chapter contains the general conclusions of the work, describes the main scientific contributions and proposes future research lines.

15.1. General conclusions

In this Master's Thesis, five main tasks have been developed: a comparison of existing EMI measurement methods, the development of a method to generate synthetic signals with known PSD, the definition of a digital implementation of CISPR 16-1-1 with fixed parameters and the definition and development of two new measurement methods, RMS-A and AppQP methods, for measurements in the LV grid in the range 2 kHz – 150 kHz . The first new method, RMS-A, is designed to provide RMS spectra in the CISPR Band A. Nonetheless, the second new method provides QP values with less computational complexity and memory resources.

First, a method to generate synthetic test signals, similar to the signals that can be found in the LV distribution grid in the frequency range 2 kHz – 150 kHz, has been defined and implemented. This method allows the generation of signals as a combination of different types of emissions, patterns and levels of noise and NB-PLC transmissions. The method provides high flexibility in the definition of the level, duration and bandwidth of the different components. These components can be easily combined in resultant LV grid-like signals of known amplitude levels and spectral characteristics, which are useful to evaluate the accuracy of measurement methods. The method is based on the generation of AWGN and polar coding signals. In contrast to the test signals described in the literature, this method allows the creation of broadband emissions in which the reference values PSD are known for the whole spectrum. This feature enables the accuracy of the measurement methods to be evaluated without the bias of the measurement procedure. The synthetic test signals generated by this method were used to evaluate the amplitude, frequency and integral value accuracy of standard and experimental measurement methods.

A comparison of the existing methods, both normative and experimental, has been carried out with the synthetic test signals and a measured recording in the LV grid. In this study, the accuracy of the results of the existing EMI methods has been evaluated; in which the accuracy of the amplitude, frequency and integral values have been evaluated. The knowledge acquired in this task has served for the development of the new methods proposed in this Master's Thesis.

Then, to address the reproducibility issues of CISPR 16-1-1, a digital implementation with fixed parameters of this measurement method has been defined and implemented. As CISPR 16-1-1 is a measurement method with broad tolerances, based on a 'black box approach', different implementations compliant with the standard can provide very different results. The proposed digital implementation with specific parameters solves these reproducibility problems and is aligned with the specifications defined in the standard CISPR1 6-1-1 and the Technical Report CISPR 16-3.

The most significant contribution of this work is the development of new measurement methods for the characterization of the NIE present in the LV electrical grid in the frequency range 2 kHz – 150 kHz.

The first method, the RMS-A method, provides RMS values and it is defined as an evolution of the IEC 61000-4-7 (for frequencies below 9 kHz in the CENELEC Band A), while the second method, the AppQP method, provides QP values similar to the values provided by the CISPR 16-1-1 method, for the whole frequency range, with lower computational complexity and memory resources. This method is based on a new approach: the statistical analysis of the RMS values for measurement periods of 3 s. This process for measuring QP spectra is novel, since it is based on the statistical variability of the signal over time, instead of the specifications that define the response of a specific electronic circuit. The validation of this new measurement method with recordings from the LV grid shows that it provides QP values comparable to those of the specific digital implementation of CISPR 16-1-1.

This analysis of the relation between the QP and the RMS values and the numerical model between both metrics are additional contributions of this work. The numerical model is the basis for the proposed AppQP model.

The three measurement methods mentioned above have been developed to fill the existing shortcomings of the current EMI methods. The following table summarises the strengths of each method, with the aim of clarifying how they can be complementary to assess the amplitude of the NIEs of the LV grid.

Strength of methods	Digital CISPR 16-1-1	RMS-A	AppQP
It is a standardized method	Yes	No	Under consideration
Valid for the LV grid	No	Yes	Yes
Provides QP spectra in CISPR Band A	Yes	No	Yes
Provides RMS spectra in CISPR Band A	No	Yes	No
Consistent with CISPR 16-1-1 standard	Yes	No	Yes
Consistent with IEC 61000-4-7 standard	No	Yes	Yes
Reproducibility - No implementation tolerances	Yes	Yes	Yes
Good time and frequency domain resolution	Yes	No	No
Low computational burden and low memory requirements	No	Yes	Yes

Table 29: Strengths of the designed methods

15.2. Contributions

Different contributions have been made in this Master's Thesis: papers submitted to scientific publications, a presentation in a conference and contributions to international standardisation committees. These contributions are summarised below.

- As mentioned throughout the document, part of this Master's Thesis has already been published in scientific journal articles. Specifically, both the method to design synthetic

signals and the comparison of existing EMI methods were published in the journal IEEE Transactions on Instrumentation and Measurement [7].

- Moreover, other outcomes described in this work will be shortly submitted for publication. Research related to the design and implementation of the Approximated Quasi-Peak and the numerical model that relates CISPR 16-1-1 QP and RMS-A RMS results will be submitted to the journal IEEE Transactions on Instrumentation and Measurement.

- Additionally, within the SupraEMI project, another publication on the reproducibility issues of the CISPR 16-1-1 method is being prepared and it will be submitted to the journal IEEE Transactions on Instrumentation and Measurement.

- The methodology for generating the synthetic signals and some representative results were presented at a Webinar-Workshop organised by the European SupraEMI project's consortium. The conference's title was 'Characterisation of different types of emission in the range 2-150kHz' and was held on 11 November 2020 [32].

- The outcomes of both the AppQP method and the digital implementation of CISPR 16-1-1 were presented at three meetings of the IEC77A/WG9 standardisation committee. This IEC working group is currently discussing about including these methods as a normative annex of the IEC 61000-4-30 standard.

- Finally, the outcomes presented at the IEC, the relationship between QP (CISPR 16-1-1 method) and RMS spectra (RMS-A method), and the Approximate Quasi-peak Method, will be presented at the Working Group 11 of the CENELEC standardisation organisation.

15.3. Future work

As a result of this work, specific research opportunities are envisaged, which could continue the work described in this Master's Thesis.

First, the evolution of IEC 61000-4-7 for the 9 kHz to 150 kHz band could evolve from having a final spectrum result, which does not provide information on the time evolution of the waveforms, to additional mechanisms for a deeper evaluation of the NIEs over time, based on the storage and processing of the spectrogram. In addition, the definition of new metrics would be needed to evaluate LV grid's waveforms.

Additionally, all the knowledge acquired to characterise NIEs and design measurement methods in the 2 kHz to 150 kHz band could be used in higher frequency bands. The 150-500 kHz and 0.5-30 MHz bands are still under initial investigation, from the point of view of detection and characterisation of NIEs in the LV grid. This opens up a significant opportunity to research EMI measurement methods in higher frequencies not covered in this project.

REFERENCES

[1] REE: Red Eléctrica de España, "What are smart grids?" https://www.ree.es/en/red21/smart-grids/what-are-smart-grids (accessed Apr. 24, 2021).

[2] Spanish Government. Ministry of Industry Energy and Tourism., "Orden IET/290/2012, de 16 de febrero, por la que se modifica la Orden ITC/3860/2007, de 28 de diciembre, por la que se revisan las tarifas eléctricas a partir del 1 de enero de 2008 en lo relativo al plan de sustitución de contadores," *Boletín Oficial del Estado*, vol. 44. 2012, Accessed: Apr. 24, 2021. [Online]. Available: https://www.boe.es/diario_boe/txt.php?id=BOE-A-2012-2538.

[3] IEC, *Electromagnetic compatibility (EMC) - Environment - Compatibility levels for low-frequency conducted disturbances and signalling in public low-voltage power supply systems. IEC 61000-2-2:2002*. 2002.

[4] IEC, *Electromagnetic compatibility (EMC) - Environment - Compatibility levels for low-frequency conducted disturbances and signalling in public low-voltage power supply systems. IEC 61000-2-2:2002/A1:2017*. 2017.

[5] IEC, *Electromagnetic compatibility (EMC) - Environment - Compatibility levels for low-frequency conducted disturbances and signalling in public low-voltage power supply systems. IEC 61000-2-2:2002/A2:2018*. 2018.

[6] CISPR, *Specification for radio disturbance and immunity measuring apparatus and methods - Part 1-1: Radio disturbance and immunity measuring apparatus - Measuring apparatus. CISPR 16-1-1:2019*. 2019.

[7] D. Ritzmann *et al.*, "Comparison of Measurement Methods for 2-150-kHz Conducted Emissions in Power Networks," *IEEE Transactions on Instrumentation and Measurement*, vol. 70, 2021, doi: 10.1109/TIM.2020.3039302.

[8] European Metrology project 18NRM05 SupraEMI (2019 – 2022), "Publishable Summary for 18NRM05 SupraEMI Grid measurements of 2 kHz-150 kHz harmonics to support normative emission limits for mass-market electrical goods Overview." Accessed: Apr. 24, 2021. [Online]. Available: http://empir.npl.co.uk/supraemi/wp-content/uploads/sites/56/2021/01/18NRM05_SupraEMI_M18_Publishable-Summary-ACCEPTED.pdf.

[9] CISPR, *Specification for radio disturbance and immunity measuring apparatus and methods – Part 3: CISPR technical reports. CISPR TR 16-3:2020*. 2020.

[10] M. A. Azpurua, M. Pous, and F. Silva, "Specifying the Waveforms for the Calibration of CISPR 16-1-1 Measuring Receivers," *IEEE Transactions on Electromagnetic Compatibility*, vol. 62, no. 3, pp. 654–662, 2020, doi: 10.1109/TEMC.2019.2923813.

[11] IEC, *Electromagnetic compatibility (EMC) Part 4-7: Testing and measurement techniques - General guide on harmonics and interharmonics measurements and instrumentation, for power supply systems and equipment connected thereto. IEC 61000-4-7:2002/A1:2008*. 2008.

[12] IEC, *Electromagnetic compatibility (EMC) Part 4-7: Testing and measurement techniques - General guide on harmonics and interharmonics measurements and instrumentation, for power supply systems and equipment connected thereto. IEC 61000-4-7:2002*. 2002.

[13] IEC, *Electromagnetic compatibility (EMC) - Part 4-30: Testing and measurement techniques - Power quality measurement methods. IEC 61000-4-30: 2015*. 2015.

[14] T. M. Mendes, C. A. Duque, L. R. M. Silva, D. D. Ferreira, and J. Meyer, "Supraharmonic analysis by filter bank and compressive sensing," *Electric Power Systems Research*, vol. 169, pp. 105–114, Apr. 2019, doi: 10.1016/j.epsr.2018.12.016.

[15] S. Zhuang, W. Zhao, R. Wang, Q. Wang, and S. Huang, "New Measurement Algorithm for Supraharmonics Based on Multiple Measurement Vectors Model and Orthogonal Matching Pursuit," *IEEE Transactions on Instrumentation and Measurement*, vol. 68, no. 6, pp. 1671–1679, Jun. 2019, doi: 10.1109/TIM.2018.2878613.

[16] S. Zhuang, W. Zhao, Q. Wang, Z. Wang, L. Chen, and S. Huang, "A high-resolution algorithm for supraharmonic analysis based on multiple measurement vectors and Bayesian compressive sensing," *Energies*, vol. 12, no. 13, p. 2559, Jul. 2019, doi: 10.3390/en12132559.

[17] S. Lodetti, J. Bruna, J. J. Melero, V. Khokhlov, and J. Meyer, "A Robust Wavelet-Based Hybrid Method for the Simultaneous Measurement of Harmonic and Supraharmonic Distortion," *IEEE Transactions on Instrumentation and Measurement*, vol. 69, no. 9, pp. 6704–6712, Sep. 2020, doi: 10.1109/TIM.2020.2981987.

[18] V. Khokhlov, J. Meyer, A. Grevener, T. Busatto, and S. Ronnberg, "Comparison of measurement methods for the frequency range 2-150 kHz (Supraharmonics) based on the present standards framework," *IEEE Access*, vol. 8, pp. 77618–77630, 2020, doi: 10.1109/ACCESS.2020.2987996.

[19] G. Anne, M. Jan, and R. Sarah, "Comparison of Measurement Methods for the Frequency Range 2-150 kHz (Supraharmonics)," Oct. 2018, doi: 10.1109/AMPS.2018.8494879.

[20] M. Klatt, J. Meyer, and P. Schegner, "Comparison of measurement methods for the frequency range of 2 kHz to 150 kHz," in *Proceedings of International Conference on Harmonics and Quality of Power, ICHQP*, 2014, pp. 818–822, doi: 10.1109/ICHQP.2014.6842791.

[21] I. Fernandez *et al.*, "Characterization of non-intentional emissions from distributed energy resources up to 500 kHz: A case study in Spain," *International Journal of Electrical Power and Energy Systems*, vol. 105, pp. 549–563, Feb. 2019, doi: 10.1016/j.ijepes.2018.08.048.

[22] I. Fernández, D. de la Vega, A. Arrinda, I. Angulo, N. Uribe-Pérez, and A. Llano, "Field trials for the characterization of non-intentional emissions at low-voltage grid in the frequency range assigned to NB-PLC technologies," *Electronics (Switzerland)*, vol. 8, no. 9, p. 1044, Sep. 2019, doi: 10.3390/electronics8091044.

[23] G. Proakis John and G. Manolakis Dimitris, *Digital signal processing: principles, algorithms, and applications*, Third. New Jersey: Prentice-Hall International, Inc., 1996.

[24] ITU-T, *Narrowband Orthogonal Frequency Division Multiplexing Power Line Communication Transceivers for PRIME Networks*. document ITU-T G.9904, 2012.

[25] I. Fernández, M. Alberro, J. Montalbán, A. Arrinda, I. Angulo, and D. de la Vega, "A new voltage probe with improved performance at the 10 kHz–500 kHz frequency range for field measurements in LV networks," *Measurement: Journal of the International Measurement Confederation*, vol. 145, pp. 519–524, Oct. 2019, doi: 10.1016/j.measurement.2019.05.106.

[26] V. Khokhlov, J. Meyer, A. Grevener, T. Busatto, and S. Ronnberg, "Comparison of measurement methods for the frequency range 2-150 kHz (Supraharmonics) based on the present standards framework," *IEEE Access*, vol. 8, pp. 77618–77630, 2020, doi: 10.1109/ACCESS.2020.2987996.

[27] MathWorks, "Visualize summary statistics with box plot - MATLAB boxplot - MathWorks United Kingdom," 2020. https://uk.mathworks.com/help/stats/boxplot.html (accessed Apr. 29, 2021).

[28] L. Sandrolini and A. Mariscotti, "Impact of short-time fourier transform parameters on the accuracy of EMI spectra estimates in the 2-150 kHz supraharmonic interval," *Electric Power Systems Research*, vol. 195, p. 107130, Jun. 2021, doi: 10.1016/j.epsr.2021.107130.

[29] "Start stopwatch timer - MATLAB tic - MathWorks United Kingdom." https://uk.mathworks.com/help/matlab/ref/tic.html (accessed May 22, 2021).

[30] "Read elapsed time from stopwatch - MATLAB toc - MathWorks United Kingdom." https://uk.mathworks.com/help/matlab/ref/toc.html (accessed May 22, 2021).

[31] "CPU time used by MATLAB - MATLAB cputime - MathWorks United Kingdom." https://uk.mathworks.com/help/matlab/ref/cputime.html (accessed May 22, 2021).

[32] D. de la Vega and A. Gallarreta, "Workshop-Webinar SupraEMI - Characterisation of different types of emission in the range 2-150kHz.," Nov. 2020, Accessed: May 29, 2021. [Online]. Available: http://empir.npl.co.uk/supraemi/2020/11/11/webinar-measurement-methods-for-the-frequency-range-2-150-khz-supraharmonics/.